

**DEVELOPMENT OF A CRISPR GENE CORRECTION STRATEGY FOR  
ANIRIDIA EMPLOYING A MINIMALLY HUMANIZED MOUSE  
EMBRYONIC STEM CELL-BASED DISEASE MODEL**

by

Bethany Adair

B.Sc. (Hons), Western University, 2020

A THESE SUBMITTED IN PARTIAL FULFILLMENT OF  
THE REQUIREMENTS FOR THE DEGREE OF

MASTER OF SCIENCE

in

THE FACULTY OF GRADUATE AND POSTDOCTORAL STUDIES  
(Medical Genetics)

THE UNIVERSITY OF BRITISH COLUMBIA

(Vancouver)

June 2023

© Bethany Adair, 2023

The following individuals certify that they have read, and recommend to the Faculty of Graduate and Postdoctoral Studies for acceptance, the thesis entitled:

Development of a CRISPR Gene Correction Strategy for Aniridia Employing a Minimally Humanized Mouse Embryonic Stem Cell-Based Disease Model

---

submitted by Bethany Adair in partial fulfilment of the requirements for

the degree of Master of Science

in Medical Genetics

**Examining Committee:**

Dr. Elizabeth M. Simpson, Professor, Medical Genetics, UBC  
Supervisor

Dr. Sarah Hedtrich, Associate Professor, Pharmaceutical Sciences, UBC  
Supervisory Committee Member

Dr. Catherine Van Raamsdonk, Associate Professor, Medical Genetics, UBC  
Supervisory Committee Member

Dr. William T. Gibson, Professor, Medical Genetics, UBC  
Additional Examiner

## ABSTRACT

Aniridia is a rare congenital blindness caused by heterozygous variants in the *PAX6* gene. There is no vision-saving therapy, but one exciting approach is the gene editing capabilities of CRISPR systems to permanently correct the genomic variants. Pre-clinical studies to develop such a therapy in animal models face the challenge of showing efficacy when binding human DNA. To answer this challenge, while developing a CRISPR therapy for aniridia, we proposed the “CRISPR Humanized Minimally Mouse Models” (CHuMMMs) strategy. I hypothesize that a CRISPR gene strategy can be developed and optimized in humanized mouse embryonic stem cells that will be able to distinguish between the patient variant and non-variant chromosomes, laying the foundation for correcting aniridic congenital blindness in humans. Thus, we minimally humanized *Pax6* exon 9, the location of the most common aniridia variant c.718C>T, creating a 312 bp “landing pad” of human DNA. Initially, we generated a non-variant mouse to show humanization did not disrupt *Pax6* function. Then, we generated a CHuMMMs cell-based disease model, in which we tested five CRISPR enzymes for efficacy. In this system, base editor ABE8e had the highest correction of the variant at 76.8%. Finally, we used LNPs to deliver ABE8e to primary neurons *ex vivo*, which altered a second patient variant and rescued 24.8% *Pax6* expression. Thus, we demonstrated the CHuMMMs approach, and showed the first genomic editing by ABE8e encapsulated as an LNP-RNP. Furthermore, we laid the foundation for translation of the proposed CRISPR therapy to human cells and eventually aniridia patients.

## LAY SUMMARY

Aniridia is a rare genetic disease that is caused by defects in the paired box 6 (*PAX6*) gene. This gene is essential for normal development of the eye. Patients experience low vision at birth, which progresses to blindness by adulthood. Current interventions aim to slow progression of symptoms, but no curative options exist. One exciting approach is to harness the gene-editing capabilities of CRISPR/Cas9 to correct the genetic defects that cause aniridia. Since curing aniridia in mouse is a prerequisite to treating patients, I hypothesize that a CRISPR therapy to correct the defective copy of *PAX6* in cells derived from a mouse model of aniridia will be a suitable strategy to develop an aniridia therapy. Here, we optimize a CRISPR strategy that corrects a defect that causes aniridia, while minimally impacting the functional copy of *PAX6*. This work lays the foundation for a therapy to prevent blindness in aniridia patients.

## PREFACE

Chapter 2 is based on work conceived by Dr. Elizabeth M. Simpson. Initial stages of the project were conducted by previous MSc. student Nina Chiu, lab manager Andrea Korecki, and previous technicians Tess Lengyell and Siu Ling Lam. The project became focused under my direction. The aforementioned parties generated and performed the initial molecular characterisation of the *He9<sup>+</sup>/He9<sup>+</sup>* mice. I was responsible for conducting and analyzing results from thorough phenotyping of the strains. I was responsible for generating the novel humanized ESC lines for *in vitro* therapy optimization. I proposed and coordinated the multiple therapeutic strategies that were tested, including the ABE8e RNP. I conducted *in vitro* therapeutic trials with assistance from technicians Andrea Korecki and Diana Djaksigulova. Dr. Nada Lallous and Mr. Joseph Lee at the Gobind Khorana Protein Engineering Core provided the service of purification of the ABE8e protein. Dr. Sunita Sinha at the University of British Columbia Sequencing and Bioinformatics Consortium, Ms. Marketa Hlavon and Mr. Cillein Thorne at the British Columbia Children's Hospital Research Institute Sequencing and Bioanalyzer Core conducted Sanger sequencing. All work using lipid nanoparticles was conducted in collaboration with Incisive Genetics Inc (Vancouver, Canada). Ainsley Coquinco at Incisive Genetics conducted cortical neuron cultures. I conducted all data processing, analysis, and figure generation.

Chapter 2 has been originally published as:

**Adair BA**, Korecki AJ, Djaksigulova D, Wagner PK, Chiu NY, Lam S, Lengyell TC, Leavitt BR, Simpson, EM. (2023). ABE8e corrects *Pax6*-aniridic variant in humanized mouse ESCs and via LNPs in *ex vivo* cortical neurons. *Ophthalmol Ther* (online ahead of print), PMID: 37210469.

I wrote the initial draft, which was edited in collaboration primarily with Dr. Elizabeth M. Simpson. Additional editing support was received from Andrea Korecki and Tess Lengyell.

All animals were housed and bred in the pathogen-free Transgenic Animal facility at the Centre for Molecular Medicine and Therapeutics (CMMT) of the University of British Columbia (UBC). All mouse work was performed following protocols approved by the UBC Animal Care Committee (protocol #s A21-0410, A21-0184), in accordance with guidelines determined by the Canadian Council on Animal Care.

## TABLE OF CONTENTS

ABSTRACT .....	iii
LAY SUMMARY .....	iv
PREFACE.....	v
TABLE OF CONTENTS .....	vii
LIST OF TABLES .....	x
LIST OF FIGURES .....	xi
LIST OF ABBREVIATIONS .....	xii
ACKNOWLEDGEMENTS .....	xv
DEDICATION .....	xvi
<b>CHAPTER 1: INTRODUCTION .....</b>	<b>1</b>
1.1 GENERAL BACKGROUND .....	1
1.1.1 Development of the mammalian eye .....	1
1.1.2 <i>PAX6</i> .....	3
1.1.3 Congenital blindness, aniridia .....	6
1.1.3.1 Genotype/phenotype correlations .....	7
1.1.3.2 Clinical interventions for aniridia.....	9
1.1.4 Gene therapy.....	10
1.1.4.1 Gene augmentation .....	11
1.1.4.2 CRISPR gene editing.....	11
1.1.4.3 Delivery strategies for gene therapy .....	14
1.1.5 Minimal humanization of <i>Pax6</i> for translational therapy.....	16
1.2 HYPOTHESIS AND THESIS OBJECTIVES.....	18
<b>CHAPTER 2: ABE8E CORRECTS <i>PAX6</i>-ANIRIDIC VARIANT IN HUMANIZED MOUSE ESCS AND VIA LNPS IN <i>EX VIVO</i> CORTICAL NEURONS .....</b>	<b>19</b>
2.1 INTRODUCTION .....	19
2.2 METHODS.....	23
2.2.1 Isolation and culture of mouse embryonic stem cells.....	23
2.2.2 RNP design for humanization of ESCs .....	23
2.2.3 Cell transfection and picking single clones .....	23
2.2.4 DNA isolation, PCR genotyping, and RFLP screens .....	25

2.2.5	Sanger sequencing and peak quantification.....	26
2.2.6	Generation of humanized exon 9 mice .....	26
2.2.7	Phenotyping by visual inspection and slit lamp imaging .....	28
2.2.8	Purification of ABE8e protein.....	28
2.2.9	RNP design and complexation for CRISPR therapy .....	28
2.2.10	Preparation of Incisive DS LNPs and encapsulation of RNPs and DNA template.	29
2.2.11	<i>Ex vivo</i> genome editing.....	29
2.2.12	Statistical analysis.....	30
2.2.13	Compliance with ethics guidelines .....	30
2.3	RESULTS.....	31
2.3.1	CHuMMMs for <i>Pax6</i> -aniridia therapy development <i>in vitro</i> .....	31
2.3.2	Minimal humanization with non-variant <i>PAX6</i> results in no phenotype <i>in vivo</i> .....	32
2.3.3	<i>SpCas9</i> gave higher editing of patient variant than <i>SaCas9</i> .....	34
2.3.4	High-fidelity Cas9 gave lower alteration of non-variant chromosome than WT <i>SpCas9</i> .....	36
2.3.5	ABE8e gave superior editing of patient variant and reduced alteration of non-variant chromosome than <i>SpCas9</i> .....	37
2.3.6	ABE8e edits patient variant “additively” in humanized heterozygous variant cell line .....	40
2.3.7	LNP-encapsulated ABE8e-RNPs edited a <i>Pax6</i> patient variant in mouse <i>ex vivo</i> cortical neurons.....	41
2.4	DISCUSSION.....	45
2.5	CONCLUSIONS .....	47
<b>CHAPTER 3: STRATEGIES FOR CLINICAL TRANSLATION.....</b>		<b>49</b>
3.1	HYPOTHESIS AND THESIS OBJECTIVES .....	49
3.2	CONTRIBUTION TO THE FIELD.....	50
3.3	FUTURE DIRECTIONS .....	52
3.3.1	Off-target analyses in a human cell line .....	52
3.3.2	Generation of 3xFLAG-tagged <i>He9<sup>-</sup>/He9<sup>+</sup></i> mouse .....	54
3.3.3	Optimization of ABE8e-RNP-LNP therapy in a B6129F1- <i>FHe9</i> mouse .....	56
3.4	CONCLUSION .....	61

**REFERENCES** ..... 63

**APPENDIX: GENERATION OF *FAX* ESCS** ..... 81

## LIST OF TABLES

<b>Table 2.1 CRISPR guide RNAs (gRNAs) and DNA templates used for <i>in vitro</i> gene editing.....</b>	<b>24</b>
<b>Table 2.2 Primers and restriction enzymes used for PCR, RFLP, and Sanger sequencing for characterization of humanized clones and CRISPR-edited whole cell lysates.....</b>	<b>27</b>
<b>Table 3.1 Final breeding scheme to generate cohorts for <i>in vivo</i> ABE8e-RNP-LNP optimization studies.....</b>	<b>59</b>
<b>Table 3.2 Experimental design for <i>in vivo</i> ABE8e-RNP-LNP therapy optimization study.....</b>	<b>61</b>

## LIST OF FIGURES

Figure 1.1 Development of the human eye.....	1
Figure 1.2 Labelled diagram of a healthy adult human eye.....	3
Figure 1.3 Paired box six ( <i>PAX6</i> ) cDNA and protein structure.....	5
Figure 1.4 CRISPR gene editing systems.....	13
Figure 2.1 The average diameter distribution of LNP encapsulated ABE8e RNP.....	29
Figure 2.2 Derivation of homozygous humanized <i>Pax6</i> exon-9 mouse embryonic stem cells, including an exon-9 pathogenic patient variant.....	32
Figure 2.3 CRISPR-based minimal humanization of <i>Pax6</i> does not result in an ocular phenotype in mouse.....	33
Figure 2.4. CRISPR genome editing of the patient variant is higher using <i>SpCas9</i> than <i>SaCas9</i> .....	35
Figure 2.5 A high fidelity <i>SpCas9</i> resulted in lower CRISPR editing on the non-variant chromosome.....	37
Figure 2.6 ABE8e with a modified guide showed superior editing of the patient variant, with minimal impact on the non-variant chromosome.....	39
Figure 2.7 ABE8e edits patient variant “additively” in heterozygous variant cells.....	41
Figure 2.8 LNP delivered ABE8e RNP edited <i>Pax6</i> pathogenic patient variant in mouse cortical neurons <i>ex vivo</i> .....	43
Figure 2.9 Ratio of condensed versus non-condensed neuronal nuclei did not vary with LNP treatment.....	44
Figure A.1 Characterisation of new <i>Fax</i> ESCs.....	83

## LIST OF ABBREVIATIONS

129	129S1/SvImJ
aa	amino acid
ABE	adenine base editor
AAK	aniridia-associated keratopathy
B6	C57BL/6J
BE	base editor
bp	base pair
Cas	CRISPR-associated
CBE	cytosine base editor
CHuMMMs	CRISPR Humanized Minimally Mouse Models
CMMT	Centre for Molecular Medicine and Therapeutics
CRISPR	clustered regularly interspaced short palindromic repeats
crRNA	CRISPR RNA
DEV	day <i>ex vivo</i>
DOC	day of collection
DRR	downstream regulatory region
DSB	double-stranded break
EE	ectodermal enhancer
EMA	European Medicines Agency
ESC	embryonic stem cell
FDA	Food and Drug Administration
<i>Fey</i>	3xFLAG-tagged small eye
<i>FHe9</i>	3xFLAG-tagged humanized exon 9
gRNA	guide ribonucleic acid
HA	homology arm
HC	Health Canada
HD	homeodomain
HDAd	helper-dependent adenovirus
HDR	homology-directed repair
He9	humanized exon 9

HiFi	High Fidelity
ICC	immunocytochemistry
ICM	inner cell mass
IHC	immunohistochemistry
indel	insertion and/or deletion
JAX	The Jackson Laboratory
kDA	kilodalton
KSOM	potassium simplex optimization medium
KSR	KnockOut Serum Replacement
LNK	linker region
LNP	lipid nanoparticle
LOF	loss-of-function
LSC	limbal stem cell
MEF	mouse embryonic fibroblast
nCas9	nickase Cas9
NHEJ	non-homologous end-joining
NMD	nonsense-mediated decay
nt	nucleotide
PAM	protospacer adjacent motif
<i>PAX6</i>	paired box 6 (gene)
PBS	primer binding site
PDI	polydispersity index
PE	prime editor
pegRNA	prime editor guide RNA
PCR	polymerase chain reaction
PD	paired domain
PS	phosphorothioate
PSTD	proline-serine-threonine rich domain
PTC	premature termination codon
rAAV	recombinant adeno-associated virus
RFLP	restriction fragment length polymorphism

RNP	ribonucleoprotein complex
RT	room temperature
RTT	reverse transcriptase template
<i>SaCas9</i>	<i>Staphylococcus aureus</i> Cas9
<i>Sey</i>	small eye
<i>Shh</i>	sonic hedgehog (gene)
sgRNA	single-guide RNA
<i>SpCas</i>	<i>Streptococcus pyogenes</i> Cas9
ssODN	single-stranded oligodeoxynucleotide
TF	transcription factor
tracrRNA	tracer RNA
UTR	untranslated region
WT	wild-type

## ACKNOWLEDGEMENTS

I want to thank my supervisor, Dr. Elizabeth M. Simpson, for being everything a great mentor should be, over the last three years. Thank you for your constant willingness to provide guidance and support, while also allowing me to be independent, to take ownership of, and to have autonomy over my research project. I am so grateful to have had the opportunity to learn and grow as a scientist under your supervision. Thank you to my supervisory committee, Dr. Catherine Van Raamsdonk and Dr. Sarah Hedtrich, for providing guidance throughout the course of my project, engaging in lively discussion at our annual meetings, and helping to push the boundaries of my knowledge and understanding of the project. Thank you to Andrea Korecki for all your patience and readiness to offer help and assistance, whether it was in the early days of my training in the lab, or the later stages as I was wrapping up experiments. Thank you for sharing your expertise when training me in the various molecular biology techniques, my first introduction to tissue culture and sterile technique, and all the Neon electroporations.

Thank you to my lab members, Zeinab Mohanna, Diana Djaksigulova and Sif Kaad for your collaboration, comradery, and eagerness to lend a helping hand. Zeinab, I will always appreciate our end-of-day chats about the trials and tribulations of grad school; thank you for listening and for sharing your insights and encouragement with me. Diana, I'm so glad to have been able to bounce ideas off of you without judgement during our many lunches, and I am so grateful for the friendship that has blossomed since. Thank you to Tess Lengyell, for offering your time and expertise in training and teaching me to become rather fond of blastocyst harvesting. It has been so lovely to work with you.

Of course, I must thank my wonderful support system, without whom completing this degree may not have been possible. Thank you to Audrey, Abby, Meghan, Meleah, and Maddie for your enthusiastic support and encouragement throughout this journey. Thank you to Tommy, for making the time and effort to catch up periodically to talk science, grad school, and the great beyond, while being several time zones away. Thank you to Jonathan and Haley for always being so supportive, understanding, and loving. Finally, thank you to Brett for your patience, kindness, and quiet confidence in me throughout this journey. Your support and faith in me has made all the difference.

## **DEDICATION**

*To Mom and Dad, for encouraging me to take every opportunity  
that has been afforded to me, especially this one.  
For your unwavering love, support, and belief in me  
from 4283 km away.*

## CHAPTER 1: INTRODUCTION

### 1.1 GENERAL BACKGROUND

#### 1.1.1 Development of the mammalian eye

Mammalian development of the eye begins with division of a single eye field into bilateral hemispheres, from which each eye will develop (Chow and Lang, 2001; Graw, 2010; Heavner and Pevny, 2012; Villalba et al., 2021). Each eye arises from three embryonic tissue sources –the surface ectoderm, the neural ectoderm, and the periocular mesenchyme – which produce the distinct ocular cell types that are required for normal eye function (Diacou et al., 2022; Heavner and Pevny, 2012). Ocular development begins shortly after gastrulation, roughly 3 weeks post fertilization in human embryos, when optic grooves form on either side of the developing forebrain (Graw, 2010; Heavner and Pevny, 2012). In each optic groove, specification of the medial anterior neural plate is observed, from which the progenitor cells of the neural-derived eye structures emerge (Chow and Lang, 2001). Each optic groove expands

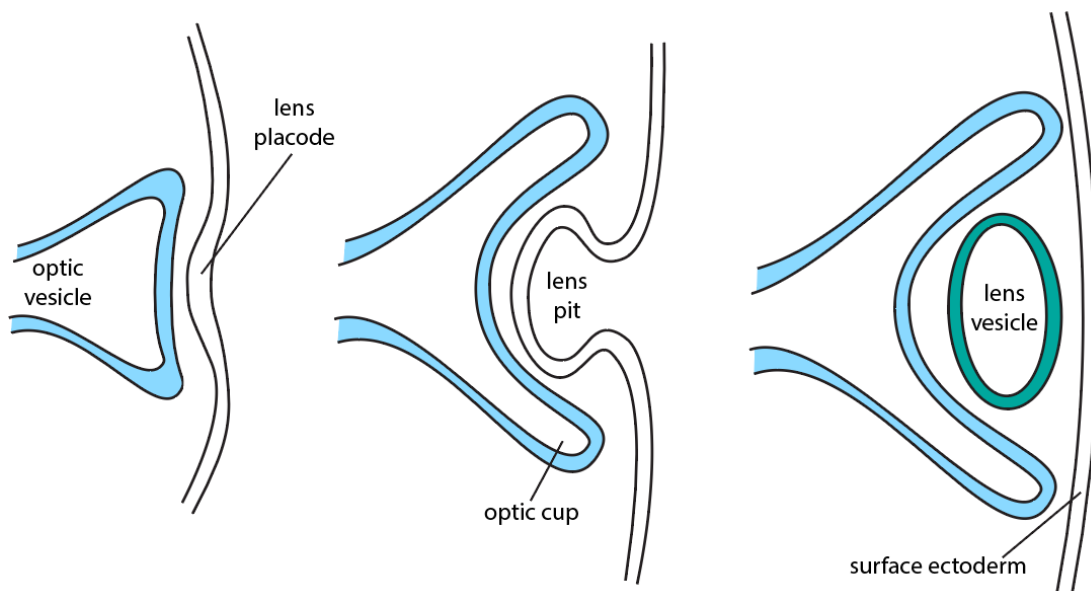


**Figure 1.1 Development of the human eye.** Formation of the optic vesicle begins at roughly 3 weeks of human gestation. The optic vesicle invaginates, forming the optic cup. At the same time, the surface ectoderm forms the lens placode, which also invaginates to create the lens pit. By week 6, the lens pit separates from the surface ectoderm, closing into a lens vesicle, from which the lens develops. Original figure.

toward the surface ectoderm as the medial anterior neural plate (now neural tube) closes, resulting in the formation of an optic vesicle (Collinson et al., 2000; Graw, 2010; Heavner and Pevny, 2012). The surface ectoderm thickens to form the lens placode, then invaginates to form the lens pit, which deepens until it pinches off from the surface ectoderm to form a lens vesicle. The lens develops further by progressive delamination of cells that form the solid lens mass (Ashery-Padan et al., 2000; Heavner and Pevny, 2012). Further migration of lens cells away from the surface ectoderm result in the detachment of the lens vesicle and closing of the surface ectoderm (Figure 1.1) (Ashery-Padan et al., 2000; Heavner and Pevny, 2012). Once this occurs, the corneal epithelium develops from the surface ectoderm. In parallel, the optic vesicle, which contains retinal stem cells that give rise to all neuroectoderm-derived cells of the eye, invaginates and forms the optic cup, which continues to develop to form the optic stalk, then the optic nerve, as well as the neural retina, and retinal pigment epithelial layers (Heavner and Pevny, 2012; Richardson et al., 2017). The periocular mesenchyme is made up of primarily neural crest cells which contribute to the stroma and endothelium of the cornea, the melanocytes and stroma of the uvea, the meningeal sheath and connective tissue of the optic nerve, the sclera, and extraocular muscles (Bales et al., 2023).

These early processes in ocular development are regulated by a complex network of highly-conserved transcription factors (TF), which are involved in establishing and specifying structural boundaries of the optic field (Heavner and Pevny, 2012; Zuber et al., 2003). For example, the *Sonic hedgehog* (*Shh*) gene is responsible for the initial division of the eye field into bilateral hemispheres (Echelard et al., 1993). Disruption of *Shh* function has been found to result in cyclopia in mice (Chow and Lang, 2001). Further, *OTX2*, which is a TF involved in forebrain development, cooperates with *SOX2* in the neural ectoderm to activate *RAX* expression,

whereby *OTX2* then becomes downregulated in the eye field (Hever et al., 2006; Zuber et al., 2003). *RAX* is essential for upregulating *SIX3*, *LHX2*, and *PAX6* which are all required in boundary specification of the optic vesicle (Diacou et al., 2022; Heavner and Pevny, 2012; Zuber et al., 2003). These three TFs play important roles in coordinating ocular development and fate-specification of progenitors, which give rise to distinct ocular cell types that are required for the development and function of a healthy human eye (Figure 1.2) (Zuber et al., 2003).

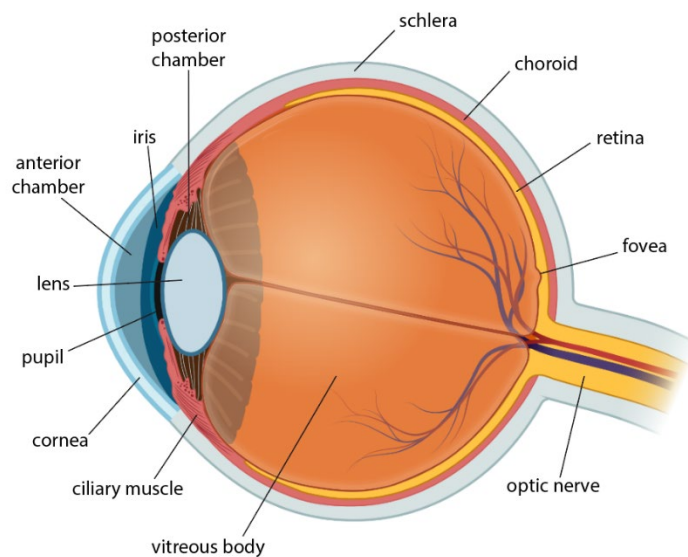


**Figure 1.2 Labelled diagram of a healthy adult human eye.** Sagittal cross-section showing anatomy of an adult human eye. Original figure made using graphics from BioRender.com.

### 1.1.2 *PAX6*

Paired box 6 (*PAX6*) is a member of the evolutionarily conserved family of TFs containing paired domains (Glaser et al., 1992; Walther and Gruss, 1991). *PAX6* spans 33 kb on chromosome 11p13 in humans (ENST00000638914.3). Canonical *PAX6* contains 13 exons, and a *PAX6* isoform contains an additional exon between canonical exons 5 and 6, called 5a (Figure 1.3A) (Sasamoto et al., 2016). Canonical *PAX6* (ENST00000241001.13) encodes a 422 amino acid (aa) protein that is approximately 46 kDA (Glaser et al., 1992). The protein contains two DNA-binding domains: the paired domain (PD) and the homeodomain (HD), which are connected by a linker region. The C-terminal end of the protein contains a proline-serine-

threonine rich domain (PSTD), which is responsible for mediating DNA binding by the HD and initiating transcription. The two subdomains of the PD (the N-terminal subdomain and the C-terminal subdomain) function to bind the respective consensus DNA sequences (Figure 1.3B) (Glaser et al., 1992; Lima Cunha et al., 2019). Each structural domain of PAX6 is required to enable optimal functioning of the protein in its role as a transcriptional regulator (Chauhan et al., 2004).

During embryogenesis *PAX6* plays an important role in establishing the optic field and is expressed on the surface and neural ectoderm (Collinson et al., 2000). By week five of human gestation, *PAX6* is expressed throughout the development of the optic vesicle, then the optic cup, and is then found to be expressed in both neural and pigmented retinal layers (Graw, 2010; Nishina et al., 1999). Postnatally, *PAX6* is expressed in the lens, cornea, conjunctiva, iris, ciliary body, and throughout the retina, in retinal ganglion, amacrine, Müller glial and horizontal cells and plays a vital role in maintaining optimal visual function throughout adolescence and adulthood (Klimova and Kozmik, 2014; Polisetti et al., 2023). Outside the eye, *PAX6* is also expressed in the pancreas, nasal epithelia, and several distinct regions of the central nervous system like the forebrain, hindbrain, and spinal cord (Duan et al., 2013; Grant et al., 2021; Hart et al., 2013).

*PAX6* regulation is controlled by various regulatory elements located both upstream and downstream of the gene (Tyas et al., 2006). Promoters P0, P1, and Pa have not been found to have any direct relationship between expression of specific *PAX6* transcripts (Xu and Saunders, 1997). The ectodermal enhancer (EE) is located approximately 3.5 kb upstream of P0 and regulates expression of *PAX6* during development of surface ectodermal-derived tissues (Lima Cunha et al., 2019). The Downstream Regulatory Region (DRR) is located 150 kb downstream

of *PAX6* and consists of several conserved elements that regulate tissue-specific *PAX6* transcription and autoregulation (Kleinjan et al., 2006). For example, SIMO is an 800 bp enhancer within the DRR that has a *PAX6* PD consensus binding sequence, and plays a prominent role in the complex regulation of *PAX6* throughout embryogenesis and postnatally (Bhatia et al., 2013).

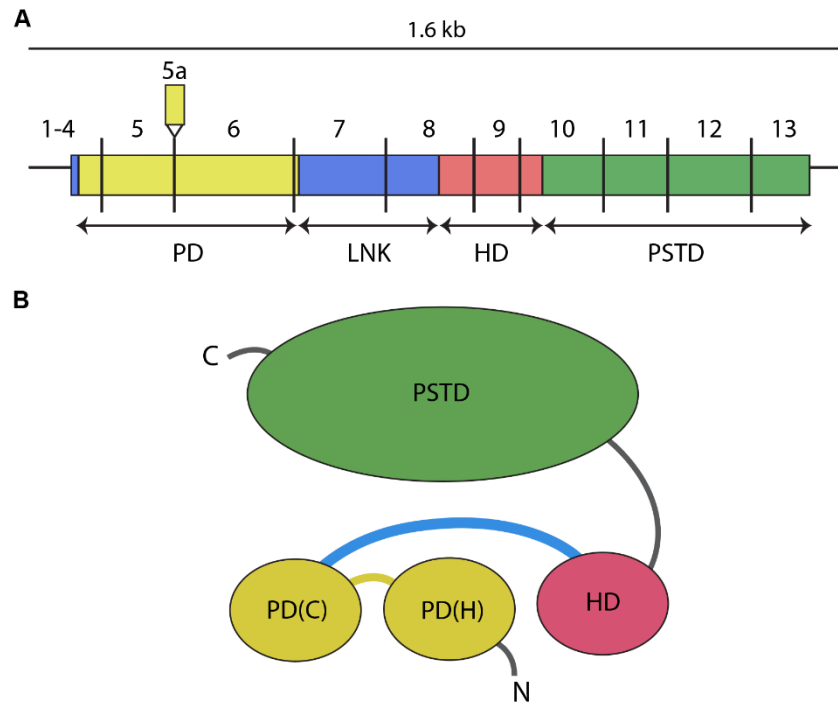


**Figure 1.3 Paired box six (*PAX6*) cDNA and protein structure. A)** Canonical *PAX6* coding sequence (ENST00000241001.13) contains 13 exons separated by vertical lines. Coloured regions indicate functional protein domains encoded by each region: paired domain (PD) (yellow), linker region (LNK) (blue), homeodomain (HD) (red), proline-serine-threonine rich domain (PSTD) (green). **B)** Schematic showing orientation of each functional domain in *PAX6* protein. PD contains two subdomains: C-terminal PD (PD(C)) and N-terminal PD (PD(N)). Original figure based on figure by Tzoulaki *et al.* 2005.

*PAX6* is considered to be a master regulator of ocular development and is required for normal ocular development in all studied mammals (Cvekl and Callaerts, 2016). Studies demonstrating that maintenance of *Lhx2* in *Pax6* null mutants, and maintenance of *Pax6* in *Lhx2* null mutants, suggests that these TFs are both independently essential for proper eye development, while also being separately insufficient (Porter et al., 1997; Zuber et al., 2003).

However, *PAX6* alone is considered a master regulator of the eye due to its role in regulating the precise patterning and formation of the multi-layered optic cup, the developing lens, and corneal epithelium (Heavner and Pevny, 2012). Additionally, exogenous expression of human *PAX6* in *Xenopus laevis* induces growth of ectopic eyes, demonstrating the essential and highly conserved function of *PAX6* in ocular development (Mirjalili Mohanna et al., 2020).

*Pax6* haploinsufficiency was first identified in the mouse small eye (*Sey*) phenotype due to a spontaneous *Pax6* loss-of-function (LOF) mutation (Hill et al., 1991; Roberts, 1967). *Sey* mice present with microphthalmia (reduced eye size), clouding and neovascularization of the cornea, and abnormal development of the cornea, iris, lens, and/or retina (Hill et al., 1991). Homozygous *Pax6* null mutant mouse embryos demonstrate sufficient generation of optic vesicles but fail to form optic cups (Porter et al., 1997). As such, homozygous LOF of *Pax6* results in anophthalmia (absence of one or both eyes) and is neonatal lethal, likely due to the critical role *Pax6* plays in brain morphogenesis (Schmahl et al., 1993).

### **1.1.3 Congenital blindness, aniridia**

*PAX6* haploinsufficiency caused by heterozygous variants results in a rare disease in humans called aniridia (Moosajee et al., 1993). Aniridia has a reported frequency of approximately 1 in every 40 000 to 100 000 live births, regardless of race or sex (Cvekl and Callaerts, 2016; Tibrewal et al., 2022). Most aniridic pathogenic variants are inherited in an autosomal dominant manner from an affected parent, but can also arise *de novo* (Dansault et al., 2007). This disease manifests at birth and the associated symptoms result in photophobia and low visual acuity, progressing over time until patients become legally blind by young adulthood (Landsend et al., 2021; Tibrewal et al., 2022). Humans with *PAX6* haploinsufficiency present with severe bilateral, ocular malformation, which typically manifests as abnormal development

of the iris, corneal cataracts, microphthalmia, and hypoplasia of the fovea, macula, and optic nerve. Other common symptoms include nystagmus, ptosis, glaucoma, corneal vascularization, and opacification caused by aniridia-associated keratopathy (AAK), among others (Guo et al., 2022; Landsend et al., 2021; Tibrewal et al., 2022). Clinical presentation is variable across patient populations, due to many unique variants reportedly being associated with aniridia etiology (Kit et al., 2021).

### **1.1.3.1 Genotype/phenotype correlations**

There have been over 600 reported unique genomic variants that cause aniridia in humans (Abdolkarimi et al., 2022; Lima Cunha et al., 2019). Intragenic variants make up approximately 96% of those reported (Lima Cunha et al., 2019; Moosajee et al., 1993; Tzoulaki et al., 2005). The majority of variants are located within exons 5, 6 (PD) and 9 (HD). 39% of reported variants are nonsense variants which result in premature termination codons (PTC), resulting in the mutant transcript being targeted for nonsense-mediated decay (NMD) (Tzoulaki et al., 2005). *PAX6* nonsense variants typically result in the most severe, classical aniridia phenotype (Moosajee et al., 1993).

27% of *PAX6* variants reported are frameshift variants. These potentially lead to a less severe phenotype, depending on how early in the sequence and in which functional domain the frameshift occurs (Tzoulaki et al., 2005). The frameshifted transcript may escape NMD if there is no PTC. 2% of reported variants have been found to result in small indels, which also typically lead to a PTC. C-terminal extension (or run-on) variants account for 2% of the reported aniridia variants. These are either frameshift or point mutations that alter stop codon location and allow for translation to continue into the 3' untranslated region (UTR) (Liang et al., 2011). These variants are thought to potentially cause a dominant negative phenotype as mutant transcripts

evade NMD since no PTC is introduced, however the mechanism is not entirely understood (Lima Cunha et al., 2019). 15% of reported *PAX6* variants are located in splice sites. The majority of these variants have been found to lead to PTCs and are generally associated with classical aniridia phenotypes (Tzoulaki et al., 2005). The majority of intronic variants are located in donor and acceptor sites at the intron-exon borders, thus affecting splicing patterns, however deep intronic variants have also been identified in large patient cohort studies (Kit et al., 2021; Plaisancie et al., 2018).

12% of reported *PAX6* variants are missense in nature and are typically associated with milder, but still atypical ocular phenotypes. In some cases, patients have been reported to present without iris defects (Azuma et al., 1998; Hanson, 2003; Lima Cunha et al., 2020). The less severe phenotype is likely dependent on how damaging the new amino acid is to *PAX6* function. Most reported missense variants occur in the PD and functional studies suggest that these variants cause differences in DNA binding and the transactivation activities of *PAX6* (Lee et al., 2020).

Variants in regulatory regions outside *PAX6* itself make up an additional 2% of causal aniridia variants (Lima Cunha et al., 2019). Severity of phenotype varies across these mutations as symptom presentation is entirely dependent on how the altered regulatory function affects *PAX6* expression. A single nucleotide (nt) change in the SIMO enhancer was described by Bhatia *et al.* to affect the *PAX6* PD binding site, resulting in decreased *PAX6* expression (Bhatia et al., 2013). An even smaller proportion of reported causal aniridia variants have been identified as chromosomal rearrangements and large deletions. These larger genomic abnormalities often result in systemic diseases when other genes proximal to *PAX6* are involved (Cheng et al., 2011). For example, disruption of *WT1* and *BDNF* in addition to *PAX6* results in WAGRO syndrome,

characterized by Wilms tumour, aniridia, genitourinary anomalies, mental disabilities, and obesity (Crolla and van Heyningen, 2002; Han et al., 2008; Lima Cunha et al., 2019).

While the many classes of variants that have been reported to cause aniridia have been found to be associated with a relative severity of symptom presentation, patients with aniridia have also been found to present with a wide phenotypic spectrum, without clear correlation between genotype and phenotype, even in patients within the same family (Kit et al., 2021; Sannan et al., 2017). This highlights the complexity of aniridia pathogenesis as patients with the same mutations can present with entirely different clinical features.

### **1.1.3.2 Clinical interventions for aniridia**

There are currently no vision-saving therapies available to treat aniridia (Landsend et al., 2021). Current treatment plans are typically directed at improving or maintaining vision by attempting to slow the progression of symptoms. A common symptom that patients experience in adulthood is aniridia-associated keratopathy (AAK) (Latta et al., 2021; Vicente et al., 2018). It is thought that AAK is caused by dysfunction and/or deficiency of limbal stem cells (LSC) of the corneal limbus (Ahmad, 2012). AAK results in dryness and opacification of the cornea, which can result in inflammation and discomfort for the patient (Lagali et al., 2019; Schlotzer-Schrehardt et al., 2021). To try to mitigate these symptoms, clinicians will often prescribe topical 2% cyclosporine drops to maintain moisture on the surface of the eye (de Paiva et al., 2019). Eye drops are also a common approach to help manage glaucoma symptoms (de Paiva et al., 2019). In severe cases of AAK, patients will undergo either allograft or LSC transplant surgery if scarring or opacification of the cornea severely impedes vision (Holland et al., 2003). This is an invasive approach that is accompanied by an extensive recovery period and only serves as a short-term treatment. Following surgery, patients' symptoms typically return (Bobba et al.,

2015). A more recent development in aniridia treatment is the surgical insertion of artificial iris prostheses (Gius et al., 2023). This procedure involves the insertion of a device into the eye to minimize glare and to improve cosmetic appearance. Other groups have also been investigating the development of a smart iris device that can respond to light stimuli and can expand or retract to allow the appropriate amount of light to reach the retina (Vasquez Quintero et al., 2021). However, this is also not a vision-saving intervention. Unfortunately, patients with aniridia will ultimately become blind, despite these therapeutic interventions. As such, there is an unmet therapeutic need.

#### **1.1.4 Gene therapy**

One exciting approach is to utilize gene therapy to address the underlying genomic cause of aniridia. Gene therapy is a medical approach that aims to treat or prevent human disease by utilizing genetic material to modify cells (Papanikolaou and Bosio, 2021; Wirth et al., 2013). Gene therapy was first conceptualized in the 1980s, but the first successful human nuclear “gene transfer” was conducted and subsequently approved by the NIH in 1989 (Rosenberg et al., 1990). This study involved advanced melanoma patients being treated with infusions of tumor-infiltrating lymphocytes that were modified *ex vivo* by retroviral gene transduction (Rosenberg et al., 1990). This was the first study to demonstrate the feasibility and safety of modifying cells with nucleic material for the purpose of treating human disease. Since the initial inception of gene therapy, the field has expanded broadly and research has been conducted to improve upon animal models and technical methods to advance gene therapy technology (Gruntman and Flotte, 2018). Today, gene therapies are being developed by many research groups globally to treat various types of cancer, genetic diseases, and infectious diseases (Lundstrom, 2019; Mendell et al., 2020). Currently there are greater than one dozen gene therapies that have been approved

globally by either the Food and Drug Administration (FDA) and/or the European Medicines Agency (EMA), while thousands of additional gene therapies are currently undergoing human clinical trials (European Medicines Agency, 2012). In Canada, four gene therapies have been approved by Health Canada (HC), including Glybera, Kymriah, Yescarta and Luxturna (Maguire et al., 2021; Mendell et al., 2020; Scott, 2015).

#### **1.1.4.1 Gene augmentation**

Gene augmentation therapy is an approach involving the delivery of a functional copy of a protein-coding gene to cells that are deficient in the protein (Xi et al., 2022). This technique is currently being developed to treat multiple types of cancer, infectious diseases, and genetic conditions that are caused by either heterozygous or homozygous haploinsufficiency of the gene. For example, Luxturna is a gene augmentation therapy that has been approved by HC to treat Leber congenital amaurosis type 2, which is an inherited retinal disease that causes progressive blindness (Maguire et al., 2021). This therapeutic approach utilizes *in vivo* viral delivery of a cDNA sequence encoding human RPE65 (Dalkara and Sahel, 2014). While approved gene augmentation therapies, like Luxturna, improve symptoms, they do not necessarily provide a complete cure for the condition. Repeat treatments tend to be required and still do not completely resolve symptoms. Thus, a permanent therapeutic approach may be more suitable to treat and cure rare genetic diseases, like aniridia.

#### **1.1.4.2 CRISPR gene editing**

Clustered regularly interspaced short palindromic repeats (CRISPR) was first described as an innate bacterial immune system that can be manipulated as a technology for gene editing purposes (Jinek et al. 2012). CRISPR enables permanent, targeted edits to the genome. Notably, the first *in vivo* CRISPR-based therapy for an inherited retinal disease, EDIT-101

(NCT03872479) (Li et al., 2023; Maeder et al., 2019), demonstrated proof-of-concept and favorable safety profile across all dose cohorts in a Phase I/II trial (<https://ir.editasmedicine.com/press-releases>, January 25, 2023). The traditional CRISPR system involves an RNA-guided, CRISPR-associated (Cas) nuclease that is targeted to a genomic region of interest (Jinek et al., 2012; Li et al., 2023). Once the Cas protein binds a protospacer adjacent motif (PAM), the double-stranded genomic DNA is unwound to facilitate protospacer or guide RNA (gRNA) binding with the target (Jinek et al., 2012; Yin et al., 2022). When the gRNA perfectly matches the target region, the Cas protein undergoes a conformational change and the two catalytic domains (HNH and RuvC) are adjusted to an active state. Once in this active state, the nuclease can catalyze a blunt-end double-stranded break (DSB). DSBs can be repaired by the endogenous cellular repair machinery through an error-prone nonhomologous end-joining (NHEJ) pathway (Jinek et al., 2012). NHEJ typically results in small insertions and deletions (indels) in the genomic sequence, disrupting the sequence and “knocking out” the gene of interest (Jinek et al., 2012; Nakagawa et al., 2015). The introduction of a single-stranded oligodeoxynucleotide (ssODN) template targets the homology-directed repair (HDR) pathway, which can result in precise alterations to the genomic sequence, by “knocking in” the DNA template (Jinek et al., 2012; Platt et al., 2014).

The most widely-investigated Cas protein is *SpCas9* (1368 aa), which is derived from *Streptococcus pyogenes* (Jinek et al., 2012). Additional wild-type (WT) Cas9 orthologs and engineered variants have also been developed, including the smaller *SaCas9* (1053 aa), derived from *Staphylococcus aureus*, and the engineered high-fidelity (HiFi) Cas9, which has been manipulated to enable more highly specific on-target editing and minimal off-target editing

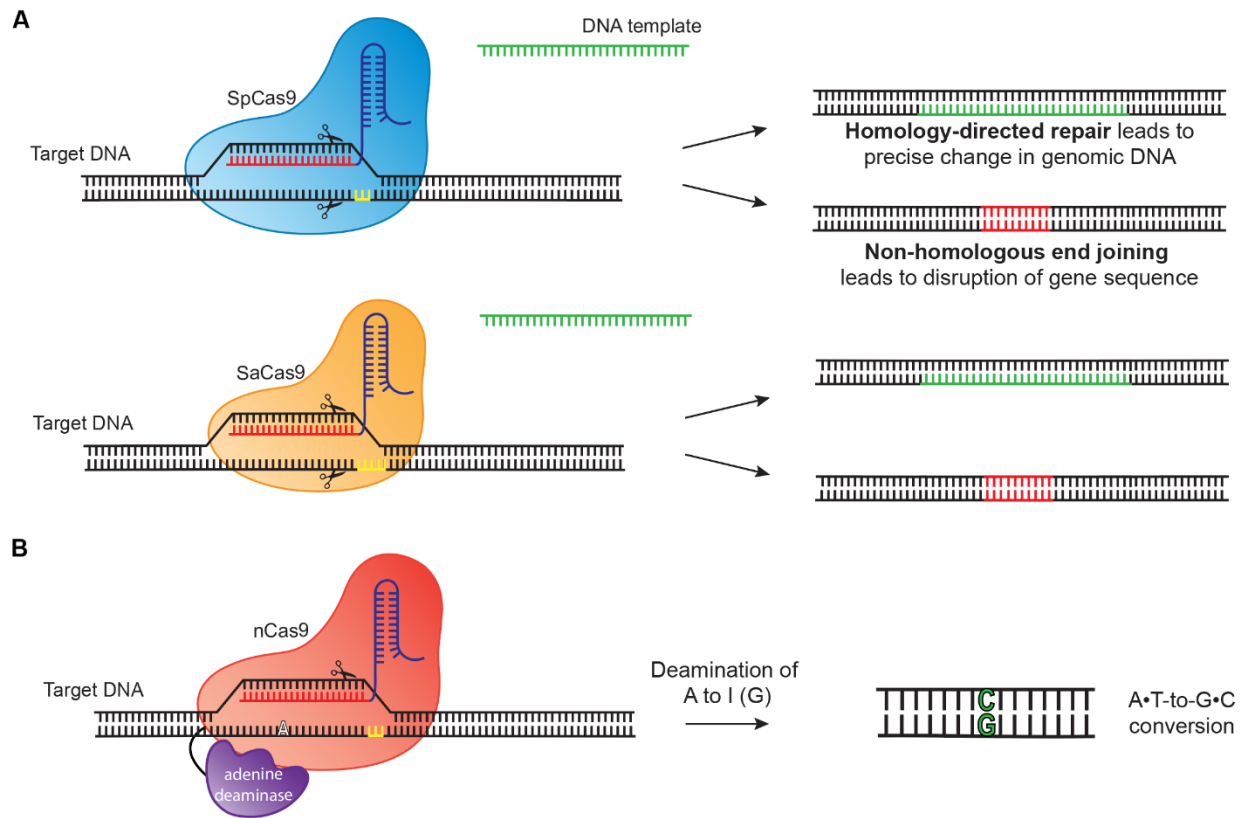


**Figure 1.4 CRISPR gene editing systems.** A) Traditional CRISPR gene editing using Cas9 nuclease to introduce double-stranded breaks in genomic DNA to target either homology-directed repair or non-homologous end joining pathways. Top, *SpCas9* ortholog. Bottom, *SaCas9* ortholog. B) Adenine base editing system involves engineered Cas9 nickase (nCas9) fused with adenine deaminase to confer single-base transition conversion from A:T base pair to G:C base pair. Original figure.

(Kleinstiver et al., 2016; Ran et al., 2015; Vakulskas et al., 2018). The many variants and orthologs present additional options for CRISPR therapy development and optimization.

Beyond the traditional CRISPR system, additional technologies have been developed. These include Cas9 nickases (nCas9), which have been engineered to inactivate one of the nuclease's two catalytic domains, so that the protein can only introduce single-stranded cleavage of genomic DNA (Shao et al., 2018). nCas9 can be fused with additional enzymes, which give rise to CRISPR base editors (BE) and primer editors (PE) (Anzalone et al., 2019; Gaudelli et al., 2017; Komor et al., 2016). Adenine and cytosine base editors (ABE and CBE, respectively) involve fusion of a deaminase enzyme to the C-terminal end of nCas9. This technology can

confer single base pair (bp) transition conversions within a particular editing window, without the need for an ssODN template and without creating DSBs (Komor et al., 2016). Once the base editor is paired with the target DNA, the deaminase enzyme removes an amine group from either a target adenine or cytosine nt, converting the single nts to either an inosine or uracil, respectively. The endogenous cellular repair machinery recognizes these inosines or uracils as either guanine or thymine, respectively, thus converting an A:T bp to a G:C bp (in the case of ABEs) or a C:G bp to a T:A bp (in the case of CBEs) (Gaudelli et al., 2017; Komor et al., 2016). This approach is very attractive for therapeutic purposes due to its lack of requirement of an ssODN and its ability to avoid introducing DSBs. However, utilizing this technology is constrained by the proximity of the target base to the PAM, and the presence of other neighbouring nucleotides, which may be vulnerable to deamination (Gaudelli et al., 2017).

Alternatively, PEs involve nCas9 fused with a reverse transcriptase enzyme (Anzalone et al., 2019). This strategy requires the design of a prime editing gRNA (pegRNA), which contains similar regions required for target recognition, CRISPR gRNA (crRNA) and Cas9 binding by tracer RNA (tracrRNA), as the above approaches. The pegRNA is also designed to contain the reverse transcriptase template (RTT), which contains the desired edit, and a primer binding site (PBS). Thus, this pegRNA binds both strands of the target DNA sequence and is constrained by proximity and orientation of the location of the desired edit, and the PAM (Anzalone et al., 2019). Base editing has been more widely studied by research groups since its invention, than prime editing, however both are powerful tools that have revolutionized the field of gene editing.

#### **1.1.4.3 Delivery strategies for gene therapy**

When developing gene editing strategies for the purposes of treating human patients, we have to consider the delivery vector by which the therapy will be administered. The most

prominent delivery method in the field currently is the recombinant adeno-associated virus (rAAV). rAAVs have been used to successfully deliver CRISPR components and produce genomic editing in multiple tissues, including the eye (Jo et al., 2023; Xiao et al., 2022; Zhang et al., 2021). However, one major disadvantage of using rAAVs is their limited packaging capacity of approximately 4.9 kb (Dong et al., 1996). With the most commonly used Cas9 enzyme, *SpCas9*, being approximately 4.1 kb in length, and a popular iteration of the adenine base editor, ABE8e (Richter et al., 2020), being approximately 4.8 kb in size, this leaves little space to encode additional components including: promoter, guide RNA (gRNA), and DNA template. Given these packaging constraints, rAAV often requires the use of a dual-virus system, which is less efficient for cellular delivery of therapeutic components (Chamberlain et al., 2016). Others have shown the use of a dual-AAV trans-splicing intein strategy to deliver one half each of a BE (Jo et al., 2023; Koblan et al., 2021).

A second common delivery method being used is to encapsulate CRISPR components in lipid nanoparticles (LNP), which are theoretically not restricted in their packaging abilities, are scalable, and non-immunogenic (Finn et al., 2018), therefore making the approach very attractive. Others have shown successful transfection and genomic editing using LNPs encapsulating *SpCas9* and ABE mRNA (Gillmore et al., 2021; Han et al., 2022; Herrera-Barrera et al., 2023; Zhang et al., 2022). However, less studied is the delivery with LNPs of the ribonucleoprotein (RNP) form of CRISPR enzymes, despite the fact that RNPs enable the use of the active form of the CRISPR enzyme and chemically modified single-guide RNAs (sgRNA), improving on-target editing, and safety by minimizing off-target editing (Chen et al., 2021; Jang et al., 2021).

One final delivery vector to consider is the episomal helper-dependent adenovirus (HDAd) (Guse et al., 2012). This class of viruses is often termed “gutless viruses”, meaning that they do not contain viral coding regions, rendering them non-integrating and dependent on a helper virus for replication. The gutless nature of HDAds enables them to have a cloning capacity of up to ~36 kb and reduced immunogenicity (Guse et al., 2012). This delivery vector has been used in preclinical studies of retinal degeneration and has been found to successfully transduce the retina. However, in one study, HDAd transduction elicited an acute inflammatory response in the rat retina (Han et al., 2019). Furthermore, HDAd has not been found to transduce the cornea, which is an important therapeutic target for aniridia. While the large cloning capacity of HDAds make them an attractive approach to consider for developing gene therapies for a variety of genetic diseases, additional development is required to make them a suitable option for a gene therapy to treat aniridia.

### **1.1.5 Minimal humanization of *Pax6* for translational therapy**

Research studies that are required to develop new therapeutics like a CRISPR-mediated therapy for aniridia rely on the use of animal models to demonstrate pre-clinical safety and efficacy (Li et al., 2020). However, the major disadvantage of using animal models in this type of study is that a CRISPR therapy optimized on mouse DNA is not directly translatable to human DNA in human cells. Thus, to enable rapid translation of a CRISPR therapy for aniridia, Dr. Simpson has proposed the CRISPR Humanized Minimally Mouse Models (CHuMMMs) strategy. CHuMMMs involve CRISPR-mediated generation of minimally humanized embryonic stem cell lines and animal strains to serve as model systems in which a CRISPR therapy for aniridia can be developed. Humanization is not a new concept. Others have worked to humanize entire genes in animal models for similar investigative and therapeutic development purposes

(Eming et al., 2002; Yuksel et al., 2015). However, humanization of entire genes has proven to be challenging and costly, as disruption of animal intronic regulatory sequences may disrupt how the newly-humanized gene may be expressed in an animal cell (Zhu et al., 2019). As such, the Simpson lab has sought to humanize a small region of interest, to circumvent these challenges. The CHuMMMs approach for aniridia involves utilizing CRISPR/Cas9 HDR to exchange a 312 bp region of interest of mouse *Pax6* sequence with an ssODN containing the human specific sequence at this locus. The 312 bp human sequence will serve as a “landing pad” on which a CRISPR therapy can be developed. The beauty of the CHuMMMs approach is that it can be applied to make model cell lines and mice to develop CRISPR therapies for other genetic diseases. The work presented here lays the foundation for such an approach to be used during pre-clinical CRISPR therapy development studies for aniridia.

## 1.2 HYPOTHESIS AND THESIS OBJECTIVES

The overarching hypothesis driving our work is that a CRISPR therapy is an effective strategy to treat aniridia. However, a broad hypothesis such as this, is not specific or testable within this thesis. Thus, a strong, more specific hypothesis is required. The more focused hypothesis is that a CRISPR gene strategy can be developed and optimized in humanized mouse ESCs that will be able to distinguish between the patient variant and non-variant chromosomes, thus laying the foundation for correcting aniridic congenital blindness in humans. My specific objectives were to:

1. Isolate and characterize humanized mouse embryonic stem cells that are homozygous for the patient variant, c.718C>T, heterozygous for the patient variant, and homozygous for the non-mutant sequence.
2. Confirm that humanization does not disrupt *Pax6* function and result in an ocular phenotype in mouse, through slit lamp imaging and visual inspection of humanized non-variant versus wild-type mice.
3. Develop and optimize a CRISPR gene therapy to correct aniridic patient variant, c.718C>T, with minimal impact on non-variant chromosomes, in humanized mouse ESCs.
4. Test *ex vivo* delivery of the optimized CRISPR therapy, encapsulated in lipid nanoparticles (LNPs), to correct another aniridia patient variant and demonstrate rescued Pax6 expression in mouse embryonic primary cortical neurons.

## **CHAPTER 2: ABE8E CORRECTS *PAX6*-ANIRIDIC VARIANT IN HUMANIZED MOUSE ESCS AND VIA LNPS IN *EX VIVO* CORTICAL NEURONS**

### **2.1 INTRODUCTION**

Congenital aniridia is a rare vision-loss disease characterised by the underdevelopment and malformation of the eye (Hingorani et al., 2012; Moosajee et al., 1993). Clinical features primarily include varying severities of hypoplasia of the iris, fovea, and optic nerve (Hingorani et al., 2012; Landsend et al., 2021; Moosajee et al., 1993). Patients experience low visual acuity and photophobia, which typically progressively worsens over time due to the occurrence of cornea keratopathy, glaucoma, and other disease manifestation, leading to blindness by young adulthood (Landsend et al., 2021; Latta et al., 2021; Schlotzer-Schrehardt et al., 2021). Aniridia is caused by greater than 600 heterozygous pathogenic variants in the transcription factor paired box 6 (*PAX6*), a master regulator of ocular development, with dosage sensitivity in the eye (Gregory-Evans et al., 2013; Heavner and Pevny, 2012; Landrum et al., 2016; Lima Cunha et al., 2019). The majority of these variants are dominant loss of function, and lead to phenotype due to *PAX6* haploinsufficiency (Pedersen et al., 2020). These include the most commonly reported aniridia patient variant, c.718C>T (p.R240X) located in exon 9 (Fokkema et al., 2011; Guo et al., 2022; Kit et al., 2021; Tyner et al., 2017), which is one of four that together account for more than 20% of aniridia cases (Lima Cunha et al., 2019). There are interventions that prolong vision (Landsend et al., 2021) and ongoing work to develop drugs that may regulate *PAX6* expression (Cole et al., 2022), but there are currently no vision-saving therapies for aniridia (Daruich et al., 2022). Thus, there is an unmet therapeutic need.

Fortunately, there has been considerable investigation and characterisation of aniridia models to study molecular pathophysiology, disease progression, and therapeutic development (Abdolkarimi et al., 2022). Importantly, there is a therapeutic window, as demonstrated by the

use of the nonsense suppressing drug, ataluren, in the small eye (*Sey*) aniridic mouse (Wang et al., 2017). The *Sey* mouse presents with similar ocular phenotypes to those observed in patients with aniridia (Hickmott et al., 2018; Hill et al., 1991) and is caused by a *Pax6* nonsense variant, c.580G>T (p.G194X), which has also been reported in human (Kit et al., 2021). Delivery of ataluren in juvenile aniridic mice positively improved phenotype, suggesting a therapeutic window in the early postnatal years in humans (Cole et al., 2022; Wang et al., 2017), despite an unsuccessful clinical trial (NCT02647359). To further improve the *Sey* mouse model, we previously added a FLAG-tag to the *Sey Pax6* allele (referred hereafter as *Fey*), which enables histological quantification of rescued Pax6 protein expression (MMRRC 066963-MU) (Mirjalili Mohanna et al., 2020).

One major challenge when undertaking therapy development with an animal model, can be the requirement for pre-clinical studies to show efficacy on human DNA, RNA, or protein. This is particularly the case for the exciting CRISPR/Cas9-based approaches to therapy development, which require binding DNA (Tay et al., 2020). To answer this challenge, we have developed the “CRISPR Humanized Minimally Mouse Models” (CHuMMMs) strategy. For the CHuMMMs strategy, we propose using CRISPR to engineer into the model a human-DNA “landing pad” to allow the CRISPR therapeutic reagents to bind human DNA at the site of the pathogenic variant. Whereas previous studies have shown humanization of entire genes is technically demanding, costly, and can have adverse consequences for gene function (Zhu et al., 2019), the CHuMMMs strategy avoids these problems by only humanizing the minimal region needed for binding of the therapeutic CRISPR reagents. This approach will enable more rapid development of directly translatable CRISPR-based therapies.

CRISPR can establish targeted, permanent edits within the genome (Jinek et al., 2012; Maeder et al., 2019). Notably, the first *in vivo* CRISPR-based therapy for a congenital vision-loss disease, EDIT-101 (NCT03872479) (Li et al., 2023; Maeder et al., 2019), demonstrated proof-of-concept and favorable safety profile across all dose cohorts in a Phase I/II trial (<https://ir.editasmedicine.com/press-releases>, January 25, 2023). Since the discovery of this gene editing platform, there has been a great deal of development to improve upon the traditional CRISPR system (Li et al., 2023). Multiple orthologous wild-type (WT) Cas9 enzymes have been widely studied, while other researchers have engineered the WT Cas9 to ease protospacer adjacent motif (PAM) requirements, increase editing activity, and decrease off-target editing (Cao et al., 2022; Shin et al., 2022; Walton et al., 2020; Yin et al., 2022). Beyond the traditional homology directed repair (HDR) approach, which aims to exchange the pathogenic genomic sequence with a WT donor DNA template (Ran et al., 2013) new CRISPR systems have been engineered. These include base editors (BEs), which can confer selective single-base transition conversions (Gaudelli et al., 2017). In addition, BEs do not require donor DNA and do not produce double-stranded breaks (DSB) in genomic DNA, resulting in low rates of indels and less off-target editing (Gaudelli et al., 2017; Li et al., 2020) which make them advantageous in developing clinical therapies. Overall, this provides many options to consider during therapy development. This rapid advancement of CRISPR technology suggests that personalized CRISPR therapies for low frequency variants may be an effective approach to treat aniridia.

There are two primary delivery options for CRISPR-based therapies, recombinant adeno-associated viruses (rAAV), and lipid nanoparticles (LNP). rAAVs have been used to successfully deliver CRISPR components and produce genomic editing in multiple tissues, including the eye (Jo et al., 2023; Xiao et al., 2022; Zhang et al., 2021). However, one major disadvantage of using

rAAVs is their limited packaging capacity, ~4.9 kb (Dong et al., 1996). With the most commonly used Cas9 enzyme, *SpCas9*, being ~4.1 kb, and a popular iteration of the adenine base editor, ABE8e (Richter et al., 2020), being ~4.8 kb in size, this leaves little space to encode additional components including: promoter, guide RNA (gRNA), and DNA template (Chamberlain et al., 2016; Jo et al., 2023; Koblan et al., 2021). The second primary delivery method is to encapsulate CRISPR components in LNPs, which are less restricted in their packaging abilities, are scalable, and non-immunogenic (Finn et al., 2018), therefore making the approach very attractive. Others have shown successful transfection and genomic editing using LNPs encapsulating *SpCas9* and ABE8e mRNA (Gillmore et al., 2021; Han et al., 2022; Herrera-Barrera et al., 2023; Zhang et al., 2022). However, less studied is the delivery with LNPs of the ribonucleoprotein (RNP) form of CRISPR, despite the fact that RNPs enable the use of the active form of the enzyme and chemically modified single-guide RNAs (sgRNA), improving on-target editing, and safety by minimizing off-target editing (Chen et al., 2021; Jang et al., 2021).

Here, we hypothesize that a CRISPR gene therapy can be developed and optimized in humanized mouse embryonic stem cells (ESC) that will be able to distinguish between the patient variant and non-variant chromosomes, thus laying the foundation for further pre-clinical studies correcting aniridic congenital blindness in mice. Having found support for this first hypothesis, a follow-up hypothesis was developed and tested, that our optimized CRISPR therapy could alter a second aniridia variant in a clinically relevant cell-type via LNPs.

## 2.2 METHODS

### 2.2.1 Isolation and culture of mouse embryonic stem cells

Male *Pax6* WT C57BL/6NTac (Taconic, Hudson, NY) ESCs (mEMS6131 (Peeters et al., 2018)) were derived as previously described (Yang et al., 2009), and cultured at 37°C with 5% CO<sub>2</sub> on either mouse embryonic fibroblasts (MEFs) or 0.1% gelatin. ESCs were maintained in ESC media and passaged as previously described (Yang et al., 2009).

### 2.2.2 RNP design for humanization of ESCs

Two gRNAs (cgEMS9, cgEMS18 (Table 2.1, guide and template sequences)) were designed to introduce two DSB in *Pax6* (Figure 2.2A). CRISPR RNAs (crRNA) and tracer RNAs (tracrRNA) were synthesized as single-strands with chemical modifications (2'-O-methyl and phosphorothioate bonds at the first two 5' and 3' terminal RNA residues) (GenScript, Piscataway, NJ). A 512 bp single-stranded oligodeoxynucleotide (ssODN) template containing the patient variant (oEMS6346) was synthesized to confer the humanization of *Pax6* exon 9 and an 84 bp ssODN (oEMS6451) was synthesized to confer correction of the variant in the resulting homozygous humanized variant cell line (Integrated DNA Technologies, Coralville, IA).

### 2.2.3 Cell transfection and picking single clones

ESCs were passaged in a 1:2 split ratio 24 hours prior to transfection and fed with fresh media 2 hours prior to transfection. Cells were dissociated using Trypsin-EDTA (catalog 25200-072, Invitrogen, Thermo Fisher) and counted using a hemocytometer. gRNAs were prepared by annealing crRNA and tracrRNA at 95°C for 5 minutes. RNP was prepared by complexing *SpCas9* protein with each gRNA for 15 minutes at room temperature (RT), prior to the addition of the ssODN and WT mouse ESCs for transfection. Each reaction consisted of 9 μL ESCs (2 x 10<sup>6</sup> per reaction) mixed with 0.3 μL of RNP and 0.2 μL of 5 μM ssODN and was electroporated

**Table 2.1 CRISPR guide RNAs (gRNAs) and DNA templates used for *in vitro* gene editing.**

<b>ID</b>	<b>Description</b>	<b>Sequence (5' - 3')</b>
<b>cgEMS9</b>	gRNA for humanization of <i>Pax6</i> exon 9.	ACACTGTCAAGCTGTCTGAT
<b>cgEMS18</b>	gRNA for humanization of <i>Pax6</i> exon 9.	CAGTGACTGGTATACAGCCA
<b>cgEMS25</b>	gRNA for correction of <i>PAX6</i> patient variant c.718C>T with <i>SpCas9</i> .	CTTTCTCAGGCAAACACATC
<b>cgEMS45</b>	gRNA for correction of <i>PAX6</i> patient variant c.718C>T with <i>SaCas9</i> .	GTCTTTCTCAGGCAAACACAT
<b>cgEMS46</b>	gRNA for correction of <i>PAX6</i> patient variant c.718C>T with ABE8e.	TTTCTCAGGCAAACACATCT
<b>oEMS6346</b>	512 base single-stranded DNA template for humanization of <i>Pax6</i> exon 9.	CCTTCGATTAGAAAACCATACCTGGAAATGCAC AGAACAGGTTAGCCCTATGCTTGCTACCACTCG GCCACAAACAAAAAGCCCTCCATCCCCACCCTT ACCTTTTTATTATATTAGTCTATAAATAAATAG TACTCTGTACAAGCACCTCTGTCTCTAGGAAAG ACAAATGGTATGAATCACAAAGTGTGAAACTGC ACAGTCTCTCGGTACCTGTATTCTTGCTTCAGGT AGATCTATTTGGCTGCTAGTCTTTCTCGGGCAA ACACATCTGGATAATGGGTTCTCTCAAACCTCTGA AAGAGTAAGTTGATTTTCCATATTGTGCCAGAA CTACACAAAATATGTTGACCAAACCTGTGCATCA AACTGGTTCCCACCTCCCCACTCCCATTACCTCC AACCAATTCCCACAGTGTGCTGACTGTACTAGC AAGAACTTTCCCACCAGGAGCAAGTTTTCTTTGG AATGACATTTAGTGTGTTGTCCTTATCTGTGGCCT AAGACAGTCA
<b>oEMS6451</b>	84 base single-stranded DNA template for correction of <i>PAX6</i> patient variant c.718C>T (bolded).	CTCTTTCAGAGTTTGAGAGAACCCATTATCCAGA TGTGTTTGCCCGAGAAAGACTAGCAGCCAAAAT AGATCTACCTGAAGCAA
<b>oEMS6453</b>	80 base single-stranded DNA template for correction of <i>PAX6</i> patient variant c.718C>T (bolded) with <i>SpCas9</i> . This template also contains silent blocking substitutions in the PAM and seed regions (underlined).	TTCAGAGTTTGAGAGAACCCATT <u>ACCAGAC</u> CGT GTTTGCCCGAGAAAGACTAGCAGCCAAAATAGA TCTACCTGAAGCAA
<b>oEMS6454</b>	80 base single-stranded DNA template for correction of <i>PAX6</i> patient variant c.718C>T (bolded) with <i>SaCas9</i> . This template also contains a silent blocking substitution in the PAM (underlined).	TTCAGAGTTTGAGAGAACCCATT <u>ACCAGAT</u> GT GTTTGCCCGAGAAAGACTAGCAGCCAAAATAGA TCTACCTGAAGCAA
<b>oEMS6455</b>	80 base single-stranded DNA template for correction of <i>PAX6</i> patient variant c.718C>T (bolded) with <i>SaCas9</i> . This template contains a silent blocking substitution in the seed region (underlined).	CTCTTTCAGAGTTTGAGAGAACCCATTATCCAGA <u>CGT</u> GTTTGCCCGAGAAAGACTAGCAGCCAAAAT AGATCTACCTGAA

**ID, identifier; cgEMS, CRISPR guide Elizabeth M. Simpson; oEMS, oligo Elizabeth M. Simpson; ABE8e, adenine base editor 8e; PAM, protospacer adjacent motif.**

using Neon Transfection System (catalog MPK5000, Invitrogen) on setting 14 (1200 mV, width 20, Pulse # 2). Electroporated ESCs were plated onto a fresh 24-well plate on either MEFs or gelatin and incubated for 48 hours at 37°C with 5% CO<sub>2</sub>. Cells were either harvested for molecular characterization or cryopreserved, as previously described (Yang et al., 2009). For ESC clones, electroporated cells were thawed and plated in serial dilutions on 0.1% gelatin in 6 cm dishes and incubated for 48 hours at 37°C with 5% CO<sub>2</sub>. Individual clones were isolated and plated on 96-well gelatinized plates and incubated at 37°C with 5% CO<sub>2</sub> until >80% confluent.

#### **2.2.4 DNA isolation, PCR genotyping, and RFLP screens**

Once ESCs became confluent, cells were digested in tissue homogenization buffer with Proteinase K according to a previously described protocol (Yang et al., 2009). DNA from lysed cell samples was amplified using *Taq* DNA Polymerase (catalog 18038042, Invitrogen) and PCR primer pairs (Table 2.2, primer sequences) specifically targeting: human sequence inside the humanized region, 5' mouse-human junction, 3' human-mouse junction, 5' mouse-3' mouse flanking the humanized region, and mouse-mouse inside of the region that was humanized, were used to confirm successful humanization of *Pax6* exon 9 (Figure 2.2A). Candidates for successful humanization were confirmed by Sanger sequencing.

To screen for heterozygous correction of patient variant c.718C>T, a restriction fragment length polymorphism (RFLP) assay using *AvaI* (catalog R0152S, NEB) and *DdeI* (catalog R0175S, NEB) restriction enzymes was used. DNA was first amplified with oEMS6223 and oEMS6224 before incubation with CutSmart Buffer (catalog B6004S, NEB) and either restriction enzyme at 37°C for 1 hour, then inactivation at either 80°C or 65°C for 10 minutes. *AvaI* cuts this DNA in presence of the cytosine base and *DdeI* cuts in presence of the thymine

base, giving rise to fragments 117 bp and 145 bp. Candidates for heterozygous and homozygous correction of patient variant were confirmed by sequencing.

### 2.2.5 Sanger sequencing and peak quantification

The region around the humanized exon (813 bp) was PCR amplified with appropriate primer pairs (Table 2.2). PCR products were run on a 2% agarose gel for 40 minutes at 130 V. Bands were excised and DNA was purified using QIAquick Gel Extraction Kit (catalog 28706, QIAGEN, Germantown, MD). Bidirectional sequencing was carried out by the CMMT DNA Sequencing Core Facility. Chromatograms were viewed using Benchling ([www.benchling.com](http://www.benchling.com)).

For CRISPR therapy optimization experiments, we sequenced unidirectionally in the reverse direction. In this direction, the target bases were sequenced prior to the cut site of Cas9. Peak height data were extracted from CRISPR-treated and mock (untreated) samples using Analysis Module Variant Analysis (VA) software (catalog A28220, Thermo Fisher) and EditR software (Kluesner et al., 2018). The treated peak height data was normalized by subtracting the average of mock untreated *He9<sup>-</sup>/He9<sup>+</sup>* replicas to remove background and conservatively calculate CRISPR editing. No samples were excluded from analysis.

### 2.2.6 Generation of humanized exon 9 mice

Mouse strains were derived by means of cytoplasmic microinjection into C57BL/6J mice (JAX 000664) using a dual RNA guide strategy (cgEMS9, cgEMS18 (Table 2.1)) and ssODN (oEMS6347) according to a previously described protocol (Mirjalili Mohanna et al., 2020).

Initially, two mouse strains were derived from two independent founders, C57BL/6J-*Pax6<sup>em6(PAX6)Ems</sup>* (MGI:7330073) and C57BL/6J-*Pax6<sup>em7(PAX6)Ems</sup>* (MGI:7330075). They were indistinguishable by casual observation, so the studies conducted here used C57BL/6J-*Pax6<sup>em7(PAX6)Ems</sup>*, which for clarity and brevity will be called humanized *Pax6* exon 9 non-variant

**Table 2.2 Primers and restriction enzymes used for PCR, RFLP, and Sanger sequencing for characterization of humanized clones and CRISPR-edited whole cell lysates.**

<b>ID</b>	<b>Description</b>	<b>Sequence (5'-3')</b>
<b>oEMS6223</b>	Forward primer for PCR screening for humanized <i>Pax6</i> exon 9.	TTGGTTGGAGGTAATGGGAG
<b>oEMS6140</b>	Forward primer for Sanger sequencing of 250 bp upstream of humanized <i>Pax6</i> exon 9.	GAAGCTCAGATGCGACTTCA
<b>oEMS6224</b>	Reverse primer for PCR screening for humanized <i>Pax6</i> exon 9; Reverse primer for Sanger sequencing of 250 bp upstream of humanized exon 9.	CAAGCACCTCTGTCTCTAGG
<b>oEMS6220</b>	Forward primer for PCR screening for 5' end of humanized <i>Pax6</i> exon 9; Forward primer for Sanger sequencing of humanized exon 9.	TCTTCTTTTCACACACCAGC
<b>oEMS6244</b>	Reverse primer for PCR screening for 5' end of humanized <i>Pax6</i> exon 9.	CCCCACCCTTACCTTTTTTATTA
<b>oEMS6391</b>	Forward primer for PCR screening for 3' end of humanized <i>Pax6</i> exon 9; Forward primer for Sanger sequencing of 250 bp downstream of humanized exon 9.	CAGTTTCACACTTTGTGATTCATAC
<b>oEMS6392</b>	Reverse primer for PCR screening for 3' end of humanized <i>Pax6</i> exon 9; Reverse primer for Sanger sequencing of 250 bp downstream of humanized exon 9.	CAGGTGACCGTCCTCTCTTAC
<b>oEMS6421</b>	Forward primer for PCR screening for mouse-specific sequence inside humanized <i>Pax6</i> exon 9.	GCTGTCTGATTGGCTGGATGA
<b>oEMS6422</b>	Reverse primer for PCR screening for mouse-specific sequence inside humanized <i>Pax6</i> exon 9.	GCATCCCAGTGCATAAAAACCA
<b>oEMS6219</b>	Forward primer for PCR screening for mouse-specific sequence outside humanized <i>Pax6</i> exon 9 to confirm length of region.	ATCAAAGGAAATGCCACAGC
<b>oEMS6222</b>	Reverse primer for PCR screening for mouse-specific sequence outside humanized <i>Pax6</i> exon 9 to confirm length of region; Reverse primer for Sanger sequencing of humanized exon 9.	GCTGCTGATAGGAATGTGAC
<b>oEMS2200</b>	Forward primer for <i>IL2</i> PCR confirming DNA sample quality.	CTAGGCCACAGAATTGAAAGATCT
<b>oEMS2201</b>	Reverse primer for <i>IL2</i> PCR confirming DNA sample quality.	GTAGGTGGAATTCTAGCATCATCC
<b><i>Ava</i>I</b>	Restriction enzyme used in RFLP to screen for correction of patient variant, c.718C>T, in humanized <i>Pax6</i> exon 9 clones. Enzyme cuts ( ) in presence of corrected base to give 117 bp and 145 bp bands.	C YCGRG GRGCY C
<b><i>Dde</i>I</b>	Restriction enzyme used in RFLP to screen for correction of patient variant, c.718C>T, in humanized <i>Pax6</i> exon 9 clones. Enzyme cuts ( ) in presence of mutant base to give 117 bp and 145 bp bands.	C TNAG GANT C

**ID, identifier; oEMS, oligo Elizabeth M. Simpson; RFLP, Restriction Fragment Length Polymorphism**

or B6-*He9*<sup>+</sup>. A third strain was then derived, 129S1.B6- *Pax6*<sup>em7(PAX6)*Ems*</sup> (MGI:7330077) by backcrossing B6-*He9*<sup>+</sup> onto the 129S1/SvImJ (JAX 002448) genetic background, which for clarity and brevity will be called 129-*He9*<sup>+</sup>.

### **2.2.7 Phenotyping by visual inspection and slit lamp imaging**

B6-*He9*<sup>+/+</sup> heterozygous N6 and N7 (backcrossed 6 and 7 times) mice were mated in trios to produce *He9*<sup>+/He9</sup><sup>+</sup>, *He9*<sup>+/+</sup>, and +/+ offspring. This breeding scheme was also repeated mating 129-*He9*<sup>+/+</sup> N6 trios to produce *He9*<sup>+/He9</sup><sup>+</sup>, *He9*<sup>+/+</sup>, and +/+ offspring. External ocular morphology of adolescent (3-4 weeks) *He9*<sup>+/He9</sup><sup>+</sup> and +/+ mice was assessed by visual inspection and scored as either normal or abnormal. Adult (~2 months old) *He9*<sup>+/He9</sup><sup>+</sup> and +/+ mice were anesthetized using isoflurane at a flow rate of 1.5-1.8% in an induction chamber using a SomnoSuite (Kent Scientific, Torrington, CA). Once a surgical plane of anesthesia was induced, mice were transferred to the nose cone and eyes were covered with 1% Isopto Tears ophthalmic solution (ALCON, Geneva, Switzerland). Micron IV Retinal Imaging Microscope (Phoenix Research Labs, Pleasanton, CA) with an anterior segment slit lamp attachment was used to image the left eyes.

### **2.2.8 Purification of ABE8e protein**

CRISPR ABE8e protein was isolated by plasmid overexpression and purification (Huang et al., 2021). pABE8e-protein plasmid (a gift from David Liu, #161788, Addgene, Watertown, MA).

### **2.2.9 RNP design and complexation for CRISPR therapy**

sgRNAs (20 bp) and ssODNs (80 bp) were designed for CRISPR HDR and ABE8e. Chemical modifications of reagents were the same as above. sgRNAs and CRISPR enzymes

were complexed for 15 minutes at RT prior to additional of ssODN (in the case of CRISPR HDR strategies) and ESCs for electroporation of two biological replicates per treatment group. ESCs were harvested characterization by sequencing, as described above.

### 2.2.10 Preparation of Incisive DS LNPs and encapsulation of RNPs and DNA template

Preparation of Incisive Delivery System LNPs was performed according to a previously described protocol (Mirjalili Mohanna et al., 2022). The size distribution and the polydispersity index (PDI) of LNPs encapsulating ABE8e were measured using a Malvern Zetasizer Nano S instrument (Worcestershire, UK) (He–Ne laser,  $\lambda = 632$  nm, detection angle =  $173^\circ$ ) (Figure 2.1).

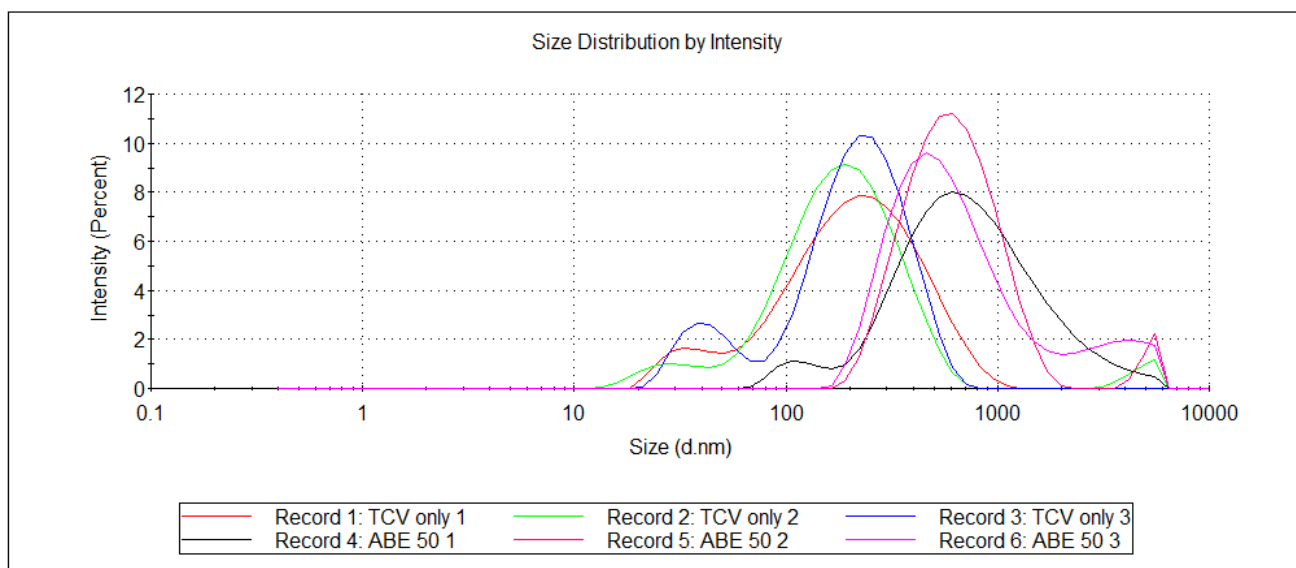


**Figure 2.1** The average diameter distribution of LNP encapsulated ABE8e RNP was  $533.8 \pm 9.5$  nm. Size distribution of LNPs encapsulating ABE8e RNP was measured using a Malvern Zetasizer Nano S instrument. Each sample was measured three times. For TCV only (nothing encapsulated), the result was Z-average:  $146.6 \pm 3.4$  nm, number mean:  $24.99 \pm 5.8$ , PDI:  $0.349 \pm 0.044$ . For encapsulation of ABE8e at 50 nM the result was Z-average:  $533.8 \pm 9.5$  nm, number mean:  $335.7 \pm 161.6$ , PDI:  $0.382 \pm 0.023$ .

### 2.2.11 *Ex vivo* genome editing

Treatment of *Fey* primary embryonic cortical neurons with LNP-encapsulated CRISPR-RNPs, and subsequent analyses (immunocytochemistry, stereology, microscopy and image processing) were performed according to a previously described protocol (Mirjalili Mohanna et

al., 2022). Minor changes were that treatments took place on day *ex vivo* (DEV) 6 and cells were collected on DEV 9.

### **2.2.12 Statistical analysis**

All statistics and plotting of graphs were conducted using GraphPad Prism version 9.4.0 for Windows (GraphPad Software, San Diego, CA). Statistical significance was determined using two-tailed unpaired t-test or Fisher's exact test for comparisons of two groups, and one-way or two-way ANOVA analysis for three or more groups, where appropriate. One-way ANOVA tests were corrected for using Tukey's multiple comparisons tests, while two-way ANOVA tests were corrected for using Sidak's multiple comparisons tests. *P* value  $\leq 0.05$  was considered to be statistically significant.

### **2.2.13 Compliance with ethics guidelines**

All animals were housed and bred in the pathogen-free Transgenic Animal facility at the Centre for Molecular Medicine and Therapeutics (CMMT) of the University of British Columbia (UBC). All mouse work was performed following protocols approved by the UBC Animal Care Committee (protocol #s A21-0410, A21-0184), in accordance with guidelines determined by the Canadian Council on Animal Care.

## 2.3 RESULTS

### 2.3.1 CHuMMMs for *Pax6*-aniridia therapy development *in vitro*

To implement the CHuMMMs strategy for aniridia *in vitro* we developed minimally humanized *Pax6* ESC lines. Mouse ESCs were chosen for their ease of genetic manipulation, their differentiation potential, and ability to derive new mouse strains (Bradley et al., 1984; Gertsenstein et al., 2020; Mathew, 2023; Mirjalili Mohanna et al., 2020). Initially, we generated two novel homozygous minimally-humanized exon-9 *PAX6* variant c.718C>T (*He9<sup>-</sup>/He9<sup>-</sup>*) ESC lines (mEMS6634 and mEMS6658). A dual-gRNA strategy enabled the HDR-mediated humanization in WT C57BL/6N mouse ESCs by electroporation of CRISPR RNPs and a ssODN template (Figure 2.2A and B) (Table 2.1, guide and template sequences). The sgRNAs introduced DSBs in *Pax6* introns 8 and 9, respectively. A 512 bp ssODN containing the patient variant, c.718C>T, conferred the exchange of a 312 bp region of mouse DNA sequence with human sequence, via flanking 100 bp mouse-specific homology arms (HAs). Single clones were picked from electroporated cells. PCR assays confirmed successful insertion of the ssODN (Figure 2.2C), and a restriction fragment length polymorphism (RFLP) screen determined that clones were either heterozygous or homozygous for the HDR event. Final confirmation of the 1.2 kb region (including 250 bp regions directly 5' and 3' of the ssODN) was completed by Sanger sequencing (Figure 2.2D).

Subsequently, we generated one novel heterozygous minimally-humanized exon-9 cell line (*He9<sup>-</sup>/He9<sup>+</sup>*; mEMS6670) and two humanized homozygous non-variant cell lines (*He9<sup>+</sup>/He9<sup>+</sup>*, mEMS6674 and mEMS6676) to complete this cell-based disease model. A sgRNA (Table 2.1) and an 84 bp ssODN were employed to correct the patient variant in the *He9<sup>-</sup>/He9<sup>-</sup>* cell line mEMS6634 derived above. Single clones were again picked, and successful correction

of the patient variant was characterized by PCR assays (Figure 2.2B), the RFLP screen (Figure 2.2C), and sequencing of the 1.2 kb region (Figure 2.2D).

(Bradley et al., 1984; Gertsenstein et al., 2020; Mathew, 2023; Mirjalili Mohanna et al., 2020).

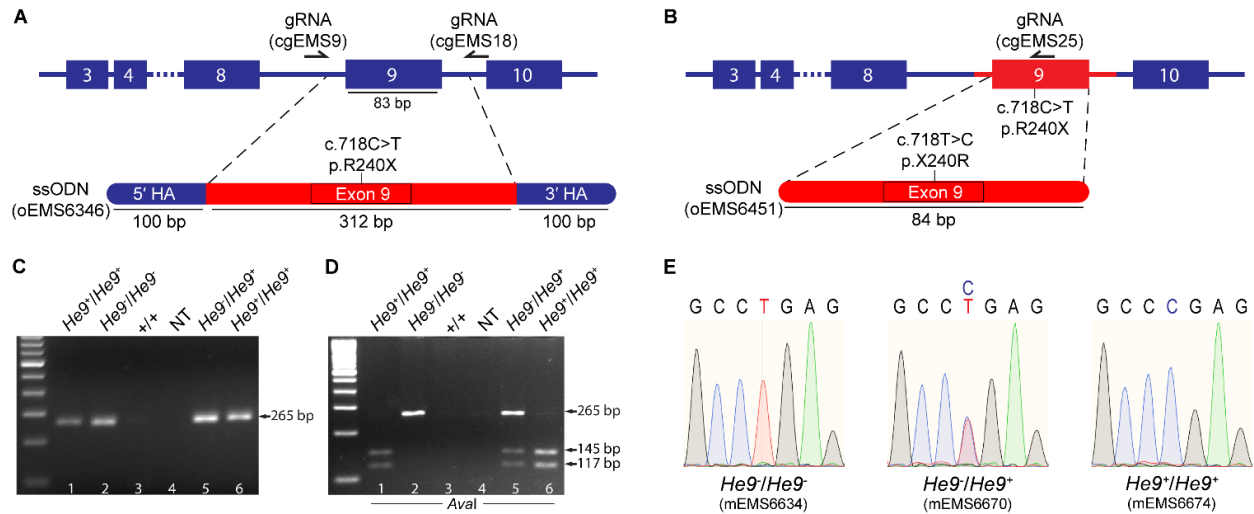


**Figure 2.2. Derivation of homozygous humanized *Pax6* exon-9 mouse ESCs, including an exon-9 pathogenic patient variant.** (A) Schematic of humanization using a dual-gRNA strategy to exchange mouse genomic sequence with a 512 bp ssODN at *Pax6* exon 9. ssODN consists of 100 bp mouse homology arms (blue) flanking 312 bp of human DNA sequence containing pathogenic patient variant, c.718C>T (red). cgEMS, CRISPR guide; oEMS, oligodeoxynucleotide; HA, homology arm. (B) Schematic of single-gRNA strategy to correct patient variant, c.718C>T, in humanized homozygous variant cell line, using an 84 bp ssODN to derive heterozygous and homozygous non-variant cell lines. (C) Human-specific DNA amplified from single embryonic stem cell clones picked following CRISPR-based humanization of *Pax6* exon 9. Lane 1, positive control DNA from a *He9<sup>+</sup>/He9<sup>+</sup>* mouse ear notch. Lane 2, DNA from a clone positive for humanization event (mEMS6634). Lane 3, negative control DNA from a B6 WT mouse. Lane 4, no template negative control. Lanes 5 and 6, DNA from clones positive for the humanization event (mEMS6670 and mEMS6674, respectively). Band at 265 bp indicates humanization. (D) Restriction fragment length polymorphism screen of the PCR products shown in B using *Ava*I restriction enzyme identifies *He9<sup>+</sup>/He9<sup>+</sup>* clones that have undergone either heterozygous (lane 5) or homozygous (lane 6) CRISPR correction of the patient variant. Fragment lengths of 145 bp and 117 bp indicate DNA cut by *Ava*I due to the presence of the non-variant base. Fragment length of 265 bp indicate uncut DNA due to presence of variant. (E) Sanger sequencing showing location of patient variant (red) from humanized cell lines demonstrating homozygosity (mEMS6634) or heterozygosity (mEMS6670) for patient variant, or homozygosity (mEMS6674) for non-variant sequence. *He9*, humanized exon 9.

### 2.3.2 Minimal humanization with non-variant *PAX6* results in no phenotype *in vivo*

Prior to therapy development using the CHuMMMs cell lines, we wanted to ensure that the minimal humanization alone did not cause adverse consequences for *Pax6* gene function.

Since there are no amino acid differences between mice and humans this seemed likely,

however, changes in codon usage, splicing sites, and potential transcription binding sites were concerns. We reasoned that the ultimate determinant of *Pax6* gene function was eye development *in vivo*.

Thus, we established CHuMMMs *He9*<sup>+/+</sup> mice through direct injection of CRISPR reagents, using the same dual-gRNA strategy described above, and the non-variant ssODN (Table 2.1). The resulting founder mice were made and bred on the C57BL/6J (B6) genetic background. The fully characterized strain was C57BL/6J-*Pax6*<sup>em7(PAX6)Ems</sup> (called B6-*He9*<sup>+</sup> hereafter). Sequencing of the 1.2 kb exon-9 region, described above, confirmed the successful molecular event. The B6-*He9*<sup>+</sup> strain was then bred onto a 129S1/SvImJ (129) genetic background to derive 129S1/SvImJ-*Pax6*<sup>em7(PAX6)Ems</sup> (called 129-*He9*<sup>+</sup> hereafter).

The observed normal ocular morphology of *He9*<sup>+/He9</sup> mice gave evidence that the minimal humanization event at exon 9 alone did not disrupt *Pax6* gene function *in vivo*. We

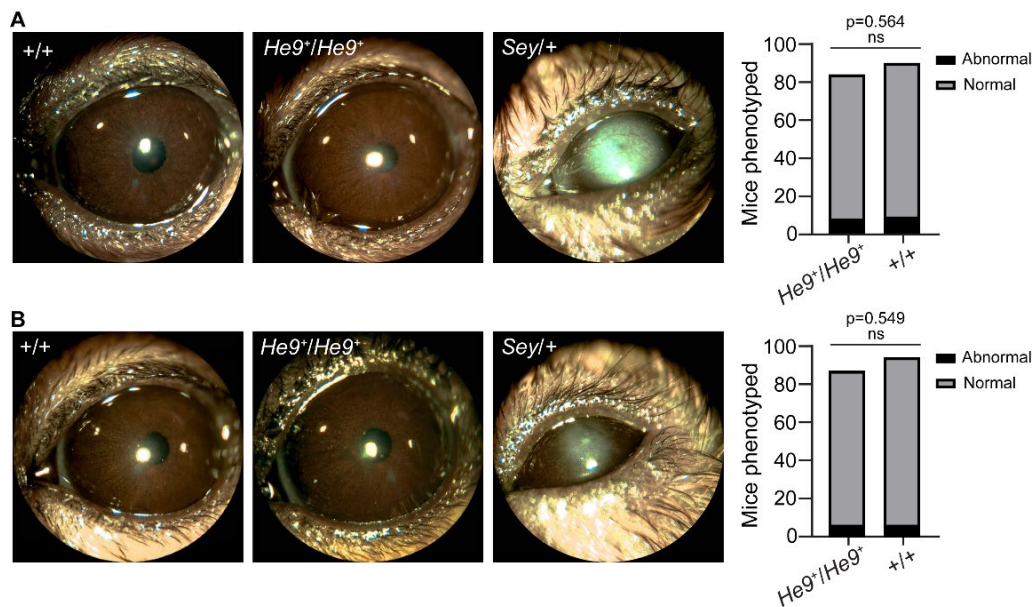


**Figure 2.3 CRISPR-based minimal humanization of *Pax6* does not result in an ocular phenotype in mouse.** (A and B) Slit lamp images of WT *He9*<sup>+/He9</sup> and *Sey*<sup>+/+</sup> mice demonstrated that *He9*<sup>+/He9</sup> ocular phenotype does not differ from WT and does differ from the *Sey*<sup>+/+</sup> mice aniridia phenotype. Mice were phenotyped by visual inspection and eyes scored as either “Normal” or “Abnormal”. (A) The *He9*<sup>+</sup> allele was bred onto a C57BL/6J background and compared to C57BL/6J WT controls (*He9*<sup>+/He9</sup>, n=84; WT, n=90). No significant difference was determined by one-sided Fisher’s exact test. (B) The *He9*<sup>+</sup> allele was bred onto a 129S1/SvImJ background and was compared to 129S1/SvImJ WT controls (*He9*<sup>+/He9</sup>, n=87; WT, n=94). No significant difference was determined by one-sided Fisher’s exact test.

characterized mice by visual inspection and found that the external ocular morphology of B6-*He9<sup>+</sup>/He9<sup>+</sup>* mice did not differ significantly from B6 WT mice. External ocular morphology of B6-*He9<sup>+</sup>/He9<sup>+</sup>* mice did, however, differ from the well-characterized B6-*Sey/+* mouse, as shown by slit lamp images (Figure 2.3A). This work was repeated with 129-*He9<sup>+</sup>/He9<sup>+</sup>* and 129 WT mice and again we observed no significant difference between the two groups (Figure 2.3B).

### 2.3.3 *SpCas9* gave higher editing of patient variant than *SaCas9*

To compare *SpCas9* versus *SaCas9* we used *He9<sup>-</sup>/He9<sup>-</sup>* and *He9<sup>+</sup>/He9<sup>+</sup>* ESCs. The *He9<sup>-</sup>/He9<sup>-</sup>* cells allowed for the observation and quantification of correction of the patient variant, and the *He9<sup>+</sup>/He9<sup>+</sup>* cells allowed for the observation and quantification of unwanted alteration on the non-variant chromosome (Figure 2.4). For *SpCas9*, a single optimal sgRNA and ssODN were chosen. For *SaCas9*, a single optimal sgRNA and two ssODN were chosen (Table 2.1). In addition to the correction of the c.718C>T, the ssODNs included synonymous single base mismatches, referred to here as “blocking mutations”, to prevent repeated targeting by Cas9 of edited alleles. These blocking mutations also enabled the quantification of on-target alteration on the non-variant chromosome. RNPs were delivered by electroporation, including replicas, and total cell lysates were harvested for characterization. To quantify CRISPR editing by Sanger sequencing, we focused our analyses on unidirectional sequencing in which the target base was prior to, and unaffected by, indels at the Cas9 cut site. Peak height was normalized by subtracting the average of mock untreated *He9<sup>-</sup>/He9<sup>-</sup>* replicas to remove background and conservatively calculate the CRISPR editing.

We found that *SpCas9* delivered to *He9<sup>-</sup>/He9<sup>-</sup>* ESCs showed significantly superior average editing of the patient variant from T to C at  $31.7 \pm 3.8\%$  (Figure 2.4A), in comparison to the average editing observed by *SaCas9* with either ssODN at  $11.5 \pm 6.3\%$  or  $9.37 \pm 2.3\%$

(Figure 2.4B). The results also showed that the average editing of the blocking mutation on the non-variant chromosome in the *He9<sup>+</sup>/He9<sup>+</sup>* cell line by *SpCas9* at  $4.02 \pm 3.6\%$ , and *SaCas9* with either ssODN at  $2.14 \pm 3.5\%$  or  $0.460 \pm 2.7\%$ , was not significantly different among the three groups. Thus, *SpCas9* was selected for further optimization in the subsequent experiments based on high editing of the patient variant and minimal editing on the non-variant chromosome.

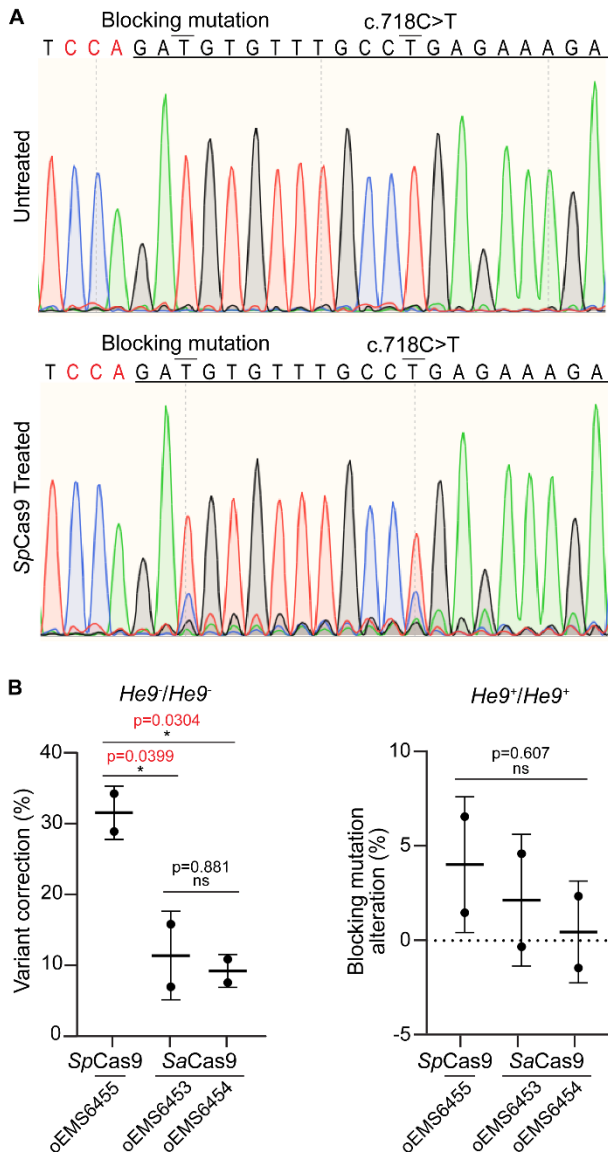


**Figure 2.4. CRISPR genome editing of the patient variant is higher using *SpCas9* than *SaCas9*.** (A) Top panel. Sanger sequencing of untreated *He9<sup>-</sup>/He9<sup>-</sup>* ESCs where patient variant c.718C>T (overlined) was homozygous for thymine as indicated by a singular red peak. Bottom panel. Sanger sequencing of *SpCas9* treated *He9<sup>-</sup>/He9<sup>-</sup>* ESCs demonstrated correction of the patient variant from T to C at 34.3%, as shown by dominant red peak and secondary blue peak. The ssODN also included a synonymous “blocking mutation” (overlined) to prevent additional targeting of previously edited alleles. The blocking mutation was edited from T to C at 25.6%. PAM highlighted in red text. Guide RNA location shown by underlined text. (B) Left panel. Quantification of editing at the patient variant in *He9<sup>-</sup>/He9<sup>-</sup>* by *SpCas9* was the highest average correction at  $31.7 \pm 3.8\%$ . This was significantly different from the average editing by *SaCas9* with oEMS6453 or oEMS6454, at  $11.5 \pm 6.3\%$  and  $9.37 \pm 2.3\%$ , respectively. Right panel. Quantification of editing at the site of the blocking mutation on the non-variant chromosome in *He9<sup>+</sup>/He9<sup>+</sup>* cells was not significantly different among the three strategies. This average editing by *SpCas9* was at  $4.02 \pm 3.6\%$ , by *SaCas9* with oEMS6453 was at  $2.14 \pm 3.5\%$ , and *SaCas9* with oEMS6454 was at  $0.460 \pm 2.7\%$ . Ordinary one-way ANOVA with Tukey’s multiple comparisons tests was used to determine significance of data.

### 2.3.4 High-fidelity Cas9 gave lower alteration of non-variant chromosome than WT *SpCas9*

To further optimize our CRISPR strategy, we compared average editing of three Cas9 nucleases from different commercial retailers: WT *SpCas9*, PNABio, Thousand Oaks, CA; “TrueCut” WT *SpCas9*, Invitrogen, Waltham, MA; and “High Fidelity” (HiFi) mutated *SpCas9*, Integrated DNA Technologies, Coralville, IA (Figure 2.5). Experimental design was the same as described above for *SpCas9* versus *SaCas9*.

First, we studied the two WT *SpCas9* enzymes (Figure 2.5A). Average editing of the patient variant by PNABio *SpCas9* at  $26.8 \pm 6.0\%$  and TrueCut *SpCas9* at  $34.9 \pm 0.62\%$  was not significantly different. Average editing of the blocking mutation on the non-variant chromosome by PNABio Cas9 at  $13.9 \pm 4.9\%$  and TrueCut Cas9 at  $13.3 \pm 3.2\%$  was also not significantly different. These results demonstrated that possible variabilities in manufacturing of nucleases by these commercial retailers did not affect average editing activity of the WT *SpCas9*.

We then tested the WT *SpCas9* from PNA Bio, versus HiFi Cas9 (Figure 2.5B, C). HiFi Cas9 has been engineered to reduce off-target editing while maintaining on-target editing through the introduction of a single point mutation in the REC1 sgRNA recognition domain to enhance specificity of sgRNA binding (Vakulskas et al., 2018). Average editing of the patient variant by PNABio Cas9 at  $37.1 \pm 2.7\%$  and HiFi Cas9 at  $26.7 \pm 4.7\%$  were not significantly different. Conversely, average editing of the blocking mutation on the non-variant chromosome by PNABio Cas9 at  $23.6 \pm 1.9\%$  and HiFi Cas9 at  $0.350 \pm 0.028\%$  were significantly different. Based on these results, we found that the engineered HiFi Cas9 functioned in our assay as expected, and was the best *SpCas9* choice for further HDR-mediated CRISPR therapy development.

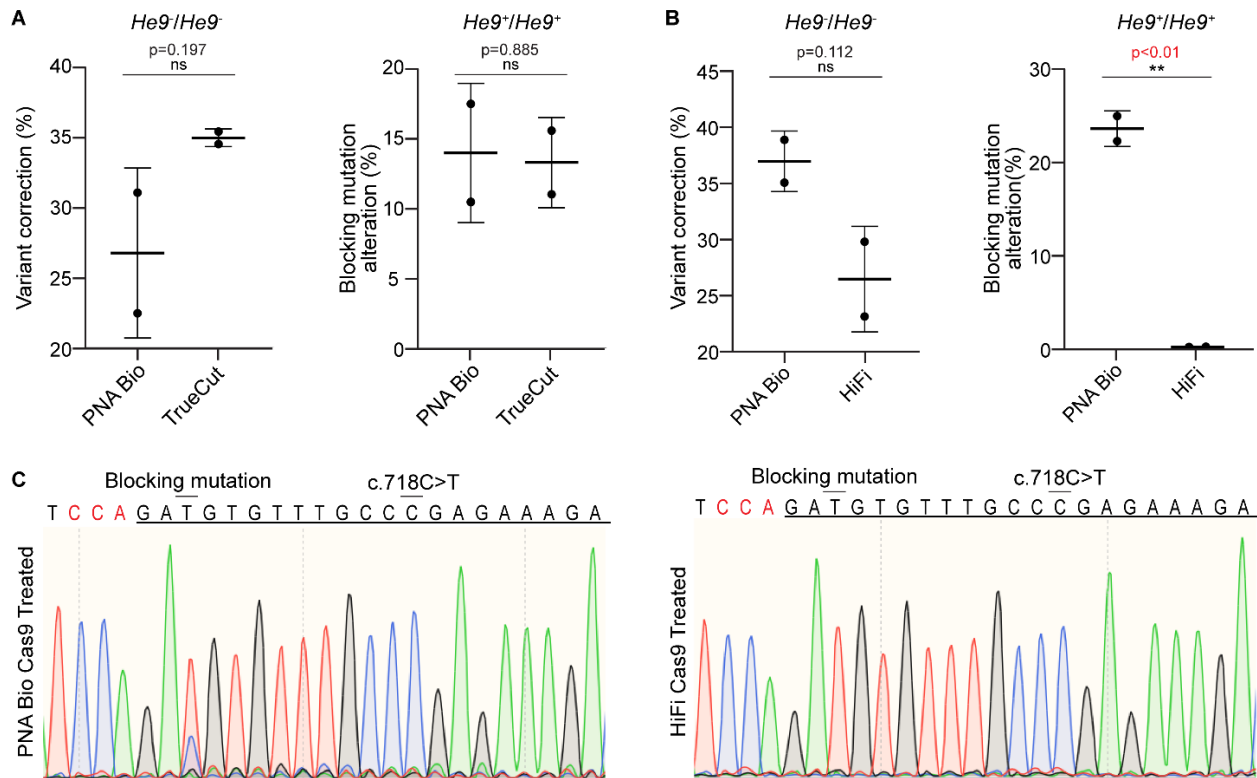


**Figure 2.5 A high fidelity *SpCas9* resulted in lower CRISPR editing on the non-variant chromosome.** (A) Left panel. Quantification of editing of the patient variant c.718C>T (overlined) in *He9<sup>-</sup>/He9<sup>-</sup>* cells found no significant difference between PNA Bio Cas9 and TrueCut Cas9 nucleases. Average editing observed by PNA Bio Cas9 was at  $26.8 \pm 6.0\%$  and TrueCut Cas9 was at  $34.9 \pm 0.62\%$ . Right panel. Quantification of editing of the synonymous blocking mutation (overlined) on the non-variant chromosome in *He9<sup>+</sup>/He9<sup>+</sup>* cells did not show a significant difference between the two nucleases. The average editing by PNA Bio Cas9 was at  $13.9 \pm 4.9\%$  and TrueCut Cas9 was at  $13.3 \pm 3.2\%$ . (B) Left panel. Quantification of editing of the patient variant in *He9<sup>-</sup>/He9<sup>-</sup>* cells found no significant difference between PNA Bio Cas9 and HiFi Cas9. Average editing observed by PNA Bio Cas9 was at  $37.1 \pm 2.7\%$  and HiFi Cas9 was at  $26.7 \pm 4.7\%$ . Right panel. Quantification of editing of the blocking mutation on the non-variant chromosome in *He9<sup>+</sup>/He9<sup>+</sup>* cells found HiFi Cas9 showed significantly lower editing than PNA Bio Cas9. The average editing by PNA Bio Cas9 was at  $23.6 \pm 1.9\%$  and HiFi Cas9 was at  $0.350 \pm 0.028\%$ . Two-tailed unpaired t-tests were used to determine significance of the data. (C) Left panel. Sanger sequencing of PNA Bio Cas9 treated *He9<sup>+</sup>/He9<sup>+</sup>* cells showed a secondary blue peak at the blocking mutation demonstrating impact on the non-variant chromosome. Also, secondary sequence is evident throughout the chromatogram 3' of Cas9 cut site due to CRISPR-based insertions and deletions (indels). Right panel. Sanger sequencing of HiFi Cas9 treated *He9<sup>+</sup>/He9<sup>+</sup>* cells demonstrated minimal CRISPR-based editing at the blocking mutation on the non-variant chromosome and minimal secondary sequence throughout chromatogram due to indels. PAM highlighted in red text. Guide RNA location shown by underlined text.

### 2.3.5 ABE8e gave superior editing of patient variant and reduced alteration of non-variant chromosome than *SpCas9*

Next, we compared average editing of the patient variant by base-editing using ABE8e versus HDR-mediated editing using WT *SpCas9* (Figure 2.6), following the same experimental design described above for *SpCas9* versus *SaCas9*. As an ssODN is not required for ABE8e

editing, we quantify on-target alteration on the non-variant chromosome by a bystander edit observed 4 bp from the target base location. We tested two sgRNAs with ABE8e: cgEMS25 (Table 2.1) targeted an optimal PAM (NGG), and placed the target base at position 8 of the reported optimal editing window of positions 4-8 for ABE8e (Richter et al., 2020); and cgEMS46 targeted a suboptimal PAM (NGA), but placed the target base at position 7 in the editing window, slightly more central to the optimal editing window, which is reported to improve on-target editing by ABE8e (Richter et al., 2020). Throughout this study, thus far, standard chemical modifications of sgRNAs have been used (Chen et al., 2021). Here, we also test unmodified sgRNAs, given that the success of using modified or unmodified sgRNAs will affect the choice of delivery methods.

We found that ABE8e complexed with cgEMS25 showed significantly higher average editing of the patient variant at  $73.0 \pm 0.644\%$  than ABE8e complexed with cgEMS46 at  $6.37 \pm 0.79\%$ , and *SpCas9* complexed with cgEMS25 at  $41.8 \pm 5.2\%$  (Figure 2.6A and B). These results demonstrate the superior editing activity of the patient variant by ABE8e versus WT *SpCas9*, as well as the importance of targeting the sgRNA to an optimal PAM. Additionally, positioning the target base more central to the editing window of ABE8e by 1 bp did not sufficiently improve editing activity, when paired with suboptimal PAM recognition by the sgRNA. Excitingly, ABE8e also showed significantly lower editing of the non-variant chromosome than *SpCas9* (Figure 2.6B). ABE8e complexed with cgEMS25 resulted in an average bystander edit on the non-variant chromosome at  $0.545 \pm 0.73\%$  and ABE8e complexed with cgEMS46 resulted in an average bystander edit at  $0.390 \pm 0.52\%$ , both of which showed significantly lower average editing of the non-variant chromosome than *SpCas9* at  $15.4 \pm 2.0\%$ . These results demonstrate

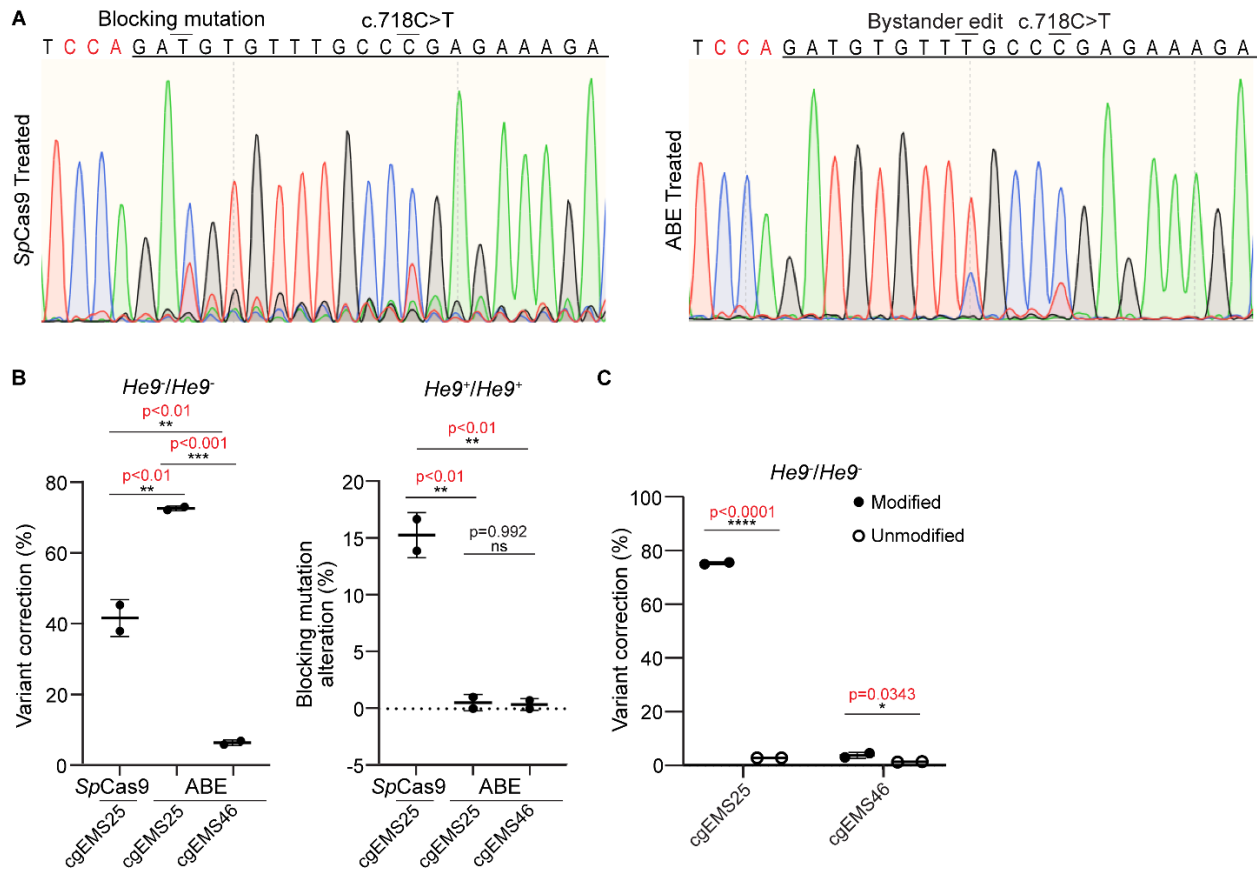


**Figure 2.6** ABE8e with a modified guide showed superior editing of the patient variant, with minimal impact on the non-variant chromosome. (A) Left panel. Sanger sequencing of *SpCas9* treated *He9/He9-* cells demonstrated CRISPR-based editing of the patient variant c.718C>T (overlined) from T to C at 57.7%, as shown by dominant blue peak and secondary red peak. Right panel. Sanger sequencing of treated *He9/He9-* cells with ABE8e complexed with cgEMS25 demonstrated highest CRISPR-based editing of the patient variant at 74.5%. Secondary peak observed 4 bp 5' of the intended edit is due to synonymous bystander editing (overlined) by ABE8e. PAM highlighted in red text. Guide RNA location shown by underlined text. (B) Left panel. Quantification of average editing of patient variant in *He9/He9-* cells showed treatment with *SpCas9* resulted in editing at  $41.8 \pm 5.2\%$ , ABE8e complexed with cgEMS25 showed significantly higher average editing at  $73.0 \pm 0.64\%$ , and ABE8e with cgEMS46 showed significantly lower average editing at  $6.37 \pm 0.79\%$ . Right panel. Treatment in *He9+/He9+* cells resulted in average editing of the synonymous blocking mutation (overlined) on the non-variant chromosome by *SpCas9* at  $15.4 \pm 2.0\%$ . Impact on the non-variant chromosome by ABE8e was assayed by the alteration of the bystander edit. ABE8e with cgEMS25 resulted in a bystander edit at  $0.545 \pm 0.73\%$ , and ABE8e with cgEMS46 resulted in a bystander edit at  $0.390 \pm 0.52\%$  on the non-variant chromosome, both of which show significantly lower average editing than *SpCas9*. Ordinary one-way ANOVA with Tukey's multiple comparisons tests were performed to determine significance of data. (C) Left panel. Quantification of ABE8e complexed with chemically modified cgEMS25 in *He9/He9-* cells showed significantly higher average editing than unmodified at  $76.8 \pm 0.48\%$  and  $2.87 \pm 0.042\%$ , respectively. ABE8e complexed with chemically modified cgEMS46 demonstrated significantly higher average editing than unmodified cgEMS46 at  $3.82 \pm 1.2\%$  and  $1.37 \pm 0.14\%$ , respectively.

the superior ability of ABE8e to differentiate the single base pair difference between the patient variant and non-variant chromosome at this locus, in comparison to the HDR-mediated approach.

To further optimize our ABE8e therapeutic strategy, we compared the use of chemically modified versus unmodified sgRNAs (Figure 2.6C). We found that the average editing efficiency of the patient variant by ABE8e complexed with chemically modified cgEMS25 at  $76.8 \pm 0.48\%$  was significantly higher than ABE8e complexed with unmodified cgEMS25 at  $2.87 \pm 0.042\%$ . We also found that the average editing efficiency by ABE8e complexed with modified cgEMS46 at  $3.82 \pm 1.2\%$  was significantly higher than ABE8e complexed with unmodified cgEMS46 at  $1.37 \pm 0.14\%$ . Overall, these results confirm the importance of chemically modified sgRNAs to editing activity by ABE8e-RNPs.

### **2.3.6 ABE8e edits patient variant “additively” in humanized heterozygous variant cell line**

To further investigate how our ABE8e-mediated therapy would behave in patient cells, we compared the editing activity of the optimized ABE8e-mediated therapy in all three of the humanized cell lines (*He9<sup>-</sup>/He9<sup>-</sup>*, *He9<sup>-</sup>/He9<sup>+</sup>*, and *He9<sup>+</sup>/He9<sup>+</sup>*) to determine whether the patient variant would be edited additively or synergistically in the heterozygous cell line (Figure 2.7). These results may give insight into how ABE8e would behave in aniridia patient cells, which are heterozygous for the pathogenic variant. The experimental design is the same as described above for *SpCas9* versus *SaCas9*.

We measured the total % cytosine (Total %C) at the site of the patient variant in the ABE8e-treated *He9<sup>-</sup>/He9<sup>-</sup>*, *He9<sup>-</sup>/He9<sup>+</sup>*, and *He9<sup>+</sup>/He9<sup>+</sup>* cell lines and found that average editing of the variant in the *He9<sup>-</sup>/He9<sup>+</sup>* cell line at  $74.8 \pm 5.0\%$  was intermediate to, but not significantly different from, treatment in the *He9<sup>-</sup>/He9<sup>-</sup>* cells at  $65.3 \pm 5.7\%$  and *He9<sup>+</sup>/He9<sup>+</sup>* cells at  $89.8 \pm 0.60\%$  (Figure 2.7A). Here, typical variation and normalization by subtracting the average of mock untreated replicas reduced the *He9<sup>+</sup>/He9<sup>+</sup>* peak value from the expected 100%. To further demonstrate the effect of the ABE8e treatment in each of these cell lines, we present the data

again but now as a change in % cytosine (Delta %C) (Figure 2.7B). We normalized ABE8e treated samples to %C at the site of the patient variant in the mock untreated samples, this time separately for each cell line. We found that the Delta %C in ABE8e treated *He9/He9*<sup>+</sup> cells at  $30.8 \pm 5.0\%$  was intermediate to, and significantly different from, the Delta %C in ABE8e treated *He9/He9*<sup>-</sup> cells at  $65.3 \pm 5.7\%$  and *He9<sup>+</sup>/He9<sup>+</sup>* cells at  $-1.98 \pm 0.60\%$ . These results demonstrate that ABE8e edited the patient variant additively in the heterozygous cell line, with no evidence of effect of the non-variant chromosome.

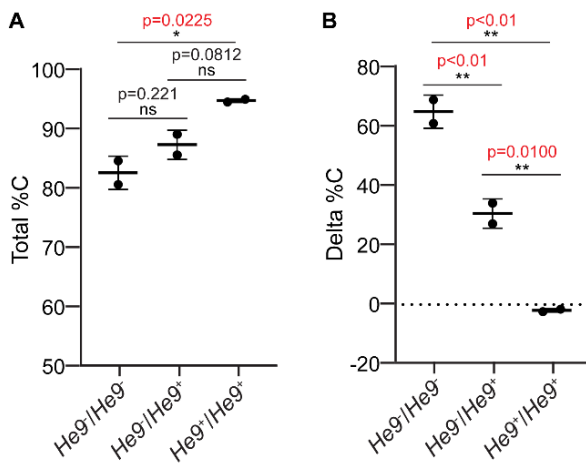


**Figure 2.7. ABE8e edits patient variant “additively” in heterozygous variant cells.** (A) Quantification of total % cytosine at site of patient variant c.718C>T following ABE8e treatment of *He9/He9*<sup>+</sup> cells was intermediate to, but not significantly different from, homozygous *He9/He9*<sup>-</sup> and *He9<sup>+</sup>/He9<sup>+</sup>* cells at  $74.8 \pm 5.0\%$ ,  $65.3 \pm 5.7\%$  and  $89.8 \pm 0.60\%$ , respectively. (B) Quantification of the change in % cytosine at site of patient variant following ABE8e treatment of *He9/He9*<sup>+</sup> cells was intermediate to, and significantly different from, homozygous *He9/He9*<sup>-</sup> and *He9<sup>+</sup>/He9<sup>+</sup>* cells at  $30.8 \pm 5.0\%$ ,  $65.3 \pm 5.7\%$  and  $-1.98 \pm 0.60\%$ , respectively. ns,  $p > 0.05$ ; \*,  $p \leq 0.05$ ; \*\*,  $p \leq 0.01$ .

### 2.3.7 LNP-encapsulated ABE8e-RNPs edited a *Pax6* patient variant in mouse *ex vivo* cortical neurons

As electroporation is not a translatable delivery method, we consider progressing development of our CRISPR therapy for aniridia to either rAAV or LNPs. Having demonstrated the importance of chemically modified sgRNAs to editing activity, which cannot be maintained when the sgRNA is encoded by rAAV, we decided to encapsulate ABE8e-RNPs in LNPs. For this we chose the Incisive Delivery System (Incisive Genetics Inc., Vancouver, Canada) for CRISPR based gene therapies, which we have used successfully before to efficiently deliver *SpCas9* RNP *in vivo* (Mirjalili Mohanna et al., 2022). In addition, we moved the study from

ESCs to the more clinically-relevant mouse primary cortical neurons. Since the patient variant c.718C>T present in the *He9* cells was not available *in vivo*, we shifted to another patient variant c.580G>T present in the *Sey* mouse. Thus, embryonic primary cortical neurons were derived from *Fey* mice. The 3xFLAG tag enabled histological quantification of correction of the *Sey* variant, by rescued Pax6 protein expression (Mirjalili Mohanna et al., 2020; Mirjalili Mohanna et al., 2022). This previously reported method found success using CRISPR *SpCas9* HDR to correct the *Sey* variant to the WT guanine base. Here, we test ABE8e which altered the variant thymine to a cytosine base, converting a stop codon to an arginine missense mutation. As such, we were initially uncertain whether this missense alteration would result in a stable Pax6 protein, and thus, detectable FLAG expression. We assayed successful transfection and genomic editing by Sanger sequencing and stereological analysis.

Excitingly, we found that ABE8e was successfully encapsulated by LNPs, transfected primary cortical neurons, altered the *Sey* variant at the genomic level, and rescued Pax6 protein expression. Transfection was first demonstrated by positive control *SpCas9* HDR-treated cells showing FLAG expression, which colabelled with PAX6, indicative of correction of the patient variant to WT (Figure 2.8A). FLAG expression and colabelling was also seen by the ABE8e (100 nM) treated cells, indicative of alteration of the patient variant despite a perhaps less stable, but certainly detectable, missense carrying *Pax6* protein.

Quantification by Sanger sequencing of whole cell lysates found that the ABE8e (100 nM) treated cells showed a genomic alteration of the *Sey* variant at an average of  $2.33 \pm 1.0\%$ , which was significantly greater than the alteration observed in the ABE8e (50 nM) at  $0.340 \pm 0.017\%$  and luciferase control group at  $0.00 \pm 0.58\%$  (Figure 2.8B). The ABE8e (50 nM) treated group was not significantly different from the negative control. Stereological quantification of

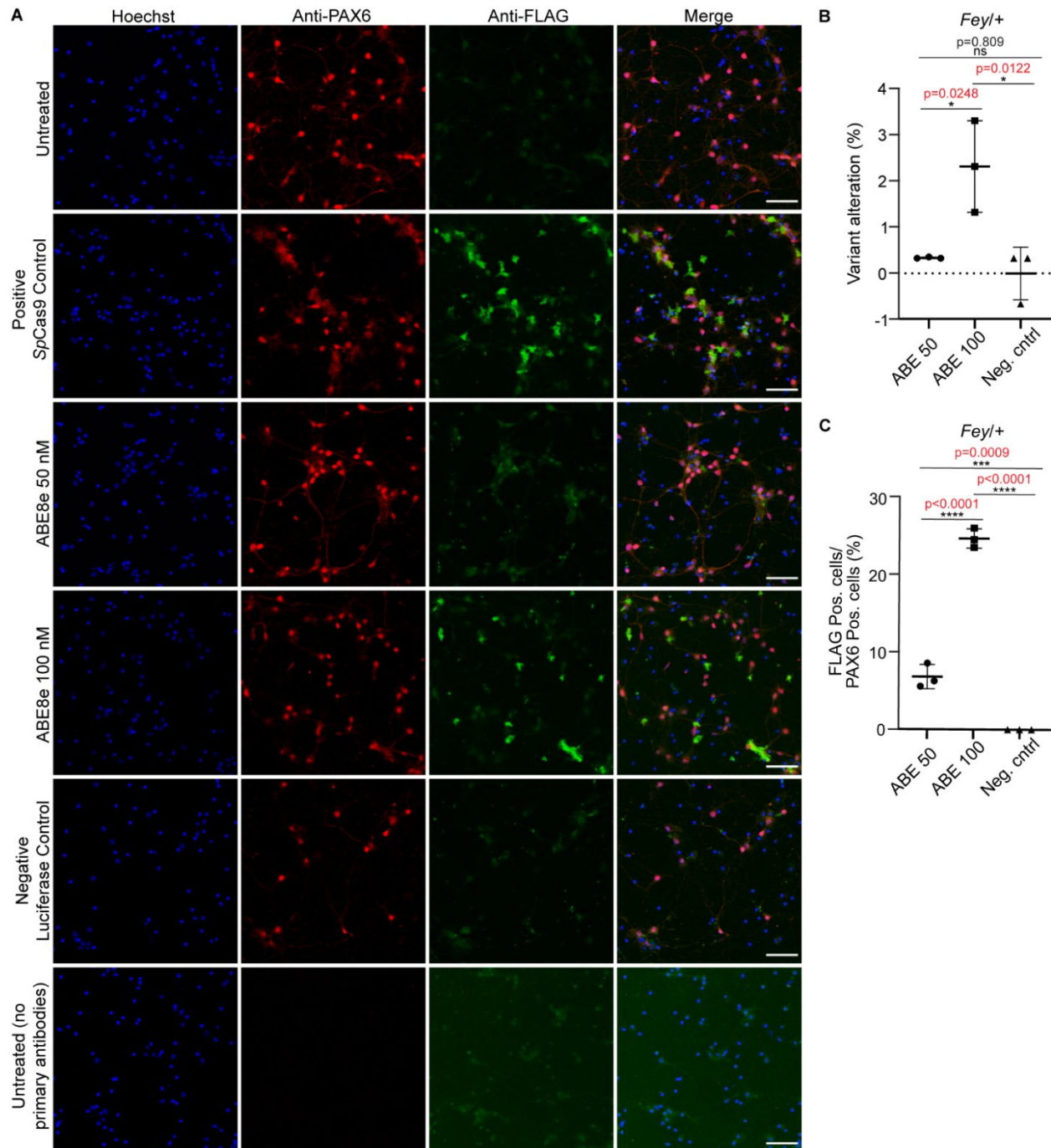


**Figure 2.8** LNP delivered ABE8e RNP edited *Pax6* pathogenic patient variant in mouse cortical neurons *ex vivo*. (A)

Immunocytochemical images of 3xFLAG-tagged Pax6 *Sey* (*Fey*) embryonic mouse cortical neurons. Hoechst (blue) was used to reveal cell nuclei. As expected for embryonic cortical neurons, anti-PAX6 (red) showed positive cells in all samples, including the heterozygous *Fey* cells. Anti-FLAG (green) showed successful editing of *Sey* variant c.580G>T leading to expression of the corrected PAX6 protein in *SpCas9* positive control and ABE8e (100 nM) RNP treated cells. Thus, as expected, anti-Pax6 and anti-FLAG showed colabelling in merge images (yellow). FLAG expression was very low in the ABE8e (50 nM) treated cells and not observed in the untreated or negative control; the latter was *SpCas9*-RNP complexed with a luciferase-targeting guide. A further negative control was samples processed with no primary antibody. Images were taken at 20x magnification. Scale bar = 50  $\mu$ M. (B) Quantification of editing of *Sey* variant in *Fey* *ex vivo* cortical neurons. ABE8e (100 nM) treated cells showed significantly higher alteration of target variant compared to ABE8e (50 nM) and the luciferase negative control at  $2.33 \pm 1.0\%$ ,  $0.340 \pm 0.017\%$ , and  $0.00 \pm 0.58\%$ , respectively. (C) Quantification of FLAG-tagged Pax6 protein expression in *Fey* *ex vivo* cortical neurons. FLAG expression was significantly different between ABE8e (50 nM), ABE8e (100 nM) and the luciferase negative control treated groups at  $6.83 \pm 1.6\%$ ,  $24.8 \pm 1.3\%$  and  $0.00 \pm 0.0\%$ , respectively. ns,  $p > 0.05$ ; \*,  $p \leq 0.05$ ; \*\*\*,  $p \leq 0.001$ ; \*\*\*\*,  $p \leq 0.0001$ .

protein expression showed that for the ABE8e (100 nM) treated cells, FLAG expression, as a percentage of total Pax6 protein-expressing cells, at  $24.8 \pm 1.3\%$  was significantly greater than that in both the ABE8e (50 nM) treated cells at  $6.83 \pm 1.6\%$  and the luciferase-targeting negative control group at  $0.00 \pm 0.0\%$  (Figure 2.8C). Thus, we can conclude that the higher molar concentration of ABE8e encapsulated in LNPs was more successful in editing the *Sey* patient variant to rescue Pax6 expression.

We suggest that the observed lower editing assayed by sequencing, compared to stereology, is a consequence of the large number of condensed nuclei (non-Pax6-expressing cells) present across all treatment groups (Figure 2.9) (Mirjalili Mohanna et al., 2022). Samples sent for sequencing were total cell lysates, and thus the non-Pax6-expressing neurons, would have diluted the result of ABE8e-mediated editing of the *Sey* patient variant. Overall, we have shown successful encapsulation, transfection, and *ex vivo* genomic editing of an aniridia variant by ABE8e-RNP-LNPs in a clinically-relevant cell type.

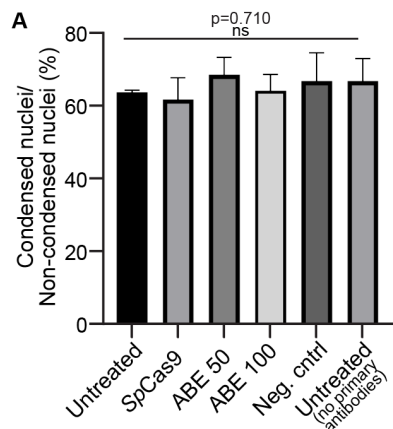


**Figure 2.9 Ratio of condensed versus non-condensed neuronal nuclei did not vary with LNP treatment.** All primary embryonic cortical neuron cultures had some cells with condensed nuclei and no Pax6 expression, possibly indicative of unhealthy or dead cells. However, no significant difference in the ratio of condensed versus non-condensed Pax6-expressing nuclei was observed across all groups, regardless of treatment (one-way ANOVA with Tukey's multiple comparisons tests).

## 2.4 DISCUSSION

We designed the CHuMMMs minimal-humanization strategy to answer the challenge of demonstrating efficacy of CRISPR-based therapies in animal *in vitro*, *ex vivo*, and *in vivo* model systems, while binding human DNA to facilitate rapid translation to the clinic. Here, we demonstrate the ease, functional tolerance, and usefulness of CHuMMMs, by developing a CRISPR-based therapeutic strategy for congenital aniridia. With ease we established three types of CHuMMMs cell lines, all homozygous for a humanized CRISPR “landing pad” of only 312 bp at exon 9 of *Pax6* (*He9*). Furthermore, they were homozygous variant (*He9<sup>-</sup>/He9<sup>-</sup>*), heterozygous (*He9<sup>-</sup>/He9<sup>+</sup>*), and homozygous non-variant (*He9<sup>+</sup>/He9<sup>+</sup>*), for the most common aniridia patient variant, c.718C>T. Functional tolerance was demonstrated by generating a CHuMMMs mouse strain (homozygous non-variant (*He9<sup>+</sup>/He9<sup>+</sup>*)) that showed humanization alone did not disrupt *Pax6* gene function *in vivo*. Finally, we used the cell lines to compare the efficacy of five different CRISPR enzymes. Overall, this work demonstrates the suitability of the CHuMMMs strategy, which can be applied widely to increase the value of all types of animal models for pre-clinical CRISPR therapy development for genetic diseases.

When comparing the efficacy of CRISPR enzymes in the *He9* CHuMMMs ESCs we found that ABE8e is the optimal enzyme for gene editing at *Pax6* exon 9 patient variant c.718C>T. ABE8e was the enzyme that demonstrated the highest average genomic correction of the patient variant at  $76.8 \pm 0.48\%$ . ABE8e also showed the lowest editing of the non-variant chromosome at  $0.545 \pm 0.73\%$ . This differential in editing activity is ideal for the purposes of treating aniridia patient cells, as they are heterozygous for the pathogenic variant. By comparing the editing activity in the three types of *He9* ESC lines, we found editing was additive, without interaction when both variant and non-variant chromosomes were present. In addition to the

variant correction, we observed bystander editing by ABE8e. Fortunately, the bystander edit results in a synonymous mutation, and therefore does not lead to an amino acid change. Overall, this work shows that ABE8e can correct the most commonly reported causal variant of aniridia. In addition, while other studies have shown successful genomic editing using ABE8e delivered *in vitro* as either plasmid, mRNA, or RNP (Alves et al., 2023; Haideri et al., 2022; Kulcsar et al., 2022; Newby et al., 2021; Richter et al., 2020; Sheriff et al., 2022), this is the first study to successfully edit the DNA of mouse ESCs utilizing the safer RNP approach.

Once we determined that ABE8e was the optimal CRISPR-based enzyme for gene editing at this locus, we sought to investigate a translatable delivery system to a more clinically relevant cell type. In choosing between rAAV and LNPs, our data showing the importance of sgRNA modification strongly favoured the use of LNPs. Our results show the first successful delivery and genomic editing by the CRISPR ABE8e encapsulated as an LNP-RNP. As a clinically relevant cell type we choose *ex vivo* mouse primary cortical neurons. This necessitated shifting to another patient variant, which strengthens the applicability of our work showing correction of two aniridia patient variants, but ABE8e was only able to correct this second genomic variant to an encoded missense mutation. Overall, correction dropped from 76.8% by electroporation in ESCs to correct the c.718C>T (p.R240X) genomic variant to wild type, versus 24.8% by LNP-RNPs in primary neurons to alter the c.580G>T (p.G194X) variant to Pax6 protein with a missense arginine. We hypothesize this difference may be due to a combination of transfection methodology, cell type, sgRNA sequence, DNA-sequence at the target site, and instability of the missense-carrying Pax6 protein.

There are two main limitations of this study to consider. First, there are over 600 *PAX6* causal variants for aniridia (Landrum et al., 2016). Here we have demonstrated a high level of

correction of the most common variant, but even that variant only represents one of four that together account for more than 20% of aniridia cases (Blanco-Kelly et al., 2021; Lima Cunha et al., 2019). We anticipated that developing a gene therapy for this variant will pave the way for similar personalized medicine approaches for other variants, but that needs future realization. Second, as with all animal model systems, it is not possible to test the off-target impact of CRISPR enzymes, which must be studied for the entire human genome. However, the finding that the base editor ABE8e was the optimal CRISPR-based enzyme is advantageous, since this enzyme does not create double stranded breaks and is well known for minimal off-target effects (Richter et al., 2020).

There are two potential approaches for clinical application of our optimized CRISPR therapeutic strategy: *ex vivo* or *in vivo*. The first application may be *ex vivo* autologous cell therapy with correction of patient-derived cells from either the retina or cornea prior to transplantation into the aniridic eye (Salman et al., 2022). A second application may be *in vivo* administration, to deliver the CRISPR therapy to multiple tissues of the patient eye (Salman et al., 2022). Nonetheless, both administration approaches require additional study to demonstrate safety and efficacy for clinical translation.

## **2.5 CONCLUSIONS**

The results of this study demonstrate support for the hypothesis that a CRISPR gene therapy can be developed and optimized in humanized mouse embryonic stem cells that will be able to distinguish between an aniridia patient variant and non-variant chromosomes. We demonstrated the usefulness of the CHuMMMs approach, and showed the first genomic editing by ABE8e encapsulated as an LNP-RNP. Overall, this study demonstrates successful ABE8e-

mediated editing of two aniridia patient variants, and thus lays the foundation for further pre-clinical *in vivo* mouse studies to rescue *Pax6* expression and prevent disease phenotype.

## CHAPTER 3: STRATEGIES FOR CLINICAL TRANSLATION

### 3.1 HYPOTHESIS AND THESIS OBJECTIVES

The work presented in this thesis has shown that I have completed all four objectives described at the outset of this study. I have successfully isolated and characterized three novel *Pax6* minimally-humanized mouse ESC lines including a homozygous patient variant, heterozygous variant, and homozygous non-variant cell line, thus completing my *in vitro* disease model of aniridia. I have demonstrated that minimal humanization of *Pax6* exon 9 does not result in an ocular phenotype *in vivo*, thus confirming it to be an acceptable humanization approach and control for future therapeutic studies in mouse. I have also demonstrated an extensive comparison of five different CRISPR enzymes as a therapeutic strategy to correct the patient variant, and have found that the ABE8e-mediated strategy shows the highest correction of the patient variant and minimal impact on non-variant chromosomes. Additionally, we investigated a promising delivery method for the optimal ABE8e-mediated strategy, by encapsulating the ABE8e-RNP in LNPs and showed successful transfection, rescued Pax6 protein expression, and genomic editing in a clinically relevant cell type.

Overall, I have demonstrated strong support for the focussed hypothesis of this thesis that a CRISPR gene strategy can be developed and optimized in humanized mouse ESCs that can distinguish between patient variant and non-variant chromosomes. This work serves as a proof-of-principle to lay the foundation for the translation of an *in vivo* CRISPR therapy to treat patients with aniridia.

### 3.2 CONTRIBUTION TO THE FIELD

The work presented here describes significant contributions made to the fields of both PAX6 aniridia (Hingorani et al., 2012) and gene editing (Cox et al., 2015) research, through the generation of new cell lines, new data, and new knowledge that will be of great use to other research groups in the aforementioned fields. In the first objective of my project, I played a key role in helping to complete a set of three novel minimally-humanized mouse ESC lines, which we used as a disease model system to initiate the development of a novel CRISPR gene therapy for aniridia. In my second objective, I generated new data which has contributed to the understanding of how minimal humanization of *Pax6* exon 9 negligibly affects Pax6 protein function *in vivo*. My work to characterize the Simpson Laboratory's novel *He9*<sup>+</sup> mouse has helped to validate the usefulness of the CHuMMMs approach, and the *He9*<sup>+</sup> mouse itself as a new control mouse model for aniridia. We have made these cell lines and the *He9*<sup>+</sup> mouse available to other groups in the field.

In the third objective, I initiated the pre-clinical development of a novel CRISPR gene therapy for the most common aniridia variant. To date, there are no curative treatment options to prevent blindness in patients with aniridia. Here, I generated new data which validated a novel therapeutic strategy for aniridia. This therapeutic strategy was validated *in vitro* and is now poised to be further optimized *in vivo*. In the final objective, we generated new data which validated a delivery strategy for the optimized CRISPR therapy. Using the optimal ABE8e-RNP strategy, we altered a second patient variant in *Fey* cortical neurons and demonstrated rescued expression of a missense-carrying Pax6 protein in a clinically relevant cell type. This experiment further demonstrated the value of the *Fey* mouse as an essential model for CRISPR therapy development for aniridia (Mirjalili Mohanna et al., 2020; Mirjalili Mohanna et al., 2022).

Additionally, this experiment demonstrated the first delivery of and genomic editing by ABE8e as an RNP encapsulated by LNPs. These exciting results demonstrate that a large enzyme, such as ABE8e, can be encapsulated by LNPs and transfected into primary cells. This was previously unknown in the field, and thus, highlights the innovative nature of this work.

Beyond the main objectives of this project, my work to isolate, culture, and characterize new *Fax* ESCs (Appendix A) contributes to the goals of the future directions of the project, to test the optimized ABE8e-RNP-LNP therapy *in vivo*. Described below in Chapter 3.3.2, the next steps of the project involve generating a novel 3xFLAG-tagged *He9/He9<sup>+</sup>* mouse for future *in vivo* studies. My work to generate *Fax* ESCs for the Simpson lab directly contributes to the future pre-clinical studies that are required to generate a new mouse model, in preparation for the clinical translation of the ABE8e therapy for aniridia.

### 3.3 FUTURE DIRECTIONS

#### 3.3.1 Off-target analyses in a human cell line

We have not yet shown or proposed any off-target analyses of the ABE8e-RNP-LNP therapy. A notable obstacle involved with conducting studies to develop CRISPR therapies in animal models is the inability to conduct off-target analyses that would yield clinically-meaningful results. This is because all the previous work has been either conducted or proposed in a model organism whose genome, outside the target locus, is not human. In the humanized *in vitro* model described in Chapter 2, the remainder of the genome outside the target locus is mouse. Thus, any results indicating the occurrence of off-target editing or lack thereof by the CRISPR therapeutic strategy would not be relevant to the purposes of treating human cells.

As such, a future direction of the work presented here would be to conduct off-target analyses in a human cell line. More specifically, I propose conducting said study in a HEK293 cell line (catalog CRL-1573, ATCC, Manassas, Virginia). I hypothesize that off-target analyses of our ABE8e-RNP-LNP therapy, conducted in HEK293 cells using CIRCLE-seq and targeted next-generation sequencing will result in no detectable (less than 0.1%) off-target editing at the determined candidate off-target loci.

Initially, we will use our previously validated method of using CRISPR-RNP HDR (described in Chapter 2) to introduce the patient variant into the HEK293 cells. The presence of the patient variant will serve as a positive control during off-target studies to ensure that ABE8e is interacting with the target variant. Mock treated cells will serve as a negative control. CIRCLE-seq will be used to determine candidate regions for off-target editing. This approach is used to enhance detection of genomic DNA fragments that have been cleaved by Cas9 and Cas9 nickases (Atkins et al., 2021; Koblan et al., 2021; Li et al., 2022; Tsai et al., 2017). In

comparison to other *in vitro* genome-wide off-target detection methods, such as Digenome seq analysis (Kim et al., 2015), CIRCLE-seq requires fewer reads and is able to identify lower frequency Cas9-induced cleavage events (Atkins et al., 2021; Tsai et al., 2017). We will deliver an *SpCas9* nuclease RNP complexed with the same sgRNA used in our ABE8e therapeutic strategy to HEK293 cells carrying the c.718C>T variant. Cells will be harvested 24-48 hours after transfection and will be lysed for molecular characterization. First, lysates will be prepped for Sanger sequencing and on-target editing efficiencies will be quantified to confirm successful transfection and genomic editing. Next, lysates will be processed for CIRCLE-seq analysis. Genomic DNA will be sheared and circularized by ligation of stem-loop adapters. Stem-loop regions will be nicked, exposing palindromic overhangs 4 nt in length, enabling intramolecular ligation. DNA fragments that have not been cleaved or nicked by Cas9 will be degraded by an exonuclease treatment. Circular DNA will then be linearized by Cas9, enabling adapter ligation, followed by PCR amplification and targeted next generation sequencing. Each read generated by Cas9 cleavage contains sequence information for a single off-target site (Tsai et al., 2017). This initial step using CIRCLE-seq is used to detect candidate off target sites.

Subsequently, primers will be designed to bind and amplify the candidate genomic regions detected in the initial CIRCLE-seq step. Amplified candidate regions will be sent for next generation sequencing. These sequencing results will determine whether any off-target editing activity will have occurred following treatment with the ABE8e therapy. The study proposed here will further enable the translation of our ABE8e-RNP-LNP therapy by demonstrating safety through determining the minimal off-target activity caused by the therapy in the human genome.

### 3.3.2 Generation of 3xFLAG-tagged *He9*/*He9*<sup>+</sup> mouse

The next step in developing a translatable *in vivo* CRISPR therapy for aniridia is to test our ABE8e-RNP-LNP *in vitro*-optimized therapy in a humanized mouse model of aniridia. This mouse model will contain a 3xFLAG-tagged *He9*<sup>-</sup> allele, hereafter called *FHe9*<sup>-</sup>, to enable histological detection of CRISPR-mediated rescue of Pax6 protein expression. First, we will generate this transgenic strain. There are many approaches that can generate transgenic mouse strains with small CRISPR-mediated genomic changes, but comparatively fewer that are able to insert the relatively large humanization region of 312 bp. The more traditional approach involves direct embryo manipulation through blastocyst microinjection of ESCs (Du et al., 2019; Papaioannou et al., 1975). The major steps of this approach involve *in vitro* manipulation of ESCs, isolation of individual clones, expansion and duplication of plates (one plate for screening of intended genomic edit and the other plate for cryopreservation), expansion of cryopreserved cells that are positive for the intended molecular manipulation, *ex vivo* microinjection of ESCs into E3.5 blastocysts isolated from a C57BL/6J-albino pregnant female, and uterus transfer of manipulated blastocysts to pseudopregnant females (Du et al., 2019).

There are many newer approaches which aim to generate CRISPR-mediated transgenic mice *in situ*, however there remains a major biological challenge. Homozygous LOF of *Pax6* is neonatal lethal (Hogan et al., 1986). The Simpson Lab and others have found that CRISPR-editing events tend to favor editing in a homozygous manner (Song et al., 2022). So, the intended heterozygous introduction of the *He9*<sup>-</sup> genomic event directly into 3xFLAG-tagged *Pax6*, hereafter called *Fax*, zygotes has proven to be challenging. As such, the traditional blastocyst microinjection approach is more favourable, due to the ability to screen many individual clones for the intended heterozygous introduction of the *He9*<sup>-</sup> allele into ESCs, prior to microinjection. I

hypothesize that blastocyst microinjection of *FHe9* ESCs will be a suitable strategy to generate a *FHe9* mouse strain to enable breeding to generate B6129F1-*FHe9*/*He9*<sup>+</sup> for *in vivo* CRISPR therapy optimization studies.

A *Fax* mouse strain has already been established by the lab by cytoplasmic microinjection of CRISPR reagents to insert the 3xFLAG tag at the *Pax6* start codon (Mirjalili Mohanna et al., 2020). I have harvested blastocysts from female C57BL/6J-*Fax* mice mated with 129S1/SvImJ-*Fax* studs, cultured and expanded these blastocysts to derive B6129F1 hybrid *Fax* ESCs for further CRISPR manipulation to introduce the *He9* allele (Appendix A). PCR assays were used to characterize newly-derived ESCs, to confirm sex and genotype as either homozygous or heterozygous for *Fax* (Figure A.1A and B). To confirm germline potential of these new *Fax* ESCs, prior to undergoing additional CRISPR manipulation, three individual *Fax* cell lines were sent to The Jackson Laboratory (JAX) (Bar Harbour, Maine) for blastocyst microinjection. All three cell lines produced litters with multiple high-chimeric male pups, indicating strong germline potential of the cells (Figure A.1C). These results instill confidence that the next stage of genomic editing to insert the *He9* allele into the newly-derived *Fax* ESCs, will also give rise to germline-capable ESCs to generate *FHe9* mice (Du et al., 2019).

To insert the *He9* allele into the newly-validated B6129F1 *Fax* ESCs, we will follow the same humanization strategy used to derive the *He9*/*He9* cell line (Figure 2.2A). The same gRNAs will be used (cgEMS9, cgEMS18) to introduce DSBs into introns 8 and 9, and the same 512 bp ssODN (oEMS6346) will introduce the human-specific landing pad, containing the patient variant, c.718C>T. The CRISPR reagents will be electroporated into the *Fax* ESCs and electroporated ESCs will be plated in serial dilutions in preparation for isolation of individual clones. Clones will be cultured and expanded to duplicate plates. One plate of clones will be

cryopreserved and the other will be lysed for characterization by PCR, RFLP, and Sanger sequencing. Once the clones have been screened for the intended heterozygous molecular event (*FHe9*<sup>+/+</sup>), they will be thawed and expanded in preparation for blastocyst microinjection at JAX. Following microinjection, once pups are born and chimerism is scored by coat colour assessment, chimeric founders will be sent to the Simpson Lab to establish the new strain. Genotype of chimeras will be confirmed by PCR, then chimeras will be backcrossed to WT inbred C57BL/6J albino females for one generation. The *FHe9*<sup>+/+</sup> strain will be backcrossed to C57BL/6J wild-type for a minimum of four additional generations (Green and Doolittle, 1963) to generate insipient congenic C57BL/6J-*FHe9*<sup>+/+</sup> (called B6-*FHe9*<sup>+/+</sup>, hereafter). In parallel, chimeras will also be backcrossed to WT inbred 129S1/SvImJ for a minimum of five total generations to generate incipient congenic 129S1/SvImJ-*FHe9*<sup>+/+</sup> (129-*FHe9*<sup>+/+</sup> hereafter) mice. Paralleling the generation of B6-*He9*<sup>+</sup> and 129-*He9*<sup>+</sup> in Chapter 2, we will then phenotype B6-*FHe9*<sup>+/+</sup> and 129-*FHe9*<sup>+/+</sup> by visual inspection and slit lamp imaging to characterize external ocular morphology of mice that are heterozygous for LOF of *Pax6*. We will expect to see phenotypes similar to those observed in *Sey* mice, including microphthalmia, corneal clouding, and neovascularization of the cornea (Hill et al., 1991). Further, based on what we observe in *Sey* mice, that the *Sey* allele on a B6 background results in a more severe phenotype than when the allele is bred on a 129 background (Hickmott et al., 2018), we will expect to see similar differences between the *FHe9*<sup>-</sup> allele bred onto the two genetic backgrounds.

### **3.3.3 Optimization of ABE8e-RNP-LNP therapy in a B6129F1-*FHe9* mouse**

Once the B6129F1-*FHe9* mice are established, we will then conduct *in vivo* studies to determine if the ABE8e-RNP-LNP strategy can rescue *Pax6* expression and prevent blindness in mouse. First, we will perform germline correction of the *FHe9*<sup>-</sup> allele to ensure that correction of

the c.718C>T variant will result in a functional allele. The CRISPR-mediated nature of the generation of the *FHe9<sup>-</sup>* allele could result in additional mutations that may be difficult to detect even by sequencing. We typically sequence 250 bp upstream and downstream from the humanized region, however additional mutations may occur elsewhere in *Pax6* coding regions or non-coding regulatory elements. Germline correction will serve as an initial step to validate that correction of the causal 1 bp variant will restore Pax6 expression and thus prevent the aniridia-like phenotype. This approach has already been validated by the Simpson Lab (Mirjalili Mohanna et al., 2020). I hypothesize that germline correction of c.718C>T by *SpCas9*-RNP HDR in B6129F1-*FHe9* will result in rescued Pax6 protein expression and rescued ocular phenotype in mouse.

To test this, we will set up timed pregnancies with the final breeders described above, using superovulated B6-*He9<sup>+</sup>/He9<sup>+</sup>*, *X<sup>+</sup>/X<sup>+</sup>* females and 129-*FHe9<sup>-</sup>/He9<sup>+</sup>*, *X<sup>lacZ</sup>/Y* males. Females will be plug-checked daily, and on the day that a PC plug is present, zygotes will be harvested and washed of cumulus cells before being placed in culture in KSOM (potassium simplex optimization medium) until the time of injection. The *SpCas9*-RNP complex will be formed and mixed with the ssODN HDR template (oEMS6451) immediately prior to microinjection into the cytoplasm of 0.5-day PC or 1-cell harvested zygotes using the XenoWorks digital microinjection system (Sutter Instrument, Novato, CA). Zygotes microinjected with RNPs and ssODNs will be placed back into KSOM and incubated until transfer into day 0.5 PC pseudopregnant surrogate females. All embryos will be allowed to develop to term. The resulting CRISPR-edited offspring will be characterized by immunohistochemistry (IHC) and western blot analysis to quantify FLAG expression and restoration of Pax6 protein expression. Phenotypic characterization by slit lamp imaging will be

conducted to assess recovery of ocular phenotype to WT morphology in developed offspring (Mirjalili Mohanna et al., 2020). Once we demonstrate functionality of the corrected *FHe9*<sup>-</sup> allele, we can be confident that our novel B6129-*FHe9* mice will serve as a robust model for ABE8e-RNP-LNP therapy development *in vivo*.

To generate “final breeders” for the cross that will be set up to generate offspring for cohorts for *in vivo* ABE therapy optimization studies, we will conduct further breeding to introduce an additional transgene to *FHe9*<sup>-</sup> mice. Here, a cohort is defined as a group of mice with shared characteristics, in this case, genotype, genetic background, age and environment, to control for confounding variables that may influence the outcome of the proposed study (Green and Doolittle, 1963). The genotypes of the final breeders will be B6-*He9*<sup>+/He9</sup><sup>+</sup>, X<sup>+/X</sup><sup>+</sup> and 129-*FHe9*<sup>-/He9</sup><sup>+</sup>, X<sup>lacZ</sup>/Y. To achieve this, 129-*FHe9*<sup>-/+</sup> will be crossed with 129-Hmgcr-lacZ (129-X<sup>lacZ</sup> hereafter), which expresses beta-galactosidase under the direction of the mouse Hmgcr promoter on the X chromosome (Mansour et al., 1990). Hemizygous X<sup>lacZ</sup> males and homozygous X<sup>lacZ</sup> females express beta-galactosidase in all tissues, while heterozygous X<sup>lacZ</sup> females do not express beta-galactosidase in all tissues, due to random X-inactivation (Tan et al., 1993). This enables histological staining and imaging of LSC migration in corneal whole mounts (Basche et al., 2018). This cross will generate a 129-*FHe9*<sup>-/+</sup>, X<sup>lacZ</sup>/X<sup>+</sup> female, which will then be crossed with a 129-*He9*<sup>+/He9</sup><sup>+</sup> male to generate a 129-*Fe9*<sup>-/He9</sup><sup>+</sup>, X<sup>lacZ</sup>/Y male to serve as a final stud to be used to generate cohorts.

The final dam B6-*He9*<sup>+/He9</sup><sup>+</sup>, X<sup>+/X</sup><sup>+</sup> will be crossed with the final stud 129-*FHe9*<sup>-/He9</sup><sup>+</sup>, X<sup>lacZ</sup>/Y to give rise to a cohort of B6129F1 hybrid mice. 50% of the offspring will be heterozygous for the *FHe9*<sup>-</sup> allele and 50% of the offspring will be homozygous for *He9*<sup>+</sup>. All the female offspring will be heterozygous for X<sup>lacZ</sup> and all the male offspring will carry WT sex

chromosomes (Table 3.1). These mice will be called B6129F1-*FHe9* hereafter, for clarity. B6129F1-*FHe9* offspring will be phenotyped by visual inspection and slit lamp imaging in preparation for *in vivo* studies optimizing the ABE8e-RNP-LNP therapy, to ensure that all offspring present with the expected external ocular morphology.

**Table 3.1 Final breeding scheme to generate cohorts for *in vivo* ABE8e-RNP-LNP optimization studies.** Litters are expected to generate 25% of each listed offspring genotype.

<b>Breeders</b>	<b>B6-<i>He9</i><sup>+</sup>/<i>He9</i><sup>+</sup>, X<sup>+</sup>/X<sup>+</sup></b>	<b>129-<i>Fe9</i><sup>+</sup>/<i>He9</i><sup>+</sup>, X<sup>lacZ</sup>/Y</b>
<b>Female offspring</b>	B6129F1- <i>Fe9</i> <sup>+</sup> / <i>He9</i> <sup>+</sup> , X <sup>lacZ</sup> /X <sup>+</sup>	B6129F1- <i>He9</i> <sup>+</sup> / <i>He9</i> <sup>+</sup> , X <sup>lacZ</sup> /X <sup>+</sup>
<b>Male offspring</b>	B6129F1- <i>Fe9</i> <sup>+</sup> / <i>He9</i> <sup>+</sup> , X <sup>+</sup> /Y	B6129F1- <i>He9</i> <sup>+</sup> / <i>He9</i> <sup>+</sup> , X <sup>+</sup> /Y

The cornea is an important therapeutic target due to AAK being a common symptom among patients with aniridia (Latta et al., 2021). More specifically, LSCs are an important target cell for a CRISPR therapy for aniridia as AAK, which is caused by LSC deficiency, is a primary cause of vision loss due to corneal opacification (Schlotzer-Schrehardt et al., 2021). In theory, restoring *PAX6* function in LSCs will ensure that all differentiated daughter cells in the same lineage will carry the corrected *PAX6* allele, and thus will not require complete widespread transfection of the CRISPR therapy to each individual cell in the cornea to have a beneficial therapeutic outcome (Landsend et al., 2021). This approach involves injection directly into the stroma of the cornea, and has been shown to achieve successful transfection of endothelial and stromal cells by CRISPR-RNP LNPs (Mirjalili Mohanna et al., 2022). However, this delivery method has not previously been used for ABE8e-RNP, nor shown to successfully deliver CRISPR-RNPs to the epithelial or LSCs (Mirjalili Mohanna et al., 2022). As such, optimizing parameters of delivery (including dose, time of harvest, and injection location) of our ABE8e-

RNP-LNP strategy to reach the various layers and cell types of the cornea is required. Due to the success of the *ex vivo* experiment detailed in Chapter 2, we will use the same LNP delivery system from Incisive Genetics, Inc.

In the initial *in vivo* study, there will be three conditions tested. The first will be intrastromal injection of ABE8e-RNP-LNP. An “cargoless LNP” group will serve as a negative control. To serve as a positive control, we will treat *ex vivo* cortical neurons with ABE8e-RNP-LNP (described in Chapter 2). For the two injected conditions, 3-month old hybrid B6129-*FHe9*<sup>-</sup>/*He9*<sup>+</sup> and B6129-*He9*<sup>+</sup>/*He9*<sup>+</sup> mice will be treated, and the injector will be blinded to all conditions and mouse genotypes (Table 3.2). B6129-*He9*<sup>+</sup>/*He9*<sup>+</sup> mice will be injected to ensure that the ABE8e-RNP-LNP therapeutic strategy does not cause adverse reactions in a healthy eye. Outcomes of the injected mice will be quantified by molecular, IHC, and phenotypic analyses. All mice will be phenotyped by visual inspection and slit lamp imaging to assess external ocular morphology prior to tissue harvest. Mice will be sacrificed at 1 month and eyes will be enucleated for molecular characterization including Sanger sequencing to quantify genomic editing efficiency in the mouse eye. Mice will be sacrificed at 1 month and utilized for IHC of sectioned eyes and confocal imaging of cryosections to assess FLAG and Pax6 expression. Confocal imaging will be followed by stereological quantification of FLAG and Pax6 expression. Mice will be harvested at five months for histological analysis of lacZ staining and imaging of beta-galactosidase patterning to demonstrate LSC migration in corneal whole mounts. Cortical neurons from the positive control group will be harvested and characterized by Sanger sequencing and ICC to assess FLAG and Pax6 expression. Confocal imaging will be followed by stereological quantification of FLAG and Pax6 expression (described in Chapter 2).

**Table 3.2 Experimental design for *in vivo* ABE8e-RNP-LNP therapy optimization study.**

<b>Experimental group</b>	<b>Delivery method</b>	<b>Genotype</b>	<b>Analysis method</b>
<b>ABE therapy</b>	Intrastromal injection	<i>He9<sup>+</sup>/He9<sup>+</sup></i> <i>FHe9<sup>+</sup>/He9<sup>+</sup></i>	Molecular Histology lacZ
<b>Cargoless LNP vector control</b>	Intrastromal injection	<i>He9<sup>+</sup>/He9<sup>+</sup></i> <i>FHe9<sup>+</sup>/He9<sup>+</sup></i>	Molecular Histology lacZ
<b>ABE8e positive control</b>	<i>Ex vivo</i> cortical neurons	<i>FHe9<sup>+</sup>/He9<sup>+</sup></i>	Molecular Histology

The proposed studies will serve as the necessary work required in the development and optimization of an ABE8e-RNP-LNP therapy to treat patients with aniridia. Optimization of the ABE8e-RNP-LNP therapy in a 3xFLAG-tagged humanized aniridia mouse will show the efficacy and safety necessary to demonstrate the suitability of translating the therapy to humans. Here, we propose a study to successfully prevent blindness in a humanized aniridic mouse, thus laying the foundation for pursuing further pre-clinical studies, prior to a Phase I/II clinical trial in human patients with aniridia.

### **3.4 CONCLUSION**

Overall, the work proposed here outlines the future preclinical research required to translate our *in vitro*-optimized ABE8e-RNP-LNP therapy to *in vivo* in mouse. This therapy aims to correct the most recurrent aniridia variant, c.718C>T (Fokkema et al., 2011; Guo et al., 2022; Kit et al., 2021; Tyner et al., 2017). This work lays the foundation for streamlining the development of additional CRISPR-based therapies to treat this currently incurable ocular disease. While there are many obstacles that lie ahead, we are confident that we present a

promising therapeutic strategy, and with optimism, a future curative intervention to prevent blindness in patients with aniridia.

## REFERENCES

- Abdolkarimi, D., Cunha, D.L., Lahne, M., and Moosajee, M. (2022). PAX6 disease models for aniridia. *Indian J Ophthalmol* 70, 4119-4129, PMID 36453299.
- Ahmad, S. (2012). Concise review: limbal stem cell deficiency, dysfunction, and distress. *Stem Cells Transl Med* 1, 110-115, PMID 23197757.
- Alves, C.R.R., Ha, L.L., Yaworski, R., Lazzarotto, C.R., Christie, K.A., Reilly, A., Beauvais, A., Doll, R.M., de la Cruz, D., Maguire, C.A., *et al.* (2023). Base editing as a genetic treatment for spinal muscular atrophy. *bioRxiv*, PMID 36711797.
- Anzalone, A.V., Randolph, P.B., Davis, J.R., Sousa, A.A., Koblan, L.W., Levy, J.M., Chen, P.J., Wilson, C., Newby, G.A., Raguram, A., *et al.* (2019). Search-and-replace genome editing without double-strand breaks or donor DNA. *Nature* 576, 149-157, PMID 31634902.
- Ashery-Padan, R., Marquardt, T., Zhou, X., and Gruss, P. (2000). Pax6 activity in the lens primordium is required for lens formation and for correct placement of a single retina in the eye. *Genes Dev* 14, 2701-2711, PMID 11069887.
- Atkins, A., Chung, C.H., Allen, A.G., Dampier, W., Gurrola, T.E., Sariyer, I.K., Nonnemacher, M.R., and Wigdahl, B. (2021). Off-Target Analysis in Gene Editing and Applications for Clinical Translation of CRISPR/Cas9 in HIV-1 Therapy. *Front Genome Ed* 3, 673022, PMID 34713260.
- Azuma, N., Hotta, Y., Tanaka, H., and Yamada, M. (1998). Missense mutations in the PAX6 gene in aniridia. *Invest Ophthalmol Vis Sci* 39, 2524-2528, PMID 9856761.
- Bales, T.R., Lopez, M.J., and Clark, J. (2023). Embryology, Eye. In *StatPearls (Treasure Island (FL))* PMID: 30860715.
- Basche, M., Kampik, D., Kawasaki, S., Branch, M.J., Robinson, M., Larkin, F., Smith, A.J., and Ali, R.R. (2018). Sustained and widespread gene delivery to the corneal epithelium via in situ transduction of limbal epithelial stem cells using lentiviral and AAV vectors. *Hum Gene Ther* 29, 1140-1152, PMID 30070149.

- Bhatia, S., Bengani, H., Fish, M., Brown, A., Divizia, M.T., de Marco, R., Damante, G., Grainger, R., van Heyningen, V., and Kleinjan, D.A. (2013). Disruption of Autoregulatory Feedback by a Mutation in a Remote, Ultraconserved PAX6 Enhancer Causes Aniridia. *Am J Hum Genet* 93, 1126-1134, PMID 24290376.
- Blanco-Kelly, F., Tarilonte, M., Villamar, M., Damian, A., Tamayo, A., Moreno-Pelayo, M.A., Ayuso, C., and Corton, M. (2021). Genetics and epidemiology of aniridia: Updated guidelines for genetic study. *Arch Soc Esp Oftalmol (Engl Ed)* 96 *Suppl 1*, 4-14, PMID 34836588.
- Bobba, S., Chow, S., Watson, S., and Di Girolamo, N. (2015). Clinical outcomes of xeno-free expansion and transplantation of autologous ocular surface epithelial stem cells via contact lens delivery: a prospective case series. *Stem Cell Res Ther* 6, 23, PMID 25889475.
- Bradley, A., Evans, M., Kaufman, M.H., and Robertson, E. (1984). Formation of germ-line chimaeras from embryo-derived teratocarcinoma cell lines. *Nature* 309, 255-256, PMID 6717601.
- Cao, X., Guo, J., Huang, S., Yu, W., Li, G., An, L., Li, X., Tao, W., Liu, Q., Huang, X., *et al.* (2022). Engineering of near-PAMless adenine base editor with enhanced editing activity and reduced off-target. *Mol Ther Nucleic Acids* 28, 732-742, PMID 35664696.
- Chamberlain, K., Riyad, J.M., and Weber, T. (2016). Expressing Transgenes That Exceed the Packaging Capacity of Adeno-Associated Virus Capsids. *Hum Gene Ther Methods* 27, 1-12, PMID 26757051.
- Chauhan, B.K., Yang, Y., Cveklova, K., and Cvekl, A. (2004). Functional properties of natural human PAX6 and PAX6(5a) mutants. *Invest Ophthalmol Vis Sci* 45, 385-392, PMID 14744876.
- Chen, Q., Zhang, Y., and Yin, H. (2021). Recent advances in chemical modifications of guide RNA, mRNA and donor template for CRISPR-mediated genome editing. *Adv Drug Deliv Rev* 168, 246-258, PMID 33122087.

- Cheng, F., Song, W., Kang, Y., Yu, S., and Yuan, H. (2011). A 556 kb deletion in the downstream region of the PAX6 gene causes familial aniridia and other eye anomalies in a Chinese family. *Molecular vision* *17*, 448-455, PMID 21321669.
- Chow, R.L., and Lang, R.A. (2001). Early eye development in vertebrates. *Annu Rev Cell Dev Biol* *17*, 255-296, PMID 11687490.
- Cole, J.D., McHaney, K.M., Rabiee, B., Gao, J., Rodriguez, C., Miller, D.A., Liu, M., Grannonico, M., Norat, P., Zhang, H.F., *et al.* (2022). Long-term retinal protection by MEK inhibition in Pax6 haploinsufficiency mice. *Exp Eye Res* *218*, 109012, PMID 35245513.
- Collinson, J.M., Hill, R.E., and West, J.D. (2000). Different roles for Pax6 in the optic vesicle and facial epithelium mediate early morphogenesis of the murine eye. *Development* *127*, 945-956, PMID 10662634.
- Cox, D.B., Platt, R.J., and Zhang, F. (2015). Therapeutic genome editing: prospects and challenges. *Nat Med* *21*, 121-131, PMID 25654603.
- Crolla, J.A., and van Heyningen, V. (2002). Frequent chromosome aberrations revealed by molecular cytogenetic studies in patients with aniridia. *Am J Hum Genet* *71*, 1138-1149, PMID 12386836.
- Cvekl, A., and Callaerts, P. (2016). PAX6: 25th anniversary and more to learn. *Exp Eye Res* *156*, 10-21, PMID 27126352.
- Dalkara, D., and Sahel, J.A. (2014). Gene therapy for inherited retinal degenerations. *C R Biol* *337*, 185-192, PMID 24702845.
- Dansault, A., David, G., Schwartz, C., Jaliffa, C., Vieira, V., de la Houssaye, G., Bigot, K., Catin, F., Tattu, L., Chopin, C., *et al.* (2007). Three new PAX6 mutations including one causing an unusual ophthalmic phenotype associated with neurodevelopmental abnormalities. *Molecular vision* *13*, 511-523, PMID 17417613.

- Daruich, A., Duncan, M., Robert, M.P., Lagali, N., Semina, E.V., Aberdam, D., Ferrari, S., Romano, V., des Roziers, C.B., Benkortebi, R., *et al.* (2022). Congenital aniridia beyond black eyes: From phenotype and novel genetic mechanisms to innovative therapeutic approaches. *Prog Retin Eye Res*, 101133, PMID 36280537.
- de Paiva, C.S., Pflugfelder, S.C., Ng, S.M., and Akpek, E.K. (2019). Topical cyclosporine A therapy for dry eye syndrome. *Cochrane Database Syst Rev* 9, CD010051, PMID 31517988.
- Diacou, R., Nandigrami, P., Fiser, A., Liu, W., Ashery-Padan, R., and Cvekl, A. (2022). Cell fate decisions, transcription factors and signaling during early retinal development. *Prog Retin Eye Res* 91, 101093, PMID 35817658.
- Dong, J.Y., Fan, P.D., and Frizzell, R.A. (1996). Quantitative analysis of the packaging capacity of recombinant adeno-associated virus. *Hum Gene Ther* 7, 2101-2112, PMID 8934224.
- Du, Y., Xie, W., Zhang, F., and Liu, C. (2019). Chimeric Mouse Generation by ES Cell Blastocyst Microinjection and Uterine Transfer. *Methods Mol Biol* 1874, 99-114, PMID 30353510.
- Duan, D., Fu, Y., Paxinos, G., and Watson, C. (2013). Spatiotemporal expression patterns of Pax6 in the brain of embryonic, newborn, and adult mice. *Brain Struct Funct* 218, 353-372, PMID 22354470.
- Echelard, Y., Epstein, D.J., St Jacques, B., Shen, L., Mohler, J., McMahon, J.A., and McMahon, A.P. (1993). Sonic hedgehog, a member of a family of putative signaling molecules, is implicated in the regulation of CNS polarity. *Cell* 75, 1417-1430, PMID 7916661.
- Eming, R., Visconti, K., Hall, F., Sekine, C., Kobayashi, K., Chen, Q., Cope, A., Kanazawa, S., Peterlin, M., Rijnders, A., *et al.* (2002). Humanized mice as a model for rheumatoid arthritis. *Arthritis Res* 4 Suppl 3, S133-140, PMID 12110132.
- European Medicines Agency (2012). European Medicines Agency recommends first gene therapy for approval (London, UK), pp. Glybera offers new medical treatment for

- patients with severe or multiple pancreatitis attacks due to lipoprotein lipase deficiency., PMID NA.
- Finn, J.D., Smith, A.R., Patel, M.C., Shaw, L., Youniss, M.R., van Heteren, J., Dirstine, T., Ciullo, C., Lescarbeau, R., Seitzer, J., *et al.* (2018). A Single Administration of CRISPR/Cas9 Lipid Nanoparticles Achieves Robust and Persistent In Vivo Genome Editing. *Cell Rep* 22, 2227-2235, PMID 29490262.
- Fokkema, I.F., Taschner, P.E., Schaafsma, G.C., Celli, J., Laros, J.F., and den Dunnen, J.T. (2011). LOVD v.2.0: the next generation in gene variant databases. *Hum Mutat* 32, 557-563, PMID 21520333.
- Gaudelli, N.M., Komor, A.C., Rees, H.A., Packer, M.S., Badran, A.H., Bryson, D.I., and Liu, D.R. (2017). Programmable base editing of A\*T to G\*C in genomic DNA without DNA cleavage. *Nature* 551, 464-471, PMID 29160308.
- Gertsenstein, M., Mianne, J., Teboul, L., and Nutter, L.M.J. (2020). Targeted Mutations in the Mouse via Embryonic Stem Cells. *Methods Mol Biol* 2066, 59-82, PMID 31512207.
- Gillmore, J.D., Gane, E., Taubel, J., Kao, J., Fontana, M., Maitland, M.L., Seitzer, J., O'Connell, D., Walsh, K.R., Wood, K., *et al.* (2021). CRISPR-Cas9 In Vivo Gene Editing for Transthyretin Amyloidosis. *N Engl J Med* 385, 493-502, PMID 34215024.
- Gius, I., Tozzi, L., De Biasi, C.S., Pizzolon, T., Parolini, B., and Frisina, R. (2023). Artificial iris: state of the art. *J Cataract Refract Surg* 49, 430-437, PMID 36719472.
- Glaser, T., Walton, D.S., and Maas, R.L. (1992). Genomic structure, evolutionary conservation and aniridia mutations in the human PAX6 gene. *Nat Genet* 2, 232-239, PMID 1345175.
- Grant, M.K., Bobilev, A.M., Branch, A., and Lauderdale, J.D. (2021). Structural and functional consequences of PAX6 mutations in the brain: implications for aniridia. *Brain Res* 1756, 147283, PMID 33515537.
- Graw, J. (2010). Eye Development. *Curr Top Dev Biol* 90C, 343-386, PMID 20691855.

- Green, E.L., and Doolittle, D.P. (1963). Theoretical consequences of systems of mating used in mammalian genetics. In *Methodology in Mammalian Genetics*, W.J. Burdette, ed. (San Francisco, Holden-Day), pp. 3-41.
- Gregory-Evans, C.Y., Wang, X., Wasan, K.M., Zhao, J., Metcalfe, A.L., and Gregory-Evans, K. (2013). Postnatal manipulation of Pax6 dosage reverses congenital tissue malformation defects. *J Clin Invest* 124, 111-116, PMID 24355924.
- Gruntman, A.M., and Flotte, T.R. (2018). The rapidly evolving state of gene therapy. *FASEB J* 32, 1733-1740, PMID 31282760.
- Guo, R., Zhang, X., Liu, A., Ji, J., and Liu, W. (2022). Novel clinical presentation and PAX6 mutation in families with congenital aniridia. *Front Med (Lausanne)* 9, 1042588, PMID 36582291.
- Guse, K., Suzuki, M., Sule, G., Bertin, T.K., Tynismaa, H., Ahola-Erkkila, S., Palmer, D., Suomalainen, A., Ng, P., Cerullo, V., *et al.* (2012). Capsid-modified adenoviral vectors for improved muscle-directed gene therapy. *Hum Gene Ther* 23, 1065-1070, PMID 22888960.
- Haideri, T., Howells, A., Jiang, Y., Yang, J., Bao, X., and Lian, X.L. (2022). Robust genome editing via modRNA-based Cas9 or base editor in human pluripotent stem cells. *Cell Rep Methods* 2, 100290, PMID 36160051.
- Han, I.C., Burnight, E.R., Ulferts, M.J., Worthington, K.S., Russell, S.R., Sohn, E.H., Mullins, R.F., Stone, E.M., Tucker, B.A., and Wiley, L.A. (2019). Helper-Dependent Adenovirus Transduces the Human and Rat Retina but Elicits an Inflammatory Reaction When Delivered Subretinally in Rats. *Hum Gene Ther* 30, 1371-1384, PMID 31456426.
- Han, J.C., Liu, Q.R., Jones, M., Levinn, R.L., Menzie, C.M., Jefferson-George, K.S., Adler-Wailes, D.C., Sanford, E.L., Lacbawan, F.L., Uhl, G.R., *et al.* (2008). Brain-derived neurotrophic factor and obesity in the WAGR syndrome. *N Engl J Med* 359, 918-927, PMID 18753648.

- Han, J.P., Kim, M., Choi, B.S., Lee, J.H., Lee, G.S., Jeong, M., Lee, Y., Kim, E.A., Oh, H.K., Go, N., *et al.* (2022). In vivo delivery of CRISPR-Cas9 using lipid nanoparticles enables antithrombin gene editing for sustainable hemophilia A and B therapy. *Sci Adv* 8, eabj6901, PMID 35061543.
- Hanson, I.M. (2003). PAX6 and congenital eye malformations. *Pediatr Res* 54, 791-796, PMID 14561779.
- Hart, A.W., Mella, S., Mendrychowski, J., van Heyningen, V., and Kleinjan, D.A. (2013). The developmental regulator Pax6 is essential for maintenance of islet cell function in the adult mouse pancreas. *PLoS ONE* 8, e54173, PMID 23326594.
- Heavner, W., and Pevny, L. (2012). Eye development and retinogenesis. *Cold Spring Harb Perspect Biol* 4, a008391, PMID 23071378.
- Herrera-Barrera, M., Ryals, R.C., Gautam, M., Jozic, A., Landry, M., Korzun, T., Gupta, M., Acosta, C., Stoddard, J., Reynaga, R., *et al.* (2023). Peptide-guided lipid nanoparticles deliver mRNA to the neural retina of rodents and nonhuman primates. *Sci Adv* 9, eadd4623, PMID 36630502.
- Hever, A.M., Williamson, K.A., and van Heyningen, V. (2006). Developmental malformations of the eye: the role of PAX6, SOX2 and OTX2. *Clin Genet* 69, 459-470, PMID 16712695.
- Hickmott, J.W., Gunawardane, U., Jensen, K., Korecki, A.J., and Simpson, E.M.a. (2018). Epistasis between *PAX6<sup>Sev</sup>* and genetic background reinforces the value of defined hybrid mouse models for therapeutic trials. *Gene Therapy* 25, 524-537, PMID 30258099.
- Hill, R.E., Favor, J., Hogan, B.L., Ton, C.C., Saunders, G.F., Hanson, I.M., Prosser, J., Jordan, T., Hastie, N.D., and van Heyningen, V. (1991). Mouse small eye results from mutations in a paired-like homeobox-containing gene. *Nature* 354, 522-525, PMID 1684639.
- Hingorani, M., Hanson, I., and van Heyningen, V. (2012). Aniridia. *Eur J Hum Genet* 20, 1011-1017, PMID 22692063.

- Hogan, B.L., Horsburgh, G., Cohen, J., Hetherington, C.M., Fisher, G., and Lyon, M.F. (1986). Small eyes (Sey): a homozygous lethal mutation on chromosome 2 which affects the differentiation of both lens and nasal placodes in the mouse. *J Embryol Exp Morphol* 97, 95-110, PMID 3794606.
- Holland, E.J., Djalilian, A.R., and Schwartz, G.S. (2003). Management of aniridic keratopathy with keratolimbic allograft: a limbal stem cell transplantation technique. *Ophthalmology* 110, 125-130, PMID 12511357.
- Huang, T.P., Newby, G.A., and Liu, D.R. (2021). Precision genome editing using cytosine and adenine base editors in mammalian cells. *Nat Protoc* 16, 1089-1128, PMID 33462442.
- Jang, H.K., Jo, D.H., Lee, S.N., Cho, C.S., Jeong, Y.K., Jung, Y., Yu, J., Kim, J.H., Woo, J.S., and Bae, S. (2021). High-purity production and precise editing of DNA base editing ribonucleoproteins. *Sci Adv* 7, eabg2661, PMID 34452911.
- Jinek, M., Chylinski, K., Fonfara, I., Hauer, M., Doudna, J.A., and Charpentier, E. (2012). A programmable dual-RNA-guided DNA endonuclease in adaptive bacterial immunity. *Science* 337, 816-821, PMID 22745249.
- Jo, D.H., Jang, H.K., Cho, C.S., Han, J.H., Ryu, G., Jung, Y., Bae, S., and Kim, J.H. (2023). Visual function restoration in a mouse model of Leber congenital amaurosis via therapeutic base editing. *Mol Ther Nucleic Acids* 31, 16-27, PMID 36589710.
- Kim, D., Bae, S., Park, J., Kim, E., Kim, S., Yu, H.R., Hwang, J., Kim, J.I., and Kim, J.S. (2015). Digenome-seq: genome-wide profiling of CRISPR-Cas9 off-target effects in human cells. *Nat Methods*, PMID 25664545.
- Kit, V., Lima Cunha, D., Hagag, A.M., and Moosajee, M. (2021). Longitudinal genotype-phenotype analysis in 86 PAX6-related aniridia patients. *JCI Insight* 6, e148406, PMID 34101622.
- Kleinjan, D.A., Seawright, A., Mella, S., Carr, C.B., Tyas, D.A., Simpson, T.I., Mason, J.O., Price, D.J., and van Heyningen, V. (2006). Long-range downstream enhancers are essential for Pax6 expression. *Dev Biol* 299, 563-581, PMID 17014839.

- Kleinstiver, B.P., Pattanayak, V., Prew, M.S., Tsai, S.Q., Nguyen, N.T., Zheng, Z., and Joung, J.K. (2016). High-fidelity CRISPR-Cas9 nucleases with no detectable genome-wide off-target effects. *Nature* 529, 490-495, PMID 26735016.
- Klimova, L., and Kozmik, Z. (2014). Stage-dependent requirement of neuroretinal Pax6 for lens and retina development. *Development* 141, 1292-1302, PMID 24523460.
- Kluesner, M.G., Nedveck, D.A., Lahr, W.S., Garbe, J.R., Abrahante, J.E., Webber, B.R., and Moriarity, B.S. (2018). EditR: A Method to Quantify Base Editing from Sanger Sequencing. *CRISPR J* 1, 239-250, PMID 31021262.
- Koblan, L.W., Erdos, M.R., Wilson, C., Cabral, W.A., Levy, J.M., Xiong, Z.M., Tavaréz, U.L., Davison, L.M., Gete, Y.G., Mao, X., *et al.* (2021). In vivo base editing rescues Hutchinson-Gilford progeria syndrome in mice. *Nature* 589, 608-614, PMID 33408413.
- Komor, A.C., Kim, Y.B., Packer, M.S., Zuris, J.A., and Liu, D.R. (2016). Programmable editing of a target base in genomic DNA without double-stranded DNA cleavage. *Nature* 533, 420-424, PMID 27096365.
- Kulcsar, P.I., Talas, A., Ligeti, Z., Krausz, S.L., and Welker, E. (2022). SuperFi-Cas9 exhibits remarkable fidelity but severely reduced activity yet works effectively with ABE8e. *Nat Commun* 13, 6858, PMID 36369279.
- Lagali, N., Wowra, B., Fries, F.N., Latta, L., Moslemani, K., Utheim, T.P., Wylegala, E., Seitz, B., and Kasmann-Kellner, B. (2019). Early phenotypic features of aniridia-associated keratopathy and association with PAX6 coding mutations. *Ocul Surf* 18, 130-140, PMID 31734509.
- Landrum, M.J., Lee, J.M., Benson, M., Brown, G., Chao, C., Chitipiralla, S., Gu, B., Hart, J., Hoffman, D., Hoover, J., *et al.* (2016). ClinVar: public archive of interpretations of clinically relevant variants. *Nucleic Acids Res* 44, D862-868, PMID 26582918.
- Landsend, E.C.S., Lagali, N., and Utheim, T.P. (2021). Congenital Aniridia - A Comprehensive Review of Clinical Features and Therapeutic Approach. *Surv Ophthalmol* 66, 1031-1050, PMID 33675823.

- Latta, L., Figueiredo, F.C., Ashery-Padan, R., Collinson, J.M., Daniels, J., Ferrari, S., Szentmary, N., Sola, S., Shalom-Feuerstein, R., Lako, M., *et al.* (2021). Pathophysiology of aniridia-associated keratopathy: Developmental aspects and unanswered questions. *Ocul Surf* 22, 245-266, PMID 34520870.
- Lee, S., Lee, S.H., Heo, H., Oh, E.H., Shin, J.H., Kim, H.S., Jung, J.H., Choi, S.Y., Choi, K.D., Lee, H., *et al.* (2020). Impaired DNA-binding affinity of novel PAX6 mutations. *Sci Rep* 10, 3062, PMID 32080308.
- Li, C., Georgakopoulou, A., Newby, G.A., Everette, K.A., Nizamis, E., Paschoudi, K., Vlachaki, E., Gil, S., Anderson, A.K., Koob, T., *et al.* (2022). In vivo base editing by a single intravenous vector injection for treatment of hemoglobinopathies. *JCI Insight* 7, e162939 PMID 36006707.
- Li, H., Yang, Y., Hong, W., Huang, M., Wu, M., and Zhao, X. (2020). Applications of genome editing technology in the targeted therapy of human diseases: mechanisms, advances and prospects. *Signal Transduct Target Ther* 5, 1, PMID 32296011.
- Li, T., Yang, Y., Qi, H., Cui, W., Zhang, L., Fu, X., He, X., Liu, M., Li, P.F., and Yu, T. (2023). CRISPR/Cas9 therapeutics: progress and prospects. *Signal Transduct Target Ther* 8, 36, PMID 36646687.
- Liang, C.L., Hsi, E., Chen, K.C., Pan, Y.R., Wang, Y.S., and Juo, S.H. (2011). A functional polymorphism at 3'UTR of the PAX6 gene may confer risk for extreme myopia in the Chinese. *Invest Ophthalmol Vis Sci* 52, 3500-3505, PMID 21421876.
- Lima Cunha, D., Arno, G., Corton, M., and Moosajee, M. (2019). The Spectrum of PAX6 Mutations and Genotype-Phenotype Correlations in the Eye. *Genes (Basel)* 10, 1050, PMID 31861090.
- Lima Cunha, D., Owen, N., Taylor, V., Corton, M., Theodorou, M., and Moosajee, M. (2020). PAX6 missense variants in two families with isolated foveal hypoplasia and nystagmus: evidence of paternal postzygotic mosaicism. *Eur J Hum Genet* 29, 349-355, PMID 33024313.

- Lundstrom, K. (2019). Gene Therapy Today and Tomorrow. *Diseases* 7, 37, PMID 31035350.
- Maeder, M.L., Stefanidakis, M., Wilson, C.J., Baral, R., Barrera, L.A., Bounoutas, G.S., Bumcrot, D., Chao, H., Ciulla, D.M., DaSilva, J.A., *et al.* (2019). Development of a gene-editing approach to restore vision loss in Leber congenital amaurosis type 10. *Nat Med* 25, 229-233, PMID 30664785.
- Maguire, A.M., Russell, S., Chung, D.C., Yu, Z.F., Tillman, A., Drack, A.V., Simonelli, F., Leroy, B.P., Reape, K.Z., High, K.A., *et al.* (2021). Durability of Voretigene Neparvovec for Biallelic RPE65-Mediated Inherited Retinal Disease: Phase 3 Results at 3 and 4 Years. *Ophthalmology* 128, 1460-1468, PMID 33798654.
- Mansour, S., KR, T., CX, D., and MR, C. (1990). Introduction of a *lacZ* reporter gene into the mouse *int-2* locus by homologous recombination. *Proceedings of the National Academy of Sciences USA* 87, 7688-7682, PMID.
- Mathew, S.M. (2023). Strategies for generation of mice via CRISPR/HDR-mediated knock-in. *Mol Biol Rep* 50, 3189-3204, PMID 36701041.
- Mendell, J.R., Al-Zaidy, S.A., Rodino-Klapac, L.R., Goodspeed, K., Gray, S.J., Kay, C.N., Boye, S.L., Boye, S.E., George, L.A., Salabarria, S., *et al.* (2020). Current Clinical Applications of in vivo Gene Therapy with AAVs. *Mol Ther* 29, 464-488, PMID 33309881.
- Mirjalili Mohanna, S.Z., Hickmott, J.W., Lam, S.L., Chiu, N.Y., Lengyell, T.C., Tam, B.M., Moritz, O.L., and Simpson, E.M. (2020). Germline CRISPR/Cas9-Mediated Gene Editing Prevents Vision Loss in a Novel Mouse Model of Aniridia. *Mol Ther Methods Clin Dev* 17, 478-490, PMID 32258211.
- Mirjalili Mohanna, S.Z.M., Djaksigulova, D., Hill, A.M., Wagner, P.K., Simpson, E.M., and Leavitt, B.R. (2022). LNP-mediated delivery of CRISPR RNP for wide-spread in vivo genome editing in mouse cornea. *J Control Release* 350, 401-413, PMID 36029893.

- Moosajee, M., Hingorani, M., and Moore, A.T. (1993). PAX6-Related Aniridia. In GeneReviews((R)), M.P. Adam, H.H. Ardinger, R.A. Pagon, S.E. Wallace, L.J.H. Bean, K. Stephens, and A. Amemiya, eds. (Seattle (WA)) PMID: 20301534.
- Nakagawa, Y., Sakuma, T., Sakamoto, T., Ohmuraya, M., Nakagata, N., and Yamamoto, T. (2015). Production of knockout mice by DNA microinjection of various CRISPR/Cas9 vectors into freeze-thawed fertilized oocytes. *BMC Biotechnol* 15, 33, PMID 25997509.
- Newby, G.A., Yen, J.S., Woodard, K.J., Mayuranathan, T., Lazzarotto, C.R., Li, Y., Sheppard-Tillman, H., Porter, S.N., Yao, Y., Mayberry, K., *et al.* (2021). Base editing of haematopoietic stem cells rescues sickle cell disease in mice. *Nature* 595, 295-302, PMID 34079130.
- Nishina, S., Kohsaka, S., Yamaguchi, Y., Handa, H., Kawakami, A., Fujisawa, H., and Azuma, N. (1999). PAX6 expression in the developing human eye. *Br J Ophthalmol* 83, 723-727, PMID 10340984.
- Papaiouannou, V.E., McBurney, M.W., Gardner, R.L., and Evans, M.J. (1975). Fate of teratocarcinoma cells injected into early mouse embryos. *Nature* 258, 70-73, PMID 1186881.
- Papanikolaou, E., and Bosio, A. (2021). The Promise and the Hope of Gene Therapy. *Front Genome Ed* 3, 618346, PMID 34713249.
- Pedersen, H.R., Baraas, R.C., Landsend, E.C.S., Utheim, O.A., Utheim, T.P., Gilson, S.J., and Neitz, M. (2020). PAX6 Genotypic and Retinal Phenotypic Characterization in Congenital Aniridia. *Invest Ophthalmol Vis Sci* 61, 14, PMID 32396632.
- Peeters, S.B., Korecki, A.J., Simpson, E.M., and Brown, C.J. (2018). Human cis-acting elements regulating escape from X-chromosome inactivation function in mouse. *Hum Mol Genet*, PMID 29401310.
- Plaisancie, J., Tarilonte, M., Ramos, P., Jeanton-Scaramouche, C., Gaston, V., Dollfus, H., Aguilera, D., Kaplan, J., Fares-Taie, L., Blanco-Kelly, F., *et al.* (2018). Implication of non-coding PAX6 mutations in aniridia. *Hum Genet* 137, 831-846, PMID 30291432.

- Platt, R.J., Chen, S., Zhou, Y., Yim, M.J., Swiech, L., Kempton, H.R., Dahlman, J.E., Parnas, O., Eisenhaure, T.M., Jovanovic, M., *et al.* (2014). CRISPR-Cas9 Knockin Mice for Genome Editing and Cancer Modeling. *Cell* 159, 440-455, PMID 25263330.
- Polisetti, N., Schlunck, G., and Reinhard, T. (2023). PAX6 Expression Patterns in the Adult Human Limbal Stem Cell Niche. *Cells* 12, 400, PMID 36766742.
- Porter, F.D., Drago, J., Xu, Y., Cheema, S.S., Wassif, C., Huang, S.P., Lee, E., Grinberg, A., Massalas, J.S., Bodine, D., *et al.* (1997). Lhx2, a LIM homeobox gene, is required for eye, forebrain, and definitive erythrocyte development. *Development* 124, 2935-2944, PMID 9247336.
- Ran, F.A., Cong, L., Yan, W.X., Scott, D.A., Gootenberg, J.S., Kriz, A.J., Zetsche, B., Shalem, O., Wu, X., Makarova, K.S., *et al.* (2015). In vivo genome editing using *Staphylococcus aureus* Cas9. *Nature* 520, 186-191, PMID 25830891.
- Ran, F.A., Hsu, P.D., Wright, J., Agarwala, V., Scott, D.A., and Zhang, F. (2013). Genome engineering using the CRISPR-Cas9 system. *Nat Protoc* 8, 2281-2308, PMID 24157548.
- Richardson, R., Tracey-White, D., Webster, A., and Moosajee, M. (2017). The zebrafish eye-a paradigm for investigating human ocular genetics. *Eye (Lond)* 31, 68-86, PMID 27612182.
- Richter, M.F., Zhao, K.T., Eton, E., Lapinaite, A., Newby, G.A., Thuronyi, B.W., Wilson, C., Koblan, L.W., Zeng, J., Bauer, D.E., *et al.* (2020). Phage-assisted evolution of an adenine base editor with improved Cas domain compatibility and activity. *Nat Biotechnol* 38, 883-891, PMID 32433547.
- Roberts, R.C. (1967). Small-eyes, a new dominant mutant in the mouse. *Genet Res* 9, 121-122, PMID.
- Rosenberg, S.A., Aebersold, P., Cornetta, K., Kasid, A., Morgan, R.A., Moen, R., Karson, E.M., Lotze, M.T., Yang, J.C., Topalian, S.L., *et al.* (1990). Gene transfer into humans--immunotherapy of patients with advanced melanoma, using tumor-infiltrating

- lymphocytes modified by retroviral gene transduction. *N Engl J Med* 323, 570-578, PMID 2381442.
- Salman, M., Verma, A., Singh, V.K., Jaffet, J., Chaurasia, S., Sahel, D.K., Ramappa, M., and Singh, V. (2022). New Frontier in the Management of Corneal Dystrophies: Basics, Development, and Challenges in Corneal Gene Therapy and Gene Editing. *Asia Pac J Ophthalmol (Phila)* 11, 346-359, PMID 36041149.
- Sannan, N.S., Gregory-Evans, C.Y., Lyons, C.J., Lehman, A.M., Langlois, S., Warner, S.J., Zakrzewski, H., and Gregory-Evans, K. (2017). Correlation of novel PAX6 gene abnormalities in aniridia and clinical presentation. *Can J Ophthalmol* 52, 570-577, PMID 29217025.
- Sasamoto, Y., Hayashi, R., Park, S.J., Saito-Adachi, M., Suzuki, Y., Kawasaki, S., Quantock, A.J., Nakai, K., Tsujikawa, M., and Nishida, K. (2016). PAX6 Isoforms, along with Reprogramming Factors, Differentially Regulate the Induction of Cornea-specific Genes. *Sci Rep* 6, 20807, PMID 26899008.
- Schlotzer-Schrehardt, U., Latta, L., Giessl, A., Zenkel, M., Fries, F.N., Kasmann-Kellner, B., Kruse, F.E., and Seitz, B. (2021). Dysfunction of the limbal epithelial stem cell niche in aniridia-associated keratopathy. *Ocul Surf* 21, 160-173, PMID 34102310.
- Schmahl, W., Knoedlseder, M., Favor, J., and Davidson, D. (1993). Defects of neuronal migration and the pathogenesis of cortical malformations are associated with Small eye (Sey) in the mouse, a point mutation at the Pax-6-locus. *Acta Neuropathol* 86, 126-135, PMID 8213068.
- Scott, L.J. (2015). Alipogene tiparvovec: a review of its use in adults with familial lipoprotein lipase deficiency. *Drugs* 75, 175-182, PMID 25559420.
- Shao, Y., Wang, L., Guo, N., Wang, S., Yang, L., Li, Y., Wang, M., Yin, S., Han, H., Zeng, L., *et al.* (2018). Cas9-nickase-mediated genome editing corrects hereditary tyrosinemia in rats. *J Biol Chem* 293, 6883-6892, PMID 29507093.

- Sheriff, A., Guri, I., Zebrowska, P., Llopis-Hernandez, V., Brooks, I.R., Tekkela, S., Subramaniam, K., Gebrezgabher, R., Naso, G., Petrova, A., *et al.* (2022). ABE8e adenine base editor precisely and efficiently corrects a recurrent COL7A1 nonsense mutation. *Sci Rep* 12, 19643, PMID 36385635.
- Shin, J.W., Hong, E.P., Park, S.S., Choi, D.E., Seong, I.S., Whittaker, M.N., Kleinstiver, B.P., Chen, R.Z., and Lee, J.M. (2022). Allele-specific silencing of the gain-of-function mutation in Huntington's disease using CRISPR/Cas9. *JCI Insight* 7, e141042, PMID 36040815.
- Song, H., Ahn, J.Y., Yan, F., Ran, Y., Koo, O., and Lee, G.J. (2022). Genetic Dissection of CRISPR-Cas9 Mediated Inheritance of Independently Targeted Alleles in Tobacco alpha-1,3-Fucosyltransferase 1 and beta-1,2-Xylosyltransferase 1 Loci. *Int J Mol Sci* 23, PMID 35269602.
- Tan, S.S., Williams, E.A., and Tam, P.P. (1993). X-chromosome inactivation occurs at different times in different tissues of the post-implantation mouse embryo. *Nat Genet* 3, 170-174, PMID 8499950.
- Tay, L.S., Palmer, N., Panwala, R., Chew, W.L., and Mali, P. (2020). Translating CRISPR-Cas Therapeutics: Approaches and Challenges. *CRISPR J* 3, 253-275, PMID 32833535.
- Tibrewal, S., Ratna, R., Gour, A., Agarkar, S., Dubey, S., Ganesh, S., Kekunnaya, R., Sangwan, V., Liu, Y., and Vanita, V. (2022). Clinical and molecular aspects of congenital aniridia - A review of current concepts. *Indian J Ophthalmol* 70, 2280-2292, PMID 35791108.
- Tsai, S.Q., Nguyen, N.T., Malagon-Lopez, J., Topkar, V.V., Aryee, M.J., and Joung, J.K. (2017). CIRCLE-seq: a highly sensitive in vitro screen for genome-wide CRISPR-Cas9 nuclease off-targets. *Nat Methods* 14, 607-614, PMID 28459458.
- Tyas, D.A., Simpson, T.I., Carr, C.B., Kleinjan, D.A., van Heyningen, V., Mason, J.O., and Price, D.J. (2006). Functional conservation of Pax6 regulatory elements in humans and mice demonstrated with a novel transgenic reporter mouse. *BMC Dev Biol* 6, 21, PMID 16674807.

- Tyner, C., Barber, G.P., Casper, J., Clawson, H., Diekhans, M., Eisenhart, C., Fischer, C.M., Gibson, D., Gonzalez, J.N., Guruvadoo, L., *et al.* (2017). The UCSC Genome Browser database: 2017 update. *Nucleic Acids Res* *45*, D626-D634, PMID 27899642.
- Tzoulaki, I., White, I.M., and Hanson, I.M. (2005). PAX6 mutations: genotype-phenotype correlations. *BMC Genet* *6*, 27, PMID 15918896.
- Vakulskas, C.A., Dever, D.P., Rettig, G.R., Turk, R., Jacobi, A.M., Collingwood, M.A., Bode, N.M., McNeill, M.S., Yan, S., Camarena, J., *et al.* (2018). A high-fidelity Cas9 mutant delivered as a ribonucleoprotein complex enables efficient gene editing in human hematopoietic stem and progenitor cells. *Nat Med* *24*, 1216-1224, PMID 30082871.
- Vasquez Quintero, A., Perez-Merino, P., Fernandez Garcia, A.I., and De Smet, H. (2021). Smart contact lens: A promising therapeutic tool in aniridia. *Arch Soc Esp Oftalmol (Engl Ed)* *96 Suppl 1*, 68-73, PMID 34836591.
- Vicente, A., Bystrom, B., Lindstrom, M., Stenevi, U., and Pedrosa Domellof, F. (2018). Aniridia-related keratopathy: Structural changes in naive and transplanted corneal buttons. *PLoS One* *13*, e0198822, PMID 29889891.
- Villalba, A., Gotz, M., and Borrell, V. (2021). The regulation of cortical neurogenesis. *Curr Top Dev Biol* *142*, 1-66, PMID 33706916.
- Walther, C., and Gruss, P. (1991). Pax-6, a murine paired box gene, is expressed in the developing CNS. *Development* *113*, 1435-1449, PMID 1687460.
- Walton, R.T., Christie, K.A., Whittaker, M.N., and Kleinstiver, B.P. (2020). Unconstrained genome targeting with near-PAMless engineered CRISPR-Cas9 variants. *Science* *368*, 290-296, PMID 32217751.
- Wang, X., Gregory-Evans, K., Wasan, K.M., Sivak, O., Shan, X., and Gregory-Evans, C.Y. (2017). Efficacy of Postnatal In Vivo Nonsense Suppression Therapy in a Pax6 Mouse Model of Aniridia. *Mol Ther Nucleic Acids* *7*, 417-428, PMID 28624217.

- Wirth, T., Parker, N., and Yla-Herttuala, S. (2013). History of gene therapy. *Gene* 525, 162-169, PMID 23618815.
- Xi, Z., Vats, A., Sahel, J.A., Chen, Y., and Byrne, L.C. (2022). Gene augmentation prevents retinal degeneration in a CRISPR/Cas9-based mouse model of PRPF31 retinitis pigmentosa. *Nat Commun* 13, 7695, PMID 36509783.
- Xiao, Q., Xu, Z., Xue, Y., Xu, C., Han, L., Liu, Y., Wang, F., Zhang, R., Han, S., Wang, X., *et al.* (2022). Rescue of autosomal dominant hearing loss by in vivo delivery of mini dCas13X-derived RNA base editor. *Sci Transl Med* 14, eabn0449, PMID 35857824.
- Xu, Z.P., and Saunders, G.F. (1997). Transcriptional regulation of the human PAX6 gene promoter. *J Biol Chem* 272, 3430-3436, PMID 9013587.
- Yang, G.S., Banks, K.G., Bonaguro, R.J., Wilson, G., Dreolini, L., de Leeuw, C.N., Liu, L., Swanson, D.J., Goldowitz, D., Holt, R.A., *et al.* (2009). Next Generation Tools for High-throughput Promoter and Expression Analysis Employing Single-copy Knock-ins at the *Hprt1* Locus. *Genomics* 93, 196–204, PMID 18950699.
- Yin, S., Zhang, M., Liu, Y., Sun, X., Guan, Y., Chen, X., Yang, L., Huo, Y., Yang, J., Zhang, X., *et al.* (2022). Engineering of efficiency enhanced Cas9 and base editors with improved gene therapy efficacies. *Mol Ther* 31, 744-759, PMID 36457249.
- Yuksel, M., Wang, Y., Tai, N., Peng, J., Guo, J., Beland, K., Lapierre, P., David, C., Alvarez, F., Colle, I., *et al.* (2015). A novel "humanized mouse" model for autoimmune hepatitis and the association of gut microbiota with liver inflammation. *Hepatology* 62, 1536-1550, PMID 26185095.
- Zhang, D., Wang, G., Yu, X., Wei, T., Farbiak, L., Johnson, L.T., Taylor, A.M., Xu, J., Hong, Y., Zhu, H., *et al.* (2022). Enhancing CRISPR/Cas gene editing through modulating cellular mechanical properties for cancer therapy. *Nat Nanotechnol* 17, 777-787, PMID 35551240.
- Zhang, Y., Nishiyama, T., Li, H., Huang, J., Atmanli, A., Sanchez-Ortiz, E., Wang, Z., Mireault, A.A., Mammen, P.P.A., Bassel-Duby, R., *et al.* (2021). A consolidated AAV system for

single-cut CRISPR correction of a common Duchenne muscular dystrophy mutation. *Mol Ther Methods Clin Dev* 22, 122-132, PMID 34485599.

Zhu, F., Nair, R.R., Fisher, E.M.C., and Cunningham, T.J. (2019). Humanising the mouse genome piece by piece. *Nat Commun* 10, 1845, PMID 31015419.

Zuber, M.E., Gestri, G., Viczian, A.S., Barsacchi, G., and Harris, W.A. (2003). Specification of the vertebrate eye by a network of eye field transcription factors. *Development* 130, 5155-5167, PMID 12944429.

## APPENDIX: GENERATION OF *FAX* ESCS

I have already generated B6129F1 *Fax* ESCs, in preparation for generating *FHe9/He9<sup>+</sup>* ESCs for microinjection. The preparation for this procedure involved superovulation of *Fax* dams and paired mating with studs that had been experienced for 10 days and then rested for five days prior to mating. The procedure itself involved the surgical removal of uterine horns from pregnant *Fax* dams, 3.5 days post-fertilization, as determined by the presence of a PC plug. Uterine horns were each flushed with FHM media (catalog MR-024-D, Sigma-Aldrich) to expel pre-implanted blastocysts and morulae. Blastocysts and morulae were collected using a mouth-pipette and washed three times through additional FHM droplets, to remove external cumulus cells. Blastocysts and morulae were then placed in KSOM (catalog MR-121-D, Sigma-Aldrich) under oil and incubated at 37°C, 5% CO<sub>2</sub>, 5% O<sub>2</sub>, nitrogen balance for 2-5 hours. Blastocysts and morulae were then transferred to 96-well plates on MEFs in KSR-ESC media (catalog 10829018, Gibco). Blastocysts and morulae were monitored for three days following day of collection (DOC) and hatching of blastocysts and embedding of inner cell mass (ICM) was noted. On DOC+7 each well with healthy, expanded ESC-like cells were trypsinized and re-plated on 24-well plates with MEFs. Cells continued to be cultured and were adapted to ESC media without KSR over four days. Wells with healthy ESC-like morphology (round, 3-dimensional clones) were further expanded to 4 x 24-wells for cryopreservation and lysis for DNA characterisation.

Lysed cells were screened using PCR assays to determine sex and *Fax* genotype. Of 51 blastocyst and morulae isolated, 19 developed into ESCs and were successfully cultured and expanded prior to characterisation. Of the lysed ESC lines eleven were female and eight were male. Of the eight male cell lines, three were *Fax/+* and two were *Fax/Fax* (Figure A.1A and B).

These five male ESCs that were either heterozygous or homozygous for *Fax* were thawed and expanded for longer term storage. Three of these cell lines were sent to JAX for microinjection to determine the germline capability of the new *Fax* ESCs. We received the chimera report from JAX, which determined that all injected ESCs produced multiple high chimeric males (>50%) demonstrating strong germline potential of the ESCs (Figure A.1C). These results give us confidence that the new *Fax* ESCs that will be used in an electroporation experiment to introduce the *He9* allele, will also produce *FHe9* cells with strong germline potential, as we work towards generating our humanized aniridia mouse for *in vivo* ABE8e therapy studies.

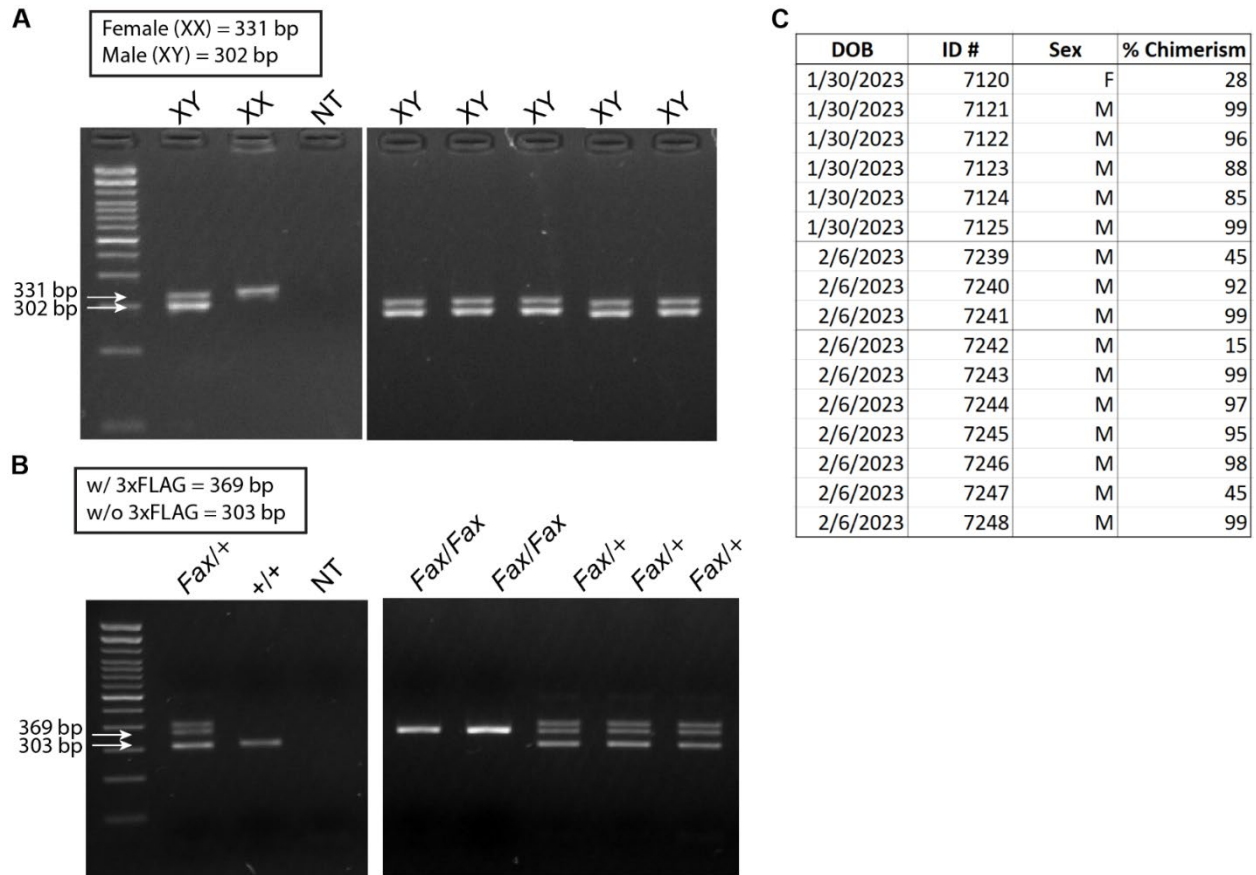


**Figure A.1 Characterisation of new *Fax* ESCs.** (A) PCR primers for X/Y assay amplify *Kdm5c* and *Kdm5d* genes on the X and Y chromosomes. Sex-chromosome specific DNA amplified from lysates of ESCs cultured from blastocysts from B6-*Fax* mice. Lane 1, XX positive control DNA from a female mouse ear notch. Lane 2, XY positive control DNA from a male mouse ear notch. Lane 3, no template negative control. Lanes 4-8, DNA from new male *Fax* ESCs. Band at 331 bp amplifies DNA from X chromosome and band at 302 bp amplifies DNA from Y chromosome. B) PCR primers for *Pax6* ATG assay bind around *Pax6* translational start site. Presence of 3xFLAG tag is indicated by 369 bp band. ATG site without 3xFLAG tag is indicated by 303 bp band. Lane 1, positive control DNA from a *Fax*/*+* mouse ear notch. Lane 2, negative control DNA from a *+/+* mouse ear notch. Lane 3, no template negative control. Lanes 4-5, DNA from cell line lysates showing singular 369 bp band, indicating homozygosity for 3xFLAG tag. Lanes 6-8, DNA from cell line lysates showing both 369 bp and 303 bp bands, indicating heterozygosity for 3xFLAG tag. C) Data from chimera report received from The Jackson Laboratory following microinjection of three of the new *Fax* ESC lines. Of the 16 male mice born from the microinjections, 12 showed high chimerism (>50%), as indicated by their coat colour.